TECHNISCHE UNIVERSITÄT MÜNCHEN

Department Chemie

Lehrstuhl Biotechnologie

The maturation of Src kinase by the molecular chaperone Hsp90 and its kinase specific cochaperone Cdc37

Edgar Erik Boczek

Vollständiger Abdruck der von der Fakultät für Chemie der Technischen Universität München zur Erlangung des akademischen Grades eines Doktors der Naturwissenschaften genehmigten Dissertation.

Vorsitzender: Univ. - Prof. Dr. Franz Hagn

Prüfer der Dissertation:

1. Univ. - Prof. Dr. Johannes Buchner
2. Univ. - Prof. Dr. Ville R.I. Kaila
3. Univ. - Prof. Dr. Sevil Weinkauf

Die Dissertation wurde am 04.12.2014 bei der Technischen Universität München eingereicht und durch die Fakultät für Chemie am 16.02.2015 angenommen.

Das deutlichste Anzeichen von Weisheit ist anhaltend gute Laune.

Michel de Montaigne

Content

1. Introduction

1.1. Chaperone assisted protein folding

Folding of the polypeptide chain is an essential prerequisite for a protein to reach its native three-dimensional structure and fulfill its tasks within the cell (Anfinsen *et al*., 1961, Dill *et al.*, 1995, Dill *et al*., 1997,). Protein folding is a cooperative process, which is not fully understood (Go & Taketomi, 1978, Kortemme, *et al*., 1998, Kloss *et al*., 2008). At intracellular protein concentrations of about 400 mg/ml and 60,000 newly synthesized proteins per minute (Zimmermann *et al.*, 1991) protein misfolding and aggregation would predominate and this would result in cell stress (Walter & Ron, 2011, Sontag *et al*., 2014, Wolozin, 2014). This issue is thought to account for the development of neurodegenerative disorders like Alzheimer (Beyreuther *et al.*, 1991 & Prusiner, 1996), lateral sclerosis (Shibata *et al.*, 2000), Morbus Parkinson (Lücking & Brice, 2000) and Chorea Huntington (Bates, 2003).

A cellular machinery has evolved to prevent or circumvent these side reactions. According to their assistance during the folding process, they are called molecular chaperones. Chaperones are involved in numerous processes, such as *de novo* folding of polypeptide chains, refolding of stress-denatured proteins, oligomer-formation and -dissociation, intracellular protein transport and proteolytic degradation. Primarily they bind hydrophobic segments on the substrate protein, prevent aggregation and reduce the concentration of folding intermediates by blocking these regions or function as disaggregases (Hartl & Hayer-Hartl, 2009). The chaperone's work starts co-translationally during ribosomal synthesis (Bergmann & Kuehl, 1979, Braakman *et al.*, 1991). In this context, the ribosome serves as a binding platform for proteins like trigger factor and nascent polypeptide-associated complex (NAC) that bind unfolded parts, thereby protecting them against unspecific interaction with other molecules and misfolding (Rutkowska *et al.*, 2008, Gautschi *et al.*, 2002). Other factors like protein disulfide isomerases (PDIs) (Freedman *et al.*, 1994, Ali Khan & Mutus, 2014) and peptidyl-prolyl *cis/trans* isomerases (PPIases) (Fischer *et al.*, 1984, Fanghänel & Fischer, 2004, Schiene & Fischer, 2000) increase the isomerization of disulfide and prolyl-peptide bonds. Since these reactions are rate-limiting steps, PDI- and PPIase-activities guarantee a significant higher speed of the folding process and consequently decrease the probability of aggregation.

Highly complex and conserved protein machines have evolved that possess the ability to suppress protein aggregation. They directly interact with aggregation-prone proteins and thus, their activity is in direct competition to the aggregation reaction (Richter *et al.*, 2010) (**Figure 1**). Their synthesis is upregulated upon cellular stress caused by parameters such as high concentrations of reactive oxygen species (Ruddock & Klappa, 1993) or heat (Georgopoulos & Welch, 1993). This enables the cell to tolerate adverse circumstances to a certain extent (Lindquist & Craig, 1988) and historically they are named heat shock proteins (Hsps). On the basis of sequence homology and size, these chaperones are categorized into five groups: (1) the Hsp60 family (GroE in bacteria), (2) the Hsp70 family, (3) the Hsp90 family, (4) the Hsp104/Clp family and (5) the family of small heat shock proteins (sHsps) (Richter *et al.*, 2010). Except for sHsps all of them are ATPases.

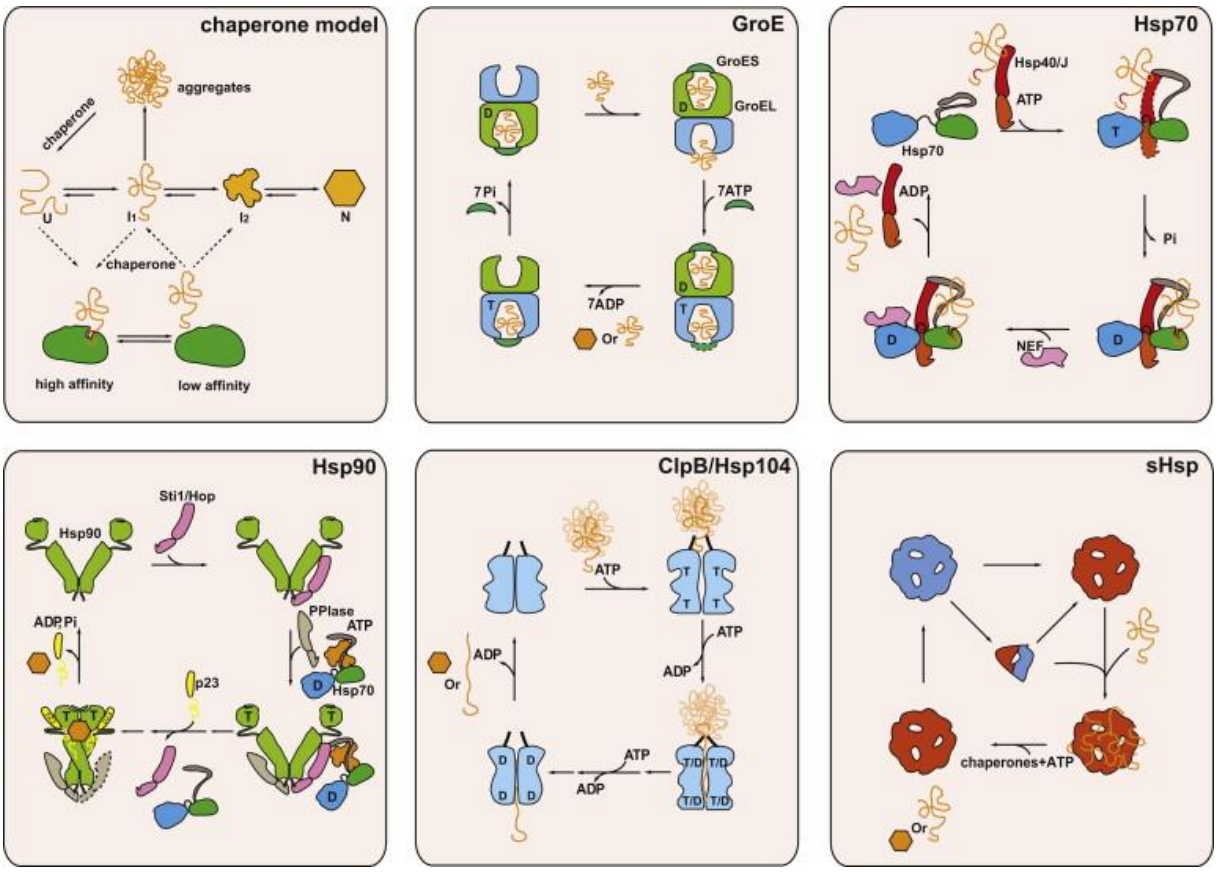

Figure 1

Molecular Chaperone Mechanisms.

Schematic representation of fundamental chaperone pathways. Chaperone model: proteins fold via intermediate steps (I_1, I_2) from unfolded (U) to a native state (N). Chaperones bind and may stabilize different stages during the folding process. GroE: in bacteria, chloroplasts and

mitochondria nonnative proteins are sterically isolated by the GroE complex and liberated upon ATP hydrolysis. Hsp70: The Hsp40-Hsp70 complex binds to extended regions exposed on not fully folded proteins and releases a partly folded, yet non-native state. Hsp90: in companion with numerous cochaperones, Hsp90 binds to pre-folded substrates (such as I_2) and liberates a fully mature protein. Clp/Hsp104: ATP-dependently disintegrates aggregated proteins by pulling them through a channel. sHsps: in their activated form these oligomeric complexes function as a reservoir for non-folded or partly folded proteins. Figure from Richter *et al.*, 2010.

1.2. Hsp90

The 90 kDa heat shock protein (Hsp90) is an abundant and ubiquitious molecular chaperone in eucaryotes. Crystal structures of yeast (19), bacterial (20) and endoplasmic reticulum (ER) Hsp90 (Dollins *et al.*, 2007) have provided a basis for further analyzing the Hsp90 machinery. Hsp90 constitutes V-shaped dimers, which close upon ATP-binding (**Figure 2**). Each subunit can be divided into three conserved domains. The N-terminal ATPase domain is connected to the middle domain via a charged linker. The middle domain itself does not hydrolyze ATP, but a catalytic arginine residue at position 380 may function as an acceptor for the γ-phosphate during ATP hydrolysis. Therefore, Hsp90 is also termed a “split ATPase”, due to the fact that the enzymatic reaction requires two separate domains (Meyer *et al.*, 2003). However, in this context, it has also been contrarily proposed that Arg380 may not be a catalytic residue, but stabilizes the closed conformation required for ATP hydrolysis (Cunningham *et al.*, 2012). ATPase activity is crucial for *in vivo* function of Hsp90 (Obermann *et al.*, 1998, Panaretou *et al.*, 1998). Client proteins and cochaperones bind to the middle domain. The 12 kDa C-terminal dimerization domain is connected to the middle domain via a long α-helix. Parts of it could not be resolved in the crystal structure, probably due to flexible regions near the C-terminus. The very C-terminus of Hsp90 is the MEEVD-motif, which is recognized by tetratricopeptide repeat (TPR)-containing cochaperones (Chen *et al.*, 1998).

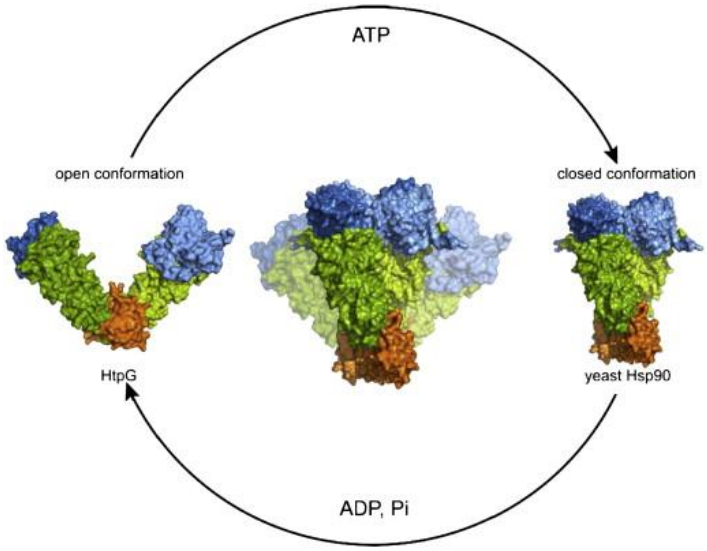

Figure 2

Hsp90 structures.

Crystal structures of full length Hsp90 from *E.coli* (HtpG) in the open conformation (left, PDB: 2IOQ) and nucleotide-bound yeast Hsp90 in the closed conformation (right, PDB: 2CG9). The N-domain is depicted in blue, the M-domain in green and the C-domain in orange. Figure from Li *et al.*, 2012.

1.2.1. Hsp90-localization and evolution

The Hsp90 family is highly conserved and ubiquitiously distributed in all organisms, except for archae. The family can be divided into five different groups: (1) cytoplasmic Hsp90, (2) ER-located Hsp90, glucose-regulated protein 94 (Grp94) in human, (3) Hsp90 in chloroplasts and (4) mitochondria, tumour necrosis factor receptor associated protein 1 (TRAP1) and (5) bacterial Hsp90, high temperature protein G (HtpG) (**Figure 3**).

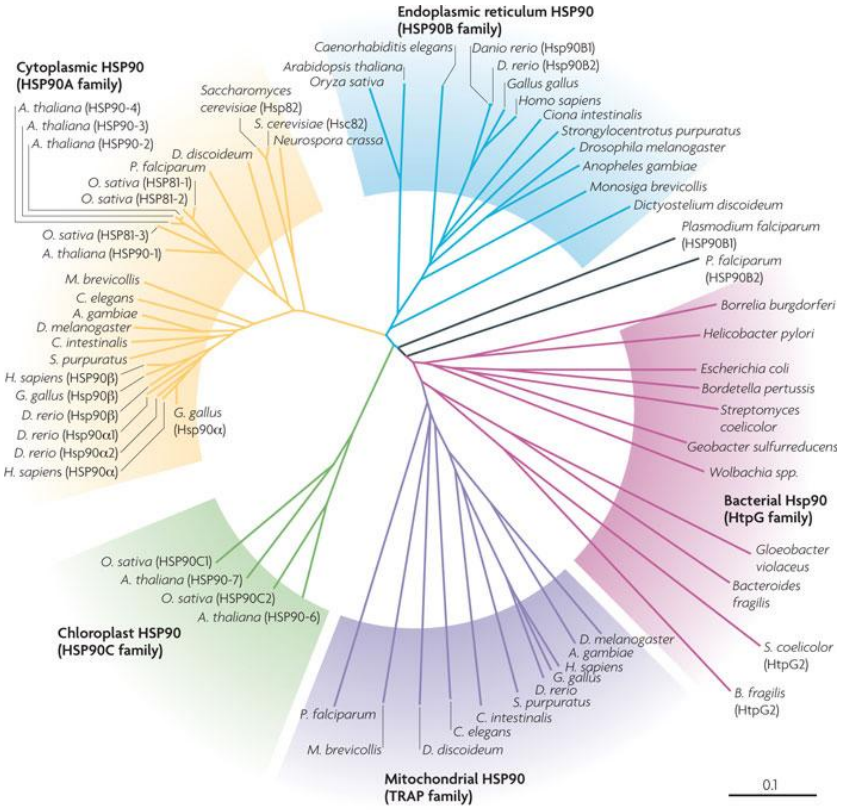

Figure 3

Evolution of the Hsp90 family.

Shown are the Hsp90 subgroups and their homology. The benchmark determines the genetic distance between the members. Figure from Taipale *et al*., 2010.

Bacterial Hsp90 is present in almost all bacteria, but not essential under physiological conditions (Obermann *et al.*, 1998, Panaretou *et al.*, 1998). Grp94 plays an important role in maintaining quality control in the ER, whereby all known substrates of Grp94 are either secreted or located in or on the extracellular membrane after maturation (Argon & Simen, 1999, Yang & Li, 2005). TRAP1 shows high sequence homology to HtpG and ensures protection of the cell against oxidative stress (Pridgeon *et al.*, 2007).

In eucaryotes Hsp90 is essential and constitutes 1-2 % of the proteome in the cytoplasm under physiological and 5 % under stress conditions (Obermann *et al.*, 1998, Panaretou *et al.* 1998, Welch & Feramisco, 1982). In man and in yeast *Saccharomyces cerevisiae*, there exist two isoforms of Hsp90 (Hsp90α and Hsp90β in human and Hsc82 and Hsp82 in yeast) (Kellis *et al.*, 2004, Langkjaer *et al.* 2003). Hsp90β and Hsc82 are constitutively expressed, whereas the expression of Hsp90α

and Hsp82 is strongly upregulated under stress conditions (Borkovich *et al.*, 1989). Since heat shock leads to protein aggregation in the cell, the significant overexpression of Hsp90 upon heat exposure indicates a crucial role of the chaperone in protecting the cell under these circumstances.

1.2.2. Hsp90-cochaperones and ATPase-cycle

Hsp90 does not act alone on substrate proteins. Its function is complemented by associated cochaperones. In the chaperone cycle, cochaperones and client proteins enter and leave the complex in order to drive protein processing (Li *et al.*, 2011). In this context, the hydrolysis of ATP plays an important role. The rate of the enzymatic reaction is significantly influenced by the type of cochaperone bound to the machinery. Hsp90 utilizes ATP binding and hydrolysis to drive large conformational changes including the transient dimerization of the N-terminal and middle domains (Richter *et al.*, 2008, Vaughan *et al.*, 2009). Recent results also propose the importance of thermal fluctuations during this process (Ratzke *et al.*, 2012). It appears that the ATP-bound form of Hsp90 has high affinity for substrate proteins and undergoes slow hydrolysis to the ADP-bound form, which has low affinity for substrate proteins and undergoes nucleotide exchange to the ATP-bound form (Young & Hartl, 2000). Interstingly, the rate of ATP-hydrolysis varies strongly among different species. Whereas human Hsp90 hydrolyzes only one ATP molecule every 20 minutes (McLaughlin *et al*., 2002), yeast and *C. elegans* Hsp90 possess a significantly increased enzymatic activity with an approximate reaction velocity of 0.8 – 1.0 hydrolysis events per minute (Panaretou *et al*., 1998 & Gaiser et al., 2009). ATP hydrolysis is tightly regulated by interactions with cochaperones. Some cochaperones slow down the ATPase cycle (Hop, Cdc37, p23 (Prodromou *et al.*, 1999, Wegele *et al.*, 2003, Gaiser *et al.*, 2010 & McLaughlin *et al.*, 2006) whereas others increase the hydrolysis rate (Aha1, Hch1) (Nathan *et al.*, 1999, Panaretou *et al.*, 2002, Mayer *et al.*, 2002). Other cochaperones interconnect chaperones, such as Hsp70-Hsp90 coordinating protein (Hop in human) and its yeast homolog stress inducible protein 1 (Sti1) that connects the Hsp70 and the Hsp90 chaperone cycles (Chen & Smith, 1998). Additionally, the cochaperones deliver specificity to the Hsp90 complex for the maturation of substrate proteins. Much of the understanding of the cellular chaperone machinery has been gained studying the group of steroid hormone receptors. During their maturation, steroid receptors are initially bound by

the chaperones Hsp70 and Hsp40 and subsequently transferred to Hsp90 (Pratt *et al.*, 2006). The cochaperone Hop serves as an adaptor protein, binding Hsp90 and Hsp70 simultaneously through its TPR-domains (Schmid *et al.*, 2012) (**Figure 4**). Hop/Sti1 stabilizes the open conformation of Hsp90 (Roe *et al.*, 2004). Other cochaperones like p23/Sba1 stabilize the closed conformation of Hsp90 (Ali *et al.*, 2006) or, like Aha1, activate ATP hydrolysis (Mayer *et al.*, 2002, Panaretou *et al.*, 2002). After Hsp70 and Hop dissociate from the intermediate complex the "late" cochaperone p23 and a TPR-containing PPIase (e.g. Cyp40, FKBP51 or FKBP52) bind to the ATP-bound, N-terminally dimerized form of Hsp90. The binding of steroid hormone may initiate the dissociation from the Hsp90 complex.

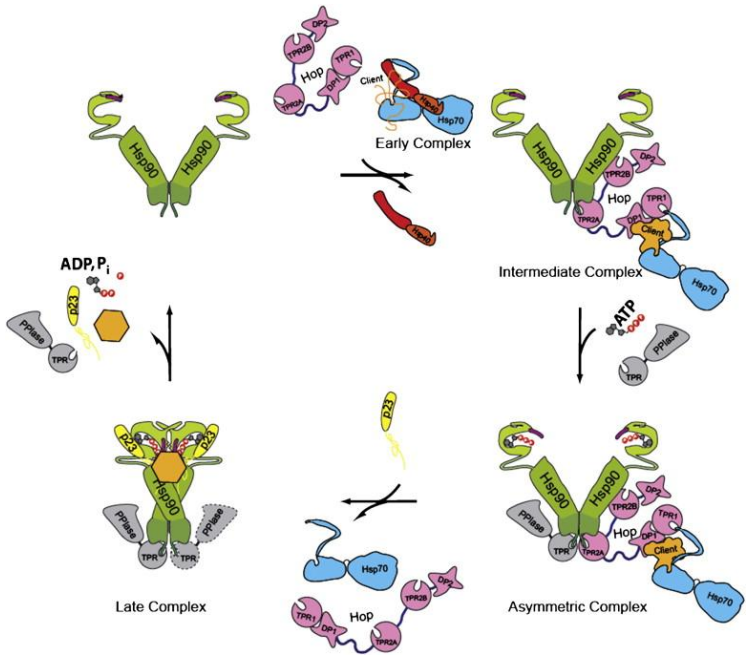

Figure 4

Cochaperone cycle of the Hsp90 machinery.

Hsp70, Hsp40 and a client protein form an „early complex". The client protein is transferred from Hsp70 to Hsp90 through the adaptor protein Hop/Sti1. One Hop/Sti1 bound is sufficient to stabilize the open conformation of Hsp90. The other TPR-acceptor site is preferentially occupied by a PPIase, leading to an asymmetric intermediate complex. Hsp90 adopts the ATPase-active (closed) conformation after binding of ATP. p23/Sba1 stabilizes the closed state of Hsp90, which weakens the binding of Hop/Sti1 and promotes its exit from the complex. Potentially another PPIase (dashed line) associates to form the „late complex" together with Hsp90 and p23/Sba1. After hydrolysis of ATP, p23/Sba1 and the folded client are released from Hsp90. Figure from Li *et al.*, 2012.

Little is known about how the ATPase-coupled chaperone cycle leads to the activation of substrate proteins or whether they are released with each cycle of the ATPase reaction. Furthermore, the question arises which conformational changes occur in the client and how these changes are effected by Hsp90 and its cochaperones.

1.2.3. Hsp90-clients

In contrast to other chaperone systems involved in general protein folding, Hsp90 shows some specificity for its substrate proteins. However, the origin of specificity and the manner in which Hsp90 interacts with its substrates are not well understood. Numerous signaling proteins like Src tyrosine kinases, Raf serine kinases and cyclin-dependent kinases 4/6 (Cdk4/6) are well-known substrates of Hsp90, as well as transcription factors such as steroid receptors, the tumor suppressor p53 and nitric oxide synthase (Picard, 2002). Thus, Hsp90 represents a platform at the interface between protein folding and regulation (Taipale *et al.*, 2010), highlighting the important position of this protein for therapeutic approaches. Interestingly, kinases comprise the biggest group of client proteins. 60 % of the human kinome depends on Hsp90 in their folding (Taipale *et al.*, 2012). In this context, one cochaperone is of particular interest and seems to be strictly connected to Hsp90-mediated maturation of kinases: Cdc37.

1.3. Cdc37

The cochaperone cell division cycle 37 (Cdc37) has been identified as a kinase-specific cochaperone of Hsp90 (Brugge *et al.*, 1981). The authors found Src kinase (pp60) interacting with Hsp90 (pp90) and Cdc37 (pp50) applying sedimentation analysis and immunoprecipitation to cell lysates. Complexed Src molecules showed mainly non-phosphorylated tyrosine residues, whereas tyrosine-phosphorylated Src was greatly found as a monomer. Phosphorylation of Tyr527 in Src leads to its inactivation (Xu *et al.*, 1999a). A temperature sensitive variant of Src showed increased interaction with Hsp90 and Cdc37 (Brugge *et al.*, 1981). In 1992, Hutchison *et al*. were able to reconstitute the heterotrimer in a cell-free reticulocyte lysate system and could furthermore show that this complex interacted with Hsp70 (Hutchison *et al.*, 1992). In 1996, eucaryotic Cdc37 was described as a kinase-targeting subunit of Hsp90. It could be shown that it interacted with the kinase Cdk4 *in vivo* and *in vitro,* preferentially in the state of the kinase that is not bound to D-type cyclins, which is the inactive state. *In vivo* inhibition of Cdc37/Hsp90 decreased the amount of newly synthesized Cdk4, indicating its role in kinase stabilization (Stepanova *et al.*, 1996). The idea of Cdc37 to be seen as a kinase-specific cochaperone became consolidated (Hunter & Poon, 1997), when it was discovered that 75% of the yeast kinome (Mandal *et al.*, 2007) and 60 % of the human kinome depend on Cdc37 chaperoning (Taipale *et al.*, 2012). Additionally it could be demonstrated that Cdc37 interacts directly after or even during translation of the kinase for stabilization, protection from misfolding, aggregation and degradation and promoting maturation (Hunter & Poon, 1997, Mandal *et al.*, 2007, Caplan *et al.*, 2007, MacLean & Picard, 2003, Gray *et al.*, 2008, Shao *et al.*, 2001, Farrel & Morgan, 2000). Cdc37 specifically stabilizes the complex of Hsp90 and the kinase (Hunter & Poon, 1997, Karnitz & Felts, 2007). The Hsp90 inhibitor geldanamycin disrupts the complex between Hsp90-Cdc37 and the kinase and prevents its maturation, while the interaction between Hsp90 and Cdc37 is not negatively influenced (Shao *et al.*, 2001). Cdc37 binds the kinase by its N-terminal domain and Hsp90 by its C-terminal region (Prince & Matts, 2004, Silverstein et al., 1998 & Zhao et al., 2004). Like Hop/Sti1, binding of Cdc37 to yeast Hsp90 inhibits the ATPase activity, which is thought to favor loading of substrate proteins (Prodromou et al., 1999, Gaiser et al., 2010, Wegele et al., 2003).

In yeast, Cdc37 is an essential protein and has been shown to possess Hsp90-independent chaperone and folding activity (Mandal *et al.*, 2007, Karnitz & Felts, 2007, Kimura *et al.*, 1997, Turnbull *et al.*, 2005) and deletion studies in yeast revealed the protein-kinase binding domain to be sufficient to maintain cell viability at lower temperatures (Lee et al., 2002). (1) *In vivo* it can compensate for decreased Hsp90 function in maintaining v-Src kinase activity but not the activity of the glucocorticoid receptor (Kimura *et al.*, 1997), (2) *in vitro* Cdc37 brings denatured β-galactosidase to an activation-competent state and (3) stabilizes mature but unstable casein kinase 2 (CK2) (Kimura *et al.*, 1997). Furthermore, in a Hop/Sti1-deficient yeast strain, Cdc37-overexpression suppressed a defect in kinase folding.

1.3.1. Cdc37-structure

Human Cdc37 is a 44,5 kDa protein comprising 378 residues. There is generally low sequence homology between different species but the most highly conserved part is located near the N-terminus (**Figure 5**).

Shao *et al*. could dissect the partial regions of Cdc37 important for partner recognition with the kinase eIF2α and showed that the Cdc37::kinase interaction is mediated via the N-terminal segment of Cdc37 (1-126) and binding of Hsp90 takes place in the middle part of Cdc37 (128-282) (Shao *et al.*, 2003). The C-terminal part (283-378) neither interacted with the kinase nor with Hsp90 and hence its function remains unknown (see Cdc37 model in **Figure 5**). On the basis of functional assays the authors suggest that the region of 127-163 serves as an “interdomain switch” that alters the ability of Cdc37 to recognize Hsp90’s conformation, thereby representing an important region for regulation of the kinase binding ability of Cdc37 by the conformation of Hsp90. Interestingly, the variant Trp7Ala with the mutation lying outside of the proposed Hsp90 binding domain decreased Hsp90 binding of the full-length protein, suggesting that global effects on the Cdc37 structure could be caused by minor changes (Shao *et al.*, 2003).

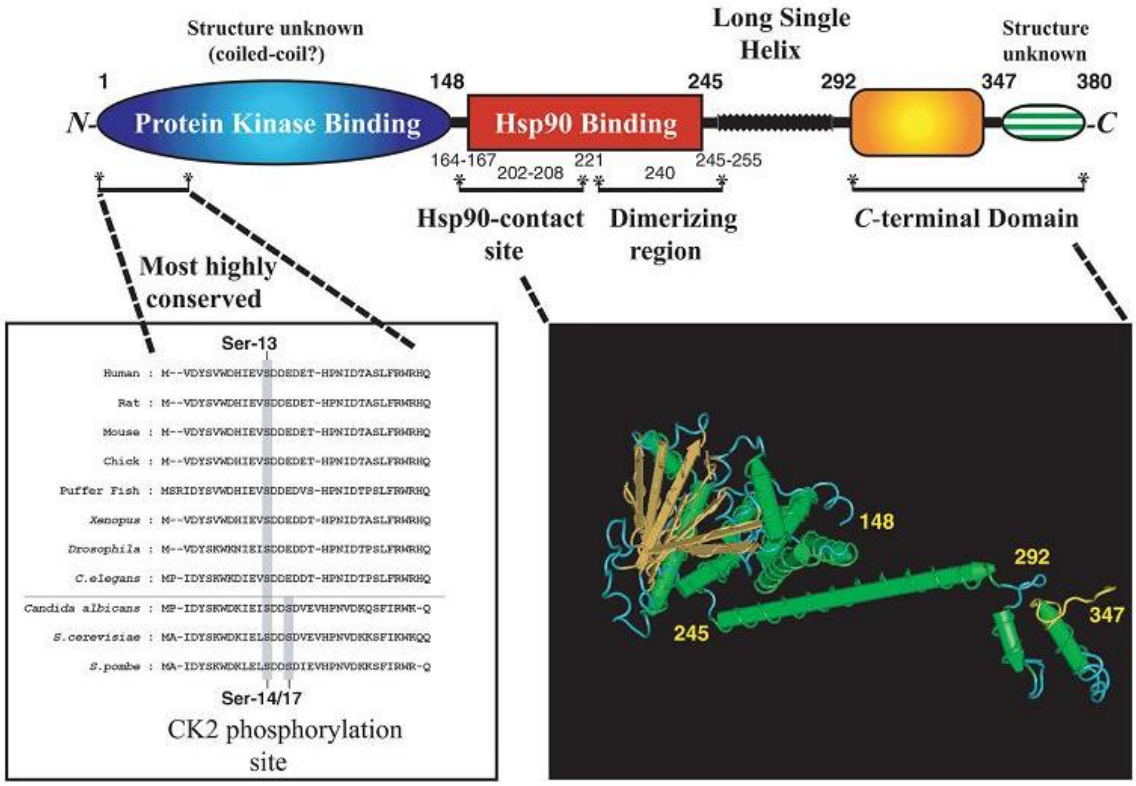

Figure 5

Structure of human Cdc37.

Domain structure of Cdc37, alignment of amino acid sequences surrounding the CK2-phosphorylation site of Cdc37, and the crystal structure of a part of Cdc37 (PDB: 1US7/MMDB) are illustrated. Figure from Miyata *et al*., 2009.

Cdc37 is a low affinity dimer (K_D ~ 80 µM) (Zhang *et al.*, 2004) and, in the phosphorylated form, it displays high affinity for multiple kinases (Shao *et al.*, 2003, Miyata & Nishida, 2004). As predicted by bioinformatic tools (Mittag & Forman-Kay, 2007, Peng *et al.*, 2005), the kinase binding domain of Cdc37 is expected to be largely unstructured.

1.3.2. Interaction of Cdc37 with Hsp90

In 2004 the crystal structure of the Cdc37 C-terminal part (148-347) was solved in complex with the N-terminal nucleotide binding domain of Hsp90 (1-220) (Roe *et al.*, 2004) shown in **Figure 6.** Under crystallizing conditions Cdc37 binds to Hsp90's N-terminal domain as a dimer, forming a heterotetramer. Cdc37 fixes the ATP-lid in an open conformation and inserts its Arg167 residue interacts with Asp33 (Asp47 in human) of Hsp90, preventing ATP-hydrolysis and interaction of the N-domains of the chaperone. The authors suggest that Cdc37 arrests the ATPase cycle and brings the Hsp90 machinery to a hold to facilitate kinase client loading. While Arg167 reaches into the ATP-binding pocket of Hsp90, this does not prevent geldanamycin (GA) to bind, as Cdc37 can bind to GA-inhibited Hsp90 (Roe *et al.*, 2004, Siligardi *et al.*, 2002, Shao *et al.*, 2001). Additional studies indicate that Cdc37 middle domains exist as monomers (Zhang *et al.*, 2004, Sreeramulu *et al.*, 2009) and low resolution cryoelectron microscopy images of the Hsp90-Cdc37-Cdk4 complex show monomeric Cdc37 binding to the Hsp90-kinase complex (Vaughan *et al.*, 2006).

The human Cdc37-Hsp90 complex was investigated by heteronuclear NMR spectroscopy utilizing the N-terminal domain of Hsp90 and the middle domain of Cdc37 (Sreeramulu *et al.*, 2009), indentifying the Cdc37 residue Leu205 as a key interactor involved in numerous hydrophobic contacts within the chaperone-cochaperone complex.

Additionally, the sensitivity of the Cdc37-Hsp90 interaction towards the binding of nucleotides on Hsp90 adds another level of complexity to this relation. Gaiser *et al*. intimately investigated this effect, which is described below.

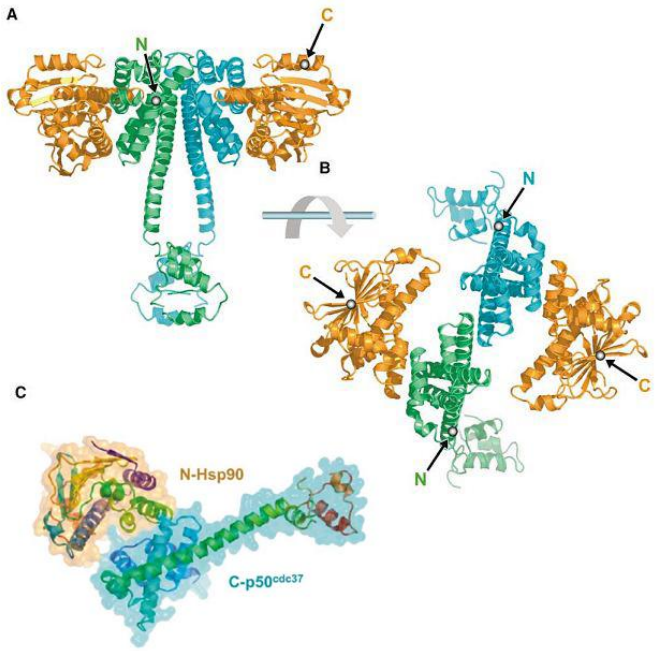

Figure 6

Structure of the Cdc37-Hsp90 complex.

Secondary structure cartoon of the $(N\text{-Hsp90})_2$-$(C\text{-Cdc37})_2$-complex. The assymetric unit in the crystal contains one N-Hsp90-C-Cdc37-dimer. N-Hsp90 in gold and C-Cdc37 in blue. The positions of the N-terminus of C-Cdc37 and of the C-terminus of N-Hsp90 are indicated. (B) As (A) but viewed from the opposite site to the long helical protusions of Cdc37. (C) Secondary structure cartoon of the N-Hsp90-C-Cdc37-complex rainbow colored and superimposed on the molecular surface of the two proteins. N-Hsp90 in gold and Cdc37 in blue. Figure adapted from Roe *et al.*, 2004.

1.3.3. Regulation of Cdc37

During kinase chaperoning, phosphorylation of Cdc37 is necessary for Hsp90-dependent kinase activation. In this context, position Ser13 (human) and Ser14/17 (yeast) are important (Vaughan *et al.*, 2008). Specific phosphorylation is facilitated by CK2. The model based on these observation is shown in **Figure 7**.

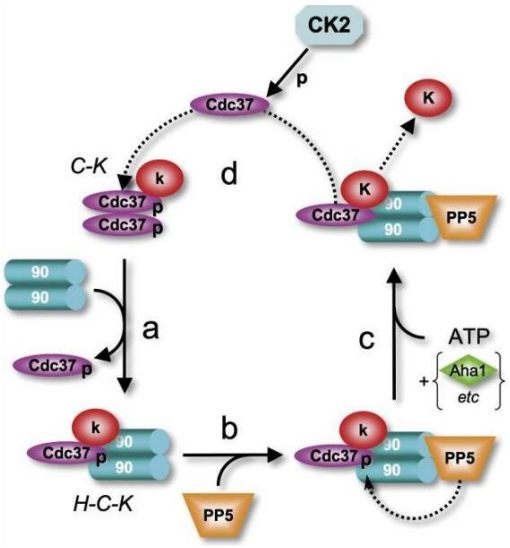

Figure 7

Illustration of coupling of CK2 phosphorylation and Hsp90-targeted dephosphorylation by PP5/Ppt1 to the role of Cdc37 in assembly and Hsp90-dependent activation of kinase clients.

Cdc37 (C) binds an inactive kinase (K) as a dimer. The C-K complex binds an Hsp90 (H) dimer with loss of one Cdc37 to give a stable H-C-K complex (a). Cdc37 is phosphorylated in both these complexes. PP5/Ppt1 can bind to Hsp90 in the H-C-K complex (b) and dephosphorylate Cdc37 prior to, or concomitant with, binding of ATP and other cochaperones, such as Aha1 (c) generating an activated kinase and dissociating the Hsp90-based complex. Free Cdc37 is rephosphorylated by the constitutive activity of CK2 (d) to regenerate the active pSer13 form of the cochaperone. Figure from Vaughan *et al.* (2008).

1.3.4. Substrates of Cdc37

Until recently, in the Picard collection the listed substrates recruited to Hsp90 by Cdc37 were ErbB2 (Her2/neu, human epidermal growth factor receptor 2), ErbB1 (EGFR, Her1), Cdk4, c-Raf (Raf-1), v-Raf (b-Raf), Akt, v-src and AR (androgen receptor), AR being the only client that is not a protein-kinase (http://www.picard.ch/downloads/Cdc37interactors.pdf). The Lindquist group greatly extended this list by applying a quantitative Lumier assay and found that in fact 60 % of the human kinome interact with Hsp90 to a certain extent (Taipale *et al.*, 2012). This holds true for the “strong” and “intermediate” clients identified, but most probably the number of kinases being dependent on Hsp90 and Cdc37 during their initial maturation is even higher, as this is also the case for the “non-client” c-Src (Xu *et al.*, 1999). In this context, Cdc37 seems to be one of the most specific cochaperones, almost exclusively delivering kinase clients to the folding machinery (Taipale *et al.*, 2012).

To date, it is suggested that stable kinases are bound transiently during maturation, whereas unstable kinases are constantly bound to Cdc37 and show a higher functional dependence on the Cdc37-Hsp90-system (Taipale et al., 2010). In cancer cells destabilized, oncogenic kinases would escape degradation via stabilization by Cdc37-Hsp90, such that Cdc37 functions as stabilizing factor for oncogenic Hsp90-substrates. Inhibition of Hsp90 leads to degradation of these unstable substrates in the cell, but also causing numerous side effects (Schneider *et al.*, 1996, Trepel *et al.*, 2010). Therefore, the idea has been raised to inhibit Cdc37 instead of Hsp90 to lead to a more kinase-specific downturn of oncogenic activity (Pearl, 2005). Although to date, there are no Cdc37-Hsp90 inhibitors in clinical trials, much hope lies in targeting a more kinase specific chaperoning with less side effects (Smith & Workman, 2009).

1.3.5. Mechanistic insights

The maturation of checkpoint kinase 1 (Chk1) has been shown to be Hsp40- and Hsp70-dependent, while in the late chaperoning complex mainly Hsp90 and Cdc37 were found (Arlander *et al.*, 2006), suggesting a mechanism in which the client kinase is brought to the Hsp90-Cdc37 complex via the Hsp40-70 pathway. Additional studies suggested that Cdc37 would bind to the active center of kinases, thereby competing with kinase inhibitors and would be released from the kinase by ATP-binding (Polier *et al.*, 2013).

Further, a carefully regulated mechanism involving the interaction with Hsp90 and many cochaperones is suggested for kinase maturation. Gaiser *et al.* could show that in *c. elegans*, this includes competitive interactions as shown with Cdc37 and Hop/Sti1 or Cdc37 and p23 (both Hsp90-ATPase inhibitors) as well as cooperative interactions as shown with the Cdc37-Hsp90 complex and Aha1 (Hsp90-ATPase activator) or protein phosphatase 1 (Pph1) (Gaiser *et al.*, 2010). The complex of Aha1, Cdc37 and Hsp90 was disrupted by the nucleotide-induced N-terminal closing reaction of Hsp90. While the complex of human Cdc37 and Hsp90 is disrupted by ATP-analogues (Zhang *et al.*, 2009), the *C. elegans* Cdc37 binds to both, the open and the closed conformation of Hsp90. In contrast to yeast Cdc37, human Cdc37 displays high affinity for Hsp90 (K_D ~ 3 µM) and shows high inhibitory impact on ATPase activity. However, human Hsp90's ATP hydrolysis rate of about 20 min^{-1} is much lower than that of *C. elegans* and yeast. Consequently, most studies were

obtained using a mixed system of human Cdc37 and yeast Hsp90, whose ATP hydrolysis rate lies around 1 min^{-1}.

Interestingly, TPR (tetratrico peptide repeat)-containing co-factors, such as protein phosphatase 5 (PP5), Hop/Sti1 and the PPIase FKBP52 seemed to block Cdc37 binding to Hsp90 at least to a certain extent, although their binding motif MEEVD lies in the C-terminal region of Hsp90, whereas Cdc37 is supposed to bind the N-terminal Hsp90 domain (Gaiser et al., 2010).

Cdc37 is not just a scaffold recruiting kinase substrates to Hsp90, but participates in the regulation of the ATPase cycle of Hsp90 (Siligardi *et al.*, 2002) suggesting a conformational control by the cochaperone.

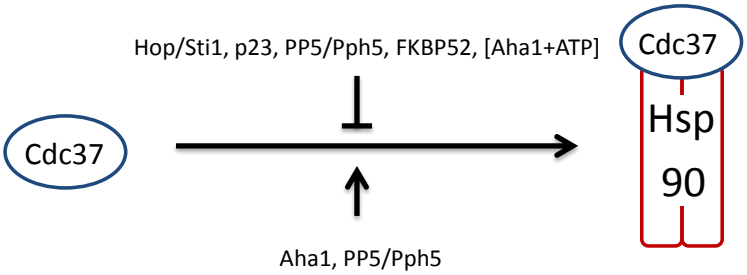

Figure 8

Summary of factors influencing Cdc37 binding to Hsp90 in different organisms.

Cochaperones found in complex or found to inhibit complex formation of Cdc37 and Hsp90 are shown. Interestingly, some cochaperones were found in complex, although having been observed to inhibit Cdc37-Hsp90 interaction at the same time (e.g. PP5/Pph1).

1.4. Protein kinases

Protein kinases represent the largest family of enzymes with 518 kinases constituting 1.7 % of the human genome (Manning *et al.*, 2002, **Figure 9**). Kinases catalyze the transfer of γ-phosphate from ATP to the hydroxyl-group of a tyrosine, a serine, a threonine or a histidine. They are divided into three subgroups, depending on their side chain specificity: Serine/Threonine kinases, Tyrosine kinases and Histidine kinases have been identified to date.

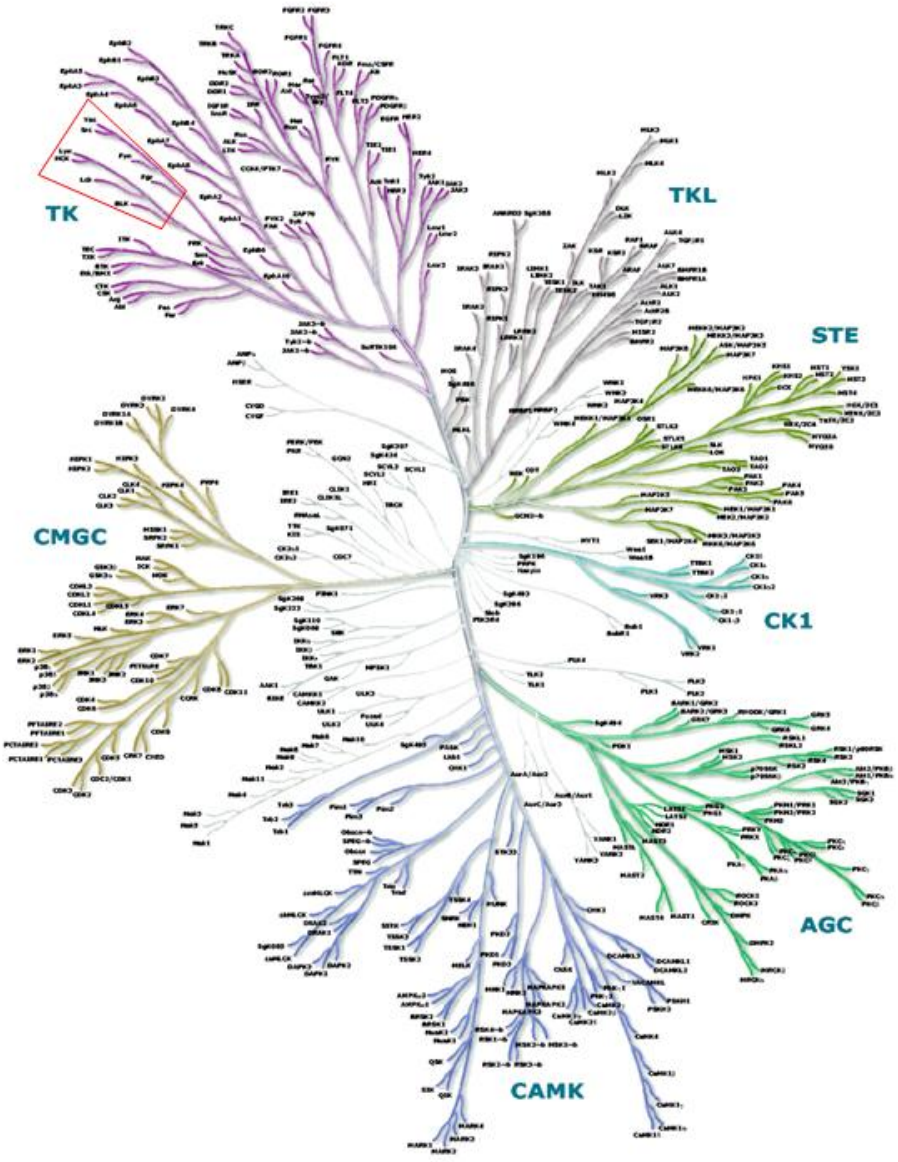

Figure 9

The human kinome.

Representation of the 518 human kinases in a phylogenetic tree. Every branch end represents one kinase. The distance between different kinases correlates with their evolutionary distance. The Src kinase family is marked by a red frame. TKL: tyrosine kinase-like, STE: homologs of yeast Sterile 7, Sterile 11, Sterile 20 kinases, CK1: casein kinase 1, AGC: Containing PKA,

PKG, PKC families, CAMK: Ca^{2+}/calmodulin-dependent kinases, CMGC: homologs of yeast Sterile 7, Sterile 11, Sterile 20 kinases, TK: tyrosine kinases. Figure from Manning *et al.* (2002).

Kinases play a key role in signal transduction and the control of fundamental cellular processes. Intracellular tyrosine kinases are involved in the cellular response to hormones and other extracellular factors binding to upstream receptors (Krauss, 2008). Upon hormone recognitition, kinases are activated downstream, often associated with autophosphorylation, thereby stepwise delivering the signal within the cell. This way, kinases are involved in the regulation of gene expression, growth, cell division, differentiation, metabolism, organization of the cytoskeleton, migration and apoptosis. Since these networks of signal transduction, involving numerous factors are highly complex and of significant importance for the emergence of many diseases, to unravel their principles is still one of the main tasks for cellular biologists.

1.4.1. Structure of kinases

Kinases are multi-domain proteins, consisting of the catalytically active kinase domain and various regulatory domains. This may include a PH- and/or WW-domain as well as the unique- (or variable) and the SH3- and SH2-domains. The PH-domain (Pleckstrin homology-domain) plays an important role in recruiting kinases to membranes of their target organelles by binding to phosphatidylinositol and in the interaction with the βγ–subunits of G-proteins and protein kinase C (Wang *et al*., 1994, Wang & Shaw, 1995, Yao *et al*., 1994). PH-domains consist of two perpendicular anti-parallel beta sheets, followed by a C-terminal amphipathic helix (**Figure 10**), (Riddihough, 1994).

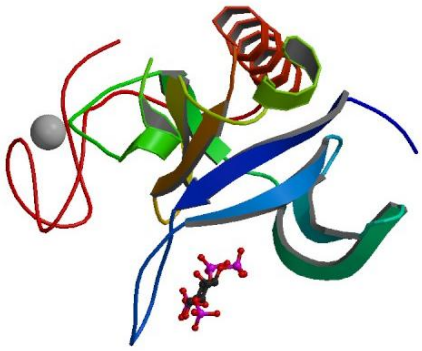

Figure 10

Structure of a PH-domain.

PH-domain of Bruton's tyrosine kinase. The protein chain is rainbow-colored from N- to C-terminus. A complexed Zn^{2+} ion is represented as white sphere and the ligand 2-(1-Hydroxybutoxy)Propyl Butyrate is depicted as stick model. PDB: 2Z0P.

The WW-domain comprises two tryptophan residues, playing a central role in regulation via protein-protein interactions. In addition to binding to proline-rich proteins, some WW-domains also recognize phospho-serine and phospho-threonine containing proteins (Chen & Sudol, 1995). WW-domains are involved in the interaction of regulatory protein complexes during signal transduction. The WW-domain represents one of the smallest protein modules (~ 40 amino acids) and structurally, it constitutes a triple-stranded beta sheet (**Figure 11**), (Macias *et al*., 1996).

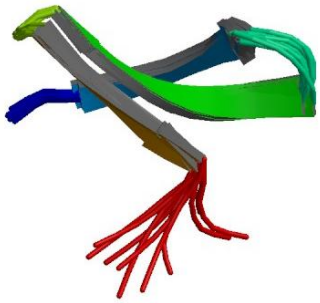

Figure 11

Structure of a WW-domain.

YJQ8WW-domain from *S. cerevisiae*. The protein chain is rainbow-colored from N- to C-terminus. PDB: 1E0N.

The unique- (or variable) domains show the lowest homology among protein kinases and their function is not clearly identified. SH-domain stands for Src-homology-

domain, showing very high homology among different kinases. The SH2-domain is found in many proteins involved in signal transduction (Russel et al., 1992). It contains two α-helices and 7 β-strands and functions as a regulatory module of signaling pathways by binding to phosphotyrosine-containing target peptides in a strictly phosphorylation-dependent manner (Moran *et al.*, 1990). The SH3 domain forms a β-barrel consisting of five or six β-strands. It binds to proline-rich substrates and increases substrate specificity of some kinases by binding far away from the active centre (Shen *et al*., 1999). Additionally, SH-domains may play a role in intramolecular autoinhibition, as it is the case for Src kinase (see chapter 1.4.4). The kinase domain is highly conserved and consists of about 260 amino acids. The domain consists of the smaller kinase domain N-lobe and the bigger C-lobe. While the N-lobe is mainly comprised of β-sheets with one single conserved α-helix (the αC-helix, carrying important active site residues), the C-lobe is mostly made up by α-helices (**Figure 12**). The active site is located at the interface of both lobes.

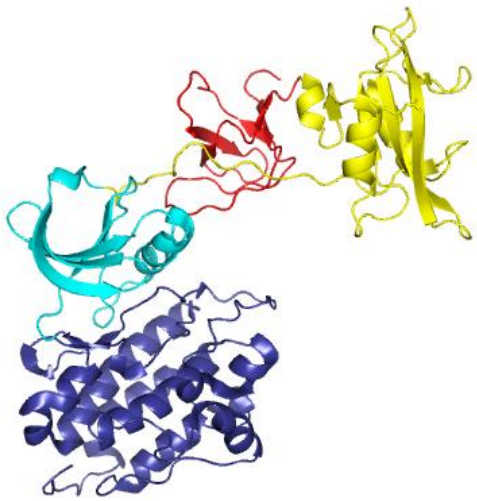

Figure 12

Structure of a protein kinase.

Representation of the secondary structure in cartoon view. The SH3-domain is colored in red, the SH2-domain in yellow and the kinase domain in blue (N-lobe, cyan and C-lobe, deep blue). PDB: 1Y57.

1.4.2. c-Src kinase

c-Src belongs to the family of non-receptor tyrosine kinases and is ubiquitiously expressed in all tissues, however differing in its expression levels (Brown & Cooper,

1996). It plays important roles in numerous signal transduction pathways ranging from cell proliferation to growth and survival. The kinase is anchored on the cytosolic side of the cell membrane via a myristoyl group on its N-terminus, which is required for its function in the cell (Courtneidge *et al.*, 1980, Kamps *et al.*, 1986). c-Src resides in its inactive state and is activated upon C-terminal dephosphorylation, and phosphorylation of the activation loop (see chapter 1.4.4). c-Src is the name-giving member of the group of Src-family kinases. This family consists of 12 kinases: the ubiquitiously expressed kinases c-Src, Fyn, Yrk and Yes and the kinases Blk, Fgr, Hck, Lck and Lyn, which are mainly expressed in hematopoietic cells as well as the kinase Srm, which is expressed in keratinocytes. Additionally, there is the group of Frk-related kinases that form a subgroup within the Src kinase family and are mainly expressed in epithelial cells and the Brk kinase, which is found in the intestine and the prostate. **Figure 13** shows the phylogenetic tree of the Src gene family.

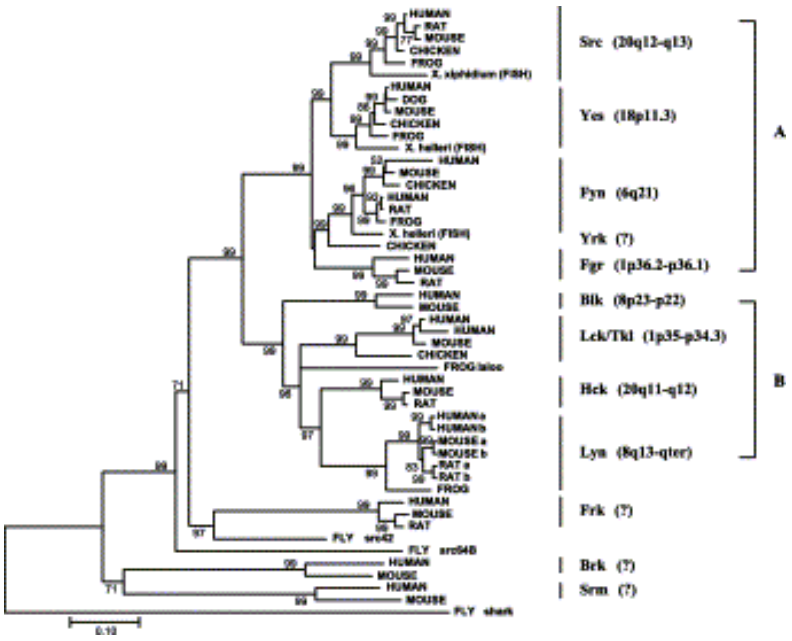

Figure 13

Phylogenetic structure of the Src gene family.

The Src family can be divided into two major distinct groups: group A including Src, Yes, Fyn, Fgr and Yrk; group B including Lyn, Hck, Lck and Blk. Kinases Frk, Brk and Srm are used as outgroups to root the NJ tree. Identified chromosomal locations of member genes are listed according to human genome map. Figure from Gu & Gu (2003).

1.4.3. Structure of Src

The Src protein consists of a unique domain containing a conserved glycine residue responsible for membrane interaction upon myristoylation. This domain is followed by the SH3- and SH2-domains, the SH2-domain-kinase linker and the kinase domain (**Figure 14**).

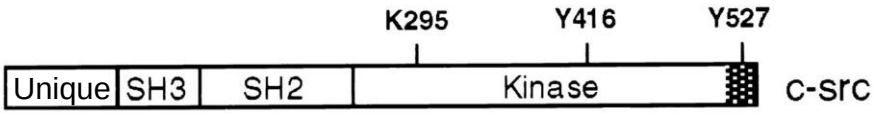

Figure 14

Domain organization of c-Src.

Domains are shown in their relative size. K295, active center; Y416, autophosphorylation site; Y527, inhibitory phosphorylation target site for CSK. Figure modified from Xu *et al*. (1999b).

The SH3-domain is responsible for binding substrate peptides. It recognizes proline-rich sequences, which form left-handed helices (Yu *et al.*, 1994). The substrates are divided into two classes: class I substrates possess a RPLPPLP-motif, while class II substrates carry a consensus sequence of ΦPPLPXR (Φ, hydrophobic amino acid; X, any residue) (Feng *et al.*, 1994). In the inactive conformation, the SH3-domain binds to the SH2-domain-kinase linker, which forms a left-handed helix, mimicking a class II substrate (**Figure 15**).

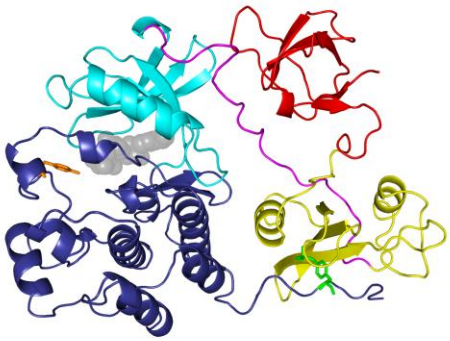

Figure 15

Crystal structure of c-Src in the inactive state.

Representation of the secondary structure in cartoon view. The SH3-domain is colored in red, the SH2-domain in yellow, the SH2-kinase-linker in magenta, the kinase domain in blue (N-lobe, cyan and C-lobe, deepblue), Tyr416 as orange sticks, pTyr527 as green sticks and AMP as grey spheres. PDB: 2SRC.

The SH2-domain binds to peptides, carrying a phospho-tyrosine in a specific manner (Moran *et al.*, 1990). Additionally, the SH2-domain is crucial for kinase regulation, since it binds intramolecularly to the phosphorylated pTyr527 in the inactive state of c-Src (Cooper *et al.*, 1986, Nada *et al.*, 1991, Okada & Nakagawa, 1988). Tyr527, which can be phosphorylated by the C-terminal Src kinase (CSK), is located in the C-terminal tail of the kinase domain and interaction with the SH2-domain leads to a compact kinase conformation, as it can be observed in the crystal structure of the inactive state (**Figure 15**).

In addition to Tyr527, the kinase domain carries another phosphorylation site at Tyr416, located within the activation loop (A-loop). Upon autophosphorylation at this site, the kinase activity is increased (Smart *et al.*, 1981).

The catalytically active kinase domain is comprised of the N- and the C-lobe with the active site located at their interface. Relative movement of the two lobes enables the kinase to adopt an open and a closed conformation. The starting and the endpoint of this activation process are shown in **Figure 16**.

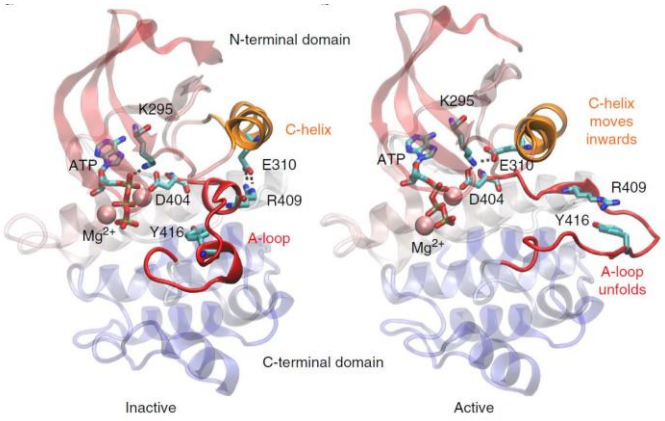

Figure 16

Crystal structures of c-Src in the inactive and active states.

The inactive and active crystal structures show structural changes in the activation loop (A-loop; red) and C-helix (orange). The kinase N-lobe is shown red and C-lobe in blue (both transparent). Figure taken from Shukla *et al*. (2014).

While in the open conformation ATP can be bound and/or ADP released, the closed form is necessary for the active center to conformationally coordinate the substrates and to adopt a catalytically competent state. Asp386 brings the substrate tyrosine residue in place, the αC-helix moves inwards and the activation loop (A-loop) outwards the active centre. The α- and β-phosphate of ATP is complexed by Lys295,

which in turn forms a salt bridge with Glu310 in the active state (Huse & Kuriyan, 2002). All these residues are crucial for enzymatic activity of Src kinase.

1.4.4. Activation of Src kinase

Due to its involvement in fundamental cellular processes c-Src is only transiently activated and is subjected to a strict cellular control. The compact, inactive conformation is mediated by the interaction between SH2-domain and pTyr527 as well as the binding of the SH3-domain to the SH2-domain-kinase-linker (**Figure 15**). Consequently, potential substrate binding sites on the SH2- and SH3-domains are blocked and the αC-helix comprising the active center is tilted, leading to a conformation incompatible with the Lys295-Glu310-salt bridge formation and thus, with enzymatic activity (Huse & Kuriyan, 2002). In addtion, the A-loop forms a α-helix, thereby sterically blocking the active center (Xu *et al.*, 1999a).

All these intramolecular interactions are characterized by low affinities. Therefore, substrate proteins are able to displace the pTyr527 and the linker from the SH2- and SH3-domains. Elimination of the SH2-pTyr527-interaction (“unlatching”) leads to a conformational change in the kinase domain, activating the enzyme in a process called “unclamping” (**Figure 17**, Xu *et al.*, 1999a).

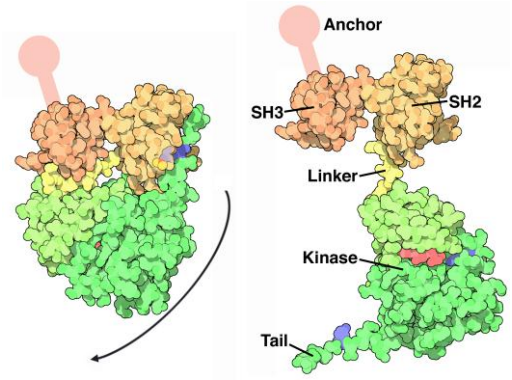

Figure 17

Conformational changes upon activation of c-Src.

Upon unlatching and unclamping, the kinase opens up leading to its active conformation and pTyr527 can be dephosphorylated. Tyr527 is shown in blue and ATP in red. Figure modified from the pdb website, www.rcsb.org/pdb, (left, PDB: 2SRC; right, PDB: 1Y57).

In this conformation, the released C-terminal pTyr527 can be dephosphorylated, the αC-helix is tilted inwards the active center, forming the Lys295-Glu310-salt bridge and the A-loop becomes unstructured (Brown & Cooper, 1996, Cowan-Jacob *et al.*,

2005). In a step called “switching” Tyr416 located in the A-loop is phosphorylated by another Src molecule, made possible by the fact that in the “unclamped” conformation, the A-loop is no longer buried in the active center. Phosphorylation at this site prevents the loop to re-interact with its former binding site and stabilizes the active state (Roskoski, 2004, Xu *et al.*, 1999a). The whole process is summarized in **Figure 18**.

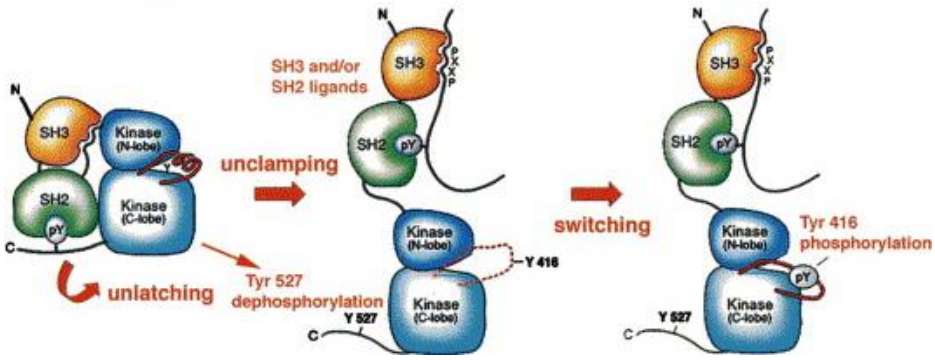

Figure 18

Model of Src activation.

After “unlatching” (release of the pTyr527::SH2-domain interaction), ligand binding to the SH2- and SH3-domains leads to “unclamping” (release of the SH3-domain::SH2-kinase-linker interaction). “Switching” is achieved by phosphorylation of the now accessible Tyr416 within the A-loop, thereby stabilizing the active state. Figure from Roskoski (2004).

1.4.5. Src signal transduction and the development of cancer

The embedment of Src in the signal transduction network of the cell and its role in the development of cancer are strictly connected. Deregulation of kinase activity is the main reason for c-Src to be involved in cancer emergence and progression, most frequently leading to hyper-phosphorylation of Src substrates (Frame, 2002). There exist many different ways to cause increased c-Src activity (Sen & Johnson, 2011). Point mutations affecting the intramolecular regulation of Src are described. This can lead to direct increase of kinase activity and is discussed in chapter 1.4.6.

For colon cancer a deletion of the C-terminal tail of c-Src carrying Tyr527 has been reported (Irby *et al.*, 1999). Since Tyr527 is phosphorylated by CSK, also altered CSK expression and activity would strongly influence Src activity. This is the case for numerous liver cell carcinoma in which CSK expression is reduced, leading to increased Src activity (Masaki *et al.*, 1999). Another way of activating Src via its Tyr527 is dephosphorylation of this site by phosphatases. Indeed elevated

expression of protein-tyrosine-phosphatase B1 (PTPB1) has been observed in breast cancer (Bjorge *et al.*, 2000). Two additional regulatory elements in the Src protein are the two SH-domains. External factors like phosphorylated focal adhesion kinase (FAK) are able to compete with their inhibiting intramolecular binding sites (Schaller *et al.*, 1994). Altered expression of FAK has been observed in a variety of cancers, indicating a close cooperation with Src to initiate invasion (Jones *et al.*, 2000). In addition to that, altered expression and/or stability of Src greatly influence its steady-state activity, as for example in the case of different dermal cancer types (Lee *et al*., 2010). Src itself regulates the proteasome system via phosphorylation of the E3-Ubiquitin-Ligase c-Cbl (Odai *et al.*, 1995, Tanaka *et al.*, 1996). This in turn may negatively affect its own degradation, suggested by the fact that hyper-phosphorylated c-Cbl has frequently been found in tumors (Kamei *et al.*, 2000).

How does increased Src activity influence the cell phenotype? c-Src interacts with and transmits the signal of different receptor tyrosine kinases (RTK), such as epidermal growth factor receptor (EGFR) and platelet derived growth factor receptor (PDGFR), that are responsive to growth hormones (**Figure 19**, Broome & Hunter, 1996, Twamley-Stein *et al.*, 1993)

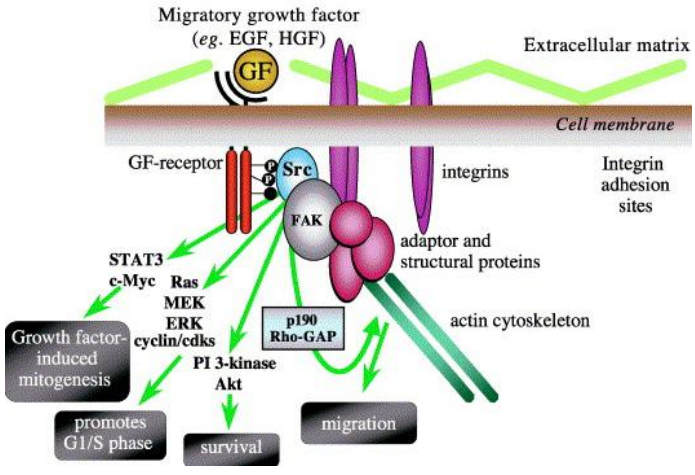

Figure 19

Important signal transduction pathways involving Src kinase.

Figure from Frame (2002).

This way, c-Src is responsible for their mitogenic activity in the cell and independent Src activity would lead to cell growth in the absence of extracellular, activating stimuli. Furthermore, Src regulates the cell cycle via Integrin-dependent

phosphorylation of FAK, leading to Grb2-interaction and thus, coupling Src to the Ras- and MEK/ERK- pathway (Schlaepfer & Hunter, 1996). Additionally, mutated Src is able to rescue the cell from apoptosis via the activation of the Phosphoinositid-3-kinase (PI3)/Akt-kinase-pathway (Johnson *et al.*, 2000). Moreover, Src interferes with actin organisation and cell adhesion by phosphorylation of adhesion protein p190Rho-GTPase-activating protein (p190RhoGAP), thereby leading to a round cell shape and potentially to the detachment of the cell from its tissue of origin (Ellis *et al.*, 1990, Fincham *et al.*, 1995). This represents the first step in the development of metastasis.

1.4.6. c-Src's oncogenic twin v-Src

c-Src was the first proto-oncogene identified (Stehelin *et al.*, 1976). Interestingly, c-Src kinase has a homologue that derives from a virus and was the first oncogene discovered: viral Src kinase (v-Src) (Stehelin, 1976, Stehelin *et al.*, 1976).

During the development of the Rous-Sarcoma virus, the c-Src gene most probably was incorporated into the viral genome (Roussel *et al.*, 1979). Due to strongly increased rates of mutation and much less evolutionary pressure within the viral carrier, the c-Src gene evolved towards its present oncogenic form, providing the virus another level of reproduction by causing sarcoma in its host. Like mutant c-Src, the creation of cancer by v-Src is due to its constitutive activity. Since v-Src carries activating point mutations and lacks the regulatory C-terminus including Tyr527, it is expected that it mimics the active c-Src conformation (Takeya & Hanefusa, 1983). A number of point mutations have been found to increase the activity of v-Src compared to c-Src and they are also present in oncogenic forms of c-Src in cancer cells (Miyazaki *et al.*, 1999, Kato *et al.*, 1986, Levy *et al.*, 1986) (**Figure 20**).

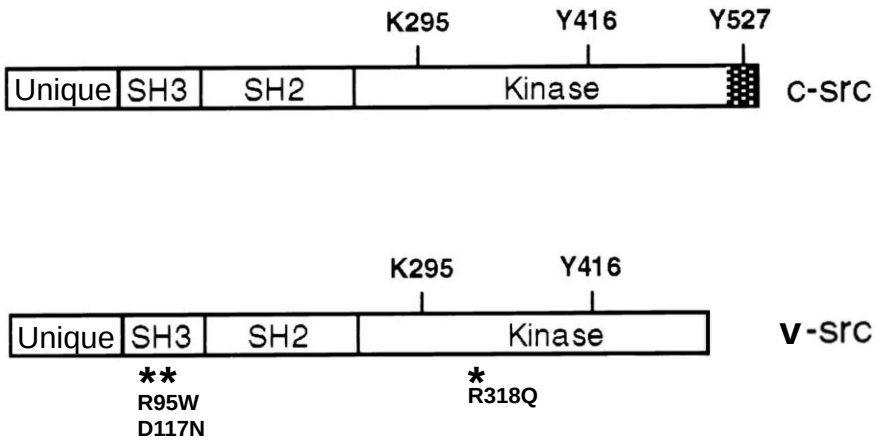

Figure 20

Comparison of c-Src and v-Src in a linear representation.

The regulatory C-terminal tail of c-Src is missing in v-Src. Additionally, several point mutations are thought to inhibit intramolecular domain interactions. Three of them showing the strongest chemical differences are marked here. Modified from Xu *et al*., 1999b.

It is thought that some of these mutations interfere with inactivating intramolecular interactions as key binding residues between SH3-domain and SH2-kinase-linker are disrupted. This is the case for the Arg95Trp and the Asp117Asn mutation (Miyazaki *et al.*, 1999). In addition, Arg318 seems to play an important role as it interacts with Asp117 in c-Src thereby mediating the SH3-domain::kinase-domain interaction in the inactive conformation (Williams *et al.*, 1997) and is involved in coordination of the active site αC-helix with Trp260 in the active conformation (Xu *et al.*, 1999a).

Correlating with increasing activity, the two kinases exhibit a strikingly different behaviour concerning their Hsp90-dependence (Xu *et al.*, 1993). The oncogenic v-Src was shown to be strictly dependent on the chaperone, whereas c-Src only transiently interacts with Hsp90 during its initial maturation (Xu *et al.*, 1999b). A recent quantification of Hsp90-client interactions revealed that v-Src is one of the strongest client kinases, whereas c-Src is one of the weakest (Taipale *et al.*, 2012). All this is even more fascinating given the fact that both genes possess 98 % sequence homology (**Figure 21**).

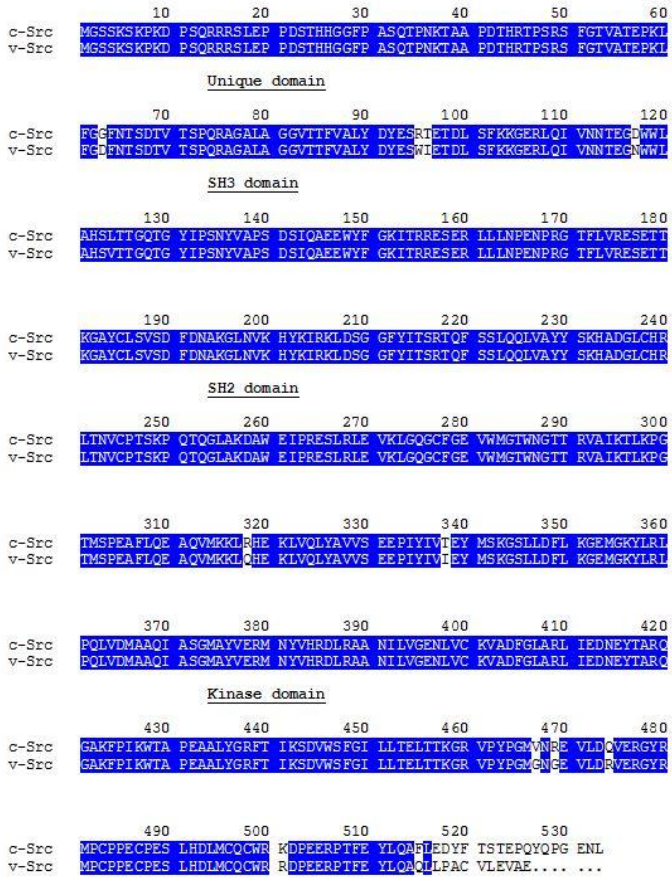

Figure 21

Sequence alignment of c-Src and v-Src.

The two kinases show 98 % sequence homology. Besides the shortened C-terminus, v-Src possesses a few point mutations in the SH3- and in the kinase domain.

First studies on this kinase pair revealed a lower stability of v-Src compared to c-Src (Falsone *et al.*, 2004). However, the role of Hsp90 in maintaining high kinase activity of v-Src and thereby facilitating its oncogenic performance in the cell remains enigmatic.

1.5. Kinases and molecular chaperones

Yeast two hybrid screens revealed that the N-lobe of a kinase is responsible for Cdc37 interaction, shown for the kinases Cdk4 (Lamphere *et al.*, 1997), Cdk1 (Cdc28) (Mort-Bontemps-Soret *et al.*, 2002) and Lck, a Src family kinase (Prince & Matts, 2004). In the latter study the primary binding region of Cdc37 to the kinase could be located to the αC-helix and part of its adjacent loop connecting the β4-strand. Additional truncation and mutational studies showed that the glycine-rich P-

loop, the αC-helix, the adjacent loop as well as β4- and β5-sheets, all located in the N-lobe of the kinase domain, are potential binding sites for Cdc37 (Prince & Matts, 2004, Prince *et al*., 2005, Citri *et al*., 2006). N-lobe binding is further supported by deletion studies for the kinases v-src (Brugge *et al.*, 1987), Fes (Nair *et al.*, 1996) and v-Raf (Silverstein *et al.*, 1998). Hsp90, also binding to the N-lobe, may additionally include regions in the kinase C-lobe, including the αE-helix (Miyata *et al*., 2001). All these findings are summarized in **Figure 22**.

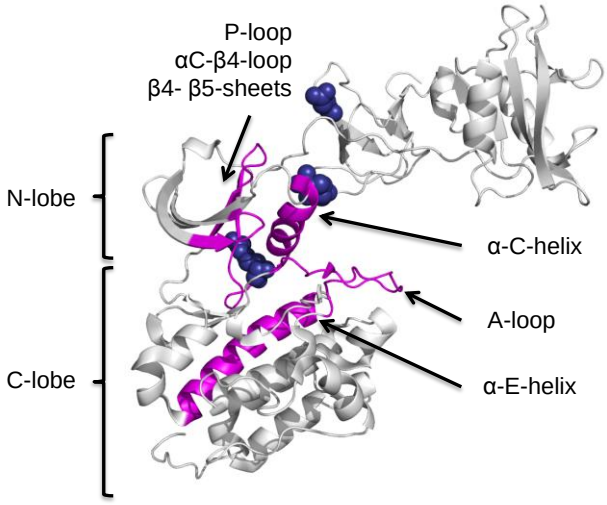

Figure 22

Summary of proposed chaperone binding sites in kinases.

Regions important for chaperone binding on kinases (magenta) have been plotted onto the crystal structure of active c-Src (white, PDB: 1Y57). The three amino acid positions in c-Src important for interdomain interaction R95, D117 and R318 are shown as blue spheres.

It has been proposed that chaperones would recognize a specific motif within the αC-β4-loop (Xu *et al.*, 2005). However, there are numerous examples of kinases carrying this motif, which are not Hsp90-dependent (Citri *et al*., 2006). It has also been shown that mutations lying outside the proposed chaperone binding sites can have great influence on the chaperone-kinase interaction (Shimamura *et al*., 2005, Grbovic *et al*., 2006). Additionally kinase activity does not seem to be the chaperone-dependence-determining factor, as kinase mutants with lower activity showed increased chaperone interaction (da Rocha Dias *et al.*, 2005). Notably, Hsp90 recognizes distinct motifs within the immature and mature fold of the same kinase (Xu *et al.*, 2005). Given the high similarities between chaperone-dependent and -independent kinases, the idea has been raised that intrinsically instable kinases

would frequently expose Hsp90 binding sites, whereas stable kinases only do so during initial folding and therefore only transiently interact with chaperones during maturation (Falsone *et al*., 2004, Caplan *et al*., 2007).

In 2006, the first and to date the only structure of Hsp90 in complex with Cdc37 and a kinase (Cdk4) could be solved by electron microscopy (EM) (Vaughan *et al.*, 2006). The structure clearly shows Hsp90 being present in a half-open conformation with a density in the region of the previously determined Cdc37-binding region (green) and additional density on one of the Hsp90-monomers (red) (**Figure 23**). Obviously, this study represents a significant advance in understanding the interaction of kinases with Cdc37 and Hsp90. Unfortunately however, the kinase binding domain of Cdc37 was not visible in the low-resolution complex. Furthermore, for other structural studies, a Cdc37 construct lacking the N-terminal part was used (Roe *et al.*, 2004, Zhang et al, 2004, Sreeramulu *et al.*, 2009). Hence, the structure of the Cdc37-kinase interaction site still remains enigmatic.

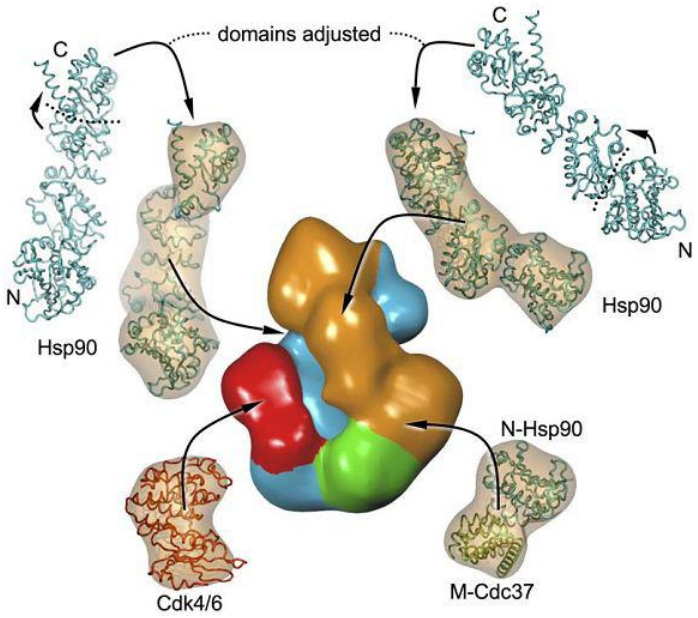

Figure 23

Electron microscopy (EM) structure of the Hsp90-Cdc37-Cdk4 complex.

In this model, the N-terminal kinase lobe interacts with Hsp90 middle domain and the C-terminal lobe is suggested to interact with either N-terminal domain of Hsp90 or Cdc37 or both. Hsp90 open monomer in orange, Hsp90 closed monomer in blue, Cdk4 in red and Cdc37 in green. Figure taken from Vaughan *et al.* (2006).

Using eIF2α as a model kinase, certain residues have been identified to play an important role in the function of Cdc37, such as Val2, Asp3, Tyr4, Trp7 and Ser13, all located within the N-terminal domain and with Ser13 as the phosphorylation site for CK2 (Shao *et al.*, 2003). But still the question remains how these residues contribute to kinase recognition. Change of the residues in the region between Trp31 and Lys60 (Trp31, Arg52, Gly53, Cys57 and Lys60) lead to gain of function variants of Cdc37 that increased cyclic AMP-dependent protein kinase (PKA) activity *in vivo* and *in vitro* and showed a higher affinity for Ste11 protein kinase (Ren *et al.*, 2007). Hence, the authors suggested that with these mutations an intramolecular autoinhibitory sequence had beed disrupted (Ren *et al.*, 2007).

Binding to Cdc37 is highly specific, and otherwise closely related protein kinases may differ substantially in their interaction. Cdk4 associates with Cdc37, whereas Cdk2 does not (Stepanova *et al.*, 1996, Dai *et al.*, 1996). Similarly, the mitogen-activated protein (MAP)-kinase MOK binds Cdc37, while extracellular-signal regulated kinase (ERK), c-Jun N-terminal kinase (JNK), and p38 do not (Miyata *et al.*, 2001).

1.6. Project objectives

1.6.1. Integration of the kinase-specific cochaperone Cdc37 into the human Hsp90 reaction cycle

Being responsible for the maturation of hundreds of kinases in the cell, which are involved in numerous signal transduction pathways controlling cell homeostasis and development, the chaperoning tandem of Cdc37 and Hsp90 has long been in the focus of research (Prodromou & Pearl, 2003, MacLean & Picard, 2003, Pearl, 2005). Surprisingly, the analysis of components from various model organisms revealed remarkable differences between the systems: the *S. cerevisiae* Cdc37 binds Hsp90 only with a K_D of ~ 100 µM (Siligardi *et al*., 2002), but has been shown to physically interact with kinases in cooperation with Hsp90 (Mandal *et al.*, 2011), thereby suggesting an adapting role of the kinase client. Recent studies showed that the chaperones of the nematode *C. elegans* exhibit a K_D for complex formation in the range of the human proteins (~ 4.0 µM), but in contrast to human Cdc37, the nematode cochaperone primarily interacts with the M-domain and not with the N-domain of Hsp90 (Eckl *et al.*, 2013). Furthermore, in contrast to human Cdc37, CeCdc37 is not expelled from a closed Hsp90 dimer induced by the nucleotide

analogues ATPγS and AMP-PNP (Gaiser *et al.*, 2010). Hence, it is obvious that kinase chaperoning has changed during evolution.

In this study, for the human cochaperone Cdc37 the stage of entry and exit of Cdc37 in the Hsp90 reaction cycle should be determined. With regard to the pharmaceutical relevance, the importance of investigating the human kinase chaperoning system is apparent. However, whenever the use of established platforms based on yeast Hsp90 was necessary, this option was not abandoned.

1.6.2. What makes a client a client: Conformational processing of v-Src kinase by Hsp90

It has previously been shown that v-Src directly interacts with Hsp90, while Hsp90 only weakly binds to c-Src (Xu *et al.*, 1993) after initial maturation. The comparison of the interaction of proteins, nearly identical in sequence but very different in their chaperone dependence, could help to understand the features that govern the recognition of client proteins by the Hsp90 machinery. Likewise, Cdc37 interacts with immature forms of Hsp90-dependent kinases and seems to be essential for their Hsp90-mediated activation (Stepanova *et al.*, 1996). Thus, Cdc37 may mediate the binding between Hsp90 and client kinases (Pearl, 2005).

c-Src and v-Src kinases will be prurified from *S. frugiperda* (*Sf*9) cells and the influence of Hsp90, Cdc37 and other (co-)chaperones on Src kinase activity will be determined *in vitro* by a radioactive transphosphorylation assay. The goal is to reconstitute chaperone-dependent maturation of v-Src kinase *in vitro* and to dissect the mechanism by which Hsp90 together with Cdc37 functions on kinases.

The functional differences between the closely related viral and cellular Src kinases make them ideal candidates for studying the substrate specificity of the human Hsp90 chaperone system. For this, chimera between c-Src and v-Src are used to pinpoint the elements that drive Hsp90-dependence in kinases. The effects of the different kinase variants will be investigated *in vivo* using *S. cerevisiae* as a model organism and *in vitro* using the above mentioned reconstitution assay. To elucidate the properties, causing the dependence on the chaperone, Hsp90-dependent and –independent Src variants will be compared by numerous biophysical methods, including circular dichroism spectroscopy, fluorescence spectroscopy, aggregation analysis and *in vitro* activity and enzyme kinetics. In addition, H/D

exchange–mass spectrometry and molecular dynamics simulations will provide further structural insights.

The results of this work will significantly contribute to the understanding of the chaperone cycle of Hsp90 and its interaction with kinases.

2. Experimental Procedures

2.1. Material

2.1.1. Chemicals

Acetic Acid	Roth, Karlsruhe, Germany
Acrylamide solution (38% with 2% bisacrylamide)	Roth, Karlsruhe, Germany
Adenosyl-imidodiphosphate (AMP-PNP)	Roche, Mannheim, Germany
Adenosin-5´-diphosphate (ADP), disodium salt	Roche, Mannheim, Germany
Adenosin-5´-triphosphate (ATP), disodium salt	Roche, Mannheim, Germany
Adenosine 5'-O-(3-thio)triphosphate (ATPγS)	Roche, Mannheim, Germany
Agar Agar	Roth, Karlsruhe, Germany
Agarose, ultra-pure	Roth, Karlsruhe, Germany
Alexa Fluor® 488 maleimide	Invitrogen, Carlsbad, USA
1-Anilino-8-Naphthalene Sulfonate (ANS)	Sigma, St. Louis, USA
Ammoniumperoxodisulfate (APS)	Roche, Mannheim, Germany
Ampicillin	Roth, Karlsruhe, Germany
Atto 550 maleimide	Sigma, St. Louis, USA
Bacto Peptone	Difco, Detroit, USA
Bacto Tryptone	Difco, Detroit, USA
Bromphenol blue S	Serva, Heidelberg, Germany
Cellfectin	Invitrogen, Carlsbad, USA
Chloramphenicol	Roth, Karlsruhe, Germany
Coomassie Brilliant Blue G-250	Serva, Heidelberg, Germany
Coomassie Protein Assay Reagent	Pierce, Rockford, USA
Desoxyribonucelotidtriphosphates (dNTP’s)	Roche, Mannheim, Germany
Dimethylsulfoxide (DMSO)	Sigma, St. Louis, USA
Dithiothreitol	Roth, Karlsruhe, Germany
EDTA	Merck, Darmstadt, Germany
Ethanol, p.a.	Roth, Karlsruhe, Germany
Ethidiumbromide	Sigma, St. Louis, USA
Galactose	Merck, Darmstadt, Germany
Gentamycine	Invitrogen, Carlsbad, USA
Glucose	Merck, Darmstadt, Germany
Glycerine, 99%	ICN, Irvine, USA

Guanidinium hydrochloride, p.a.	ICN, Irvine, USA
Imidazole	Sigma, St. Louis, USA
Isopropyl β-D-1-thiogalactopyranoside (IPTG)	Merck, Darmstadt, Germany
Kanamycin	Roth, Karlsruhe, Germany
2-Mercaptoethanol, pure	Sigma, St. Louis, USA
Milk powder	Roth, Karlsruhe, Germany
N-(2-Hydroxyethyl)-piperazine-N'-2-ethansulfonic acid (Hepes)	ICN, Irvine, USA
N,N,N',N'-Tetramethylethylendiamin (TEMED)	Roth, Karlsruhe, Germany
Polyoxyethylen-sorbitan-monolaureat (Tween-20)	Merck, Darmstadt, Germany
Ponceau S	Sigma, St. Louis, USA
Protease inhibitor mix FY	Serva, Heidelberg, Germany
Protease inhibitor mix G	Serva, Heidelberg, Germany
Protease inhibitor mix HP	Serva, Heidelberg, Germany
Protease inhibitor cocktail for His-tagged proteins	Sigma, St. Louis, USA
[γ-^{32}P]-ATP	Hartmann Analytik, Braunschweig, Germany
Radicicol	Sigma, St. Louis, USA
Raffinose	Merck, Darmstadt, Germany
Salmon Sperm carrier DNA	Sigma, St. Louis, USA
Sodiumdodecylsulfate (SDS)	Roth, Karlsruhe, Germany
Streptomycine	Roth, Karlsruhe, Germany
Trehalose	(Sigma, St. Louis, USA
Tris-(hydroxymethyl)-aminomethan (Tris)	ICN, Irvine, USA
Tetracyclin	Roth, Karlsruhe, Germany
Trypan-blue	Sigma, St. Louis, USA
X-Gal	Roth, Karlsruhe, Germany
Xylencyanol	Merck, Darmstadt, Germany
Yeast extract	Merck, Darmstadt, Germany
Yeast nitrogen base	Difco, Detroit, USA

All other chemicals were purchased from the company Merck (Darmstadt, Germany) and were of grade pro analysis (p.a.) if not stated otherwise. For the preparation of buffers Millipore-filtered water (Millipore, Bedford, USA) was used.

2.1.2. Size markers and kits

1 kb DNA ladder molecular weight standard	Peqlab, Erlangen, Germany
Calibration proteins for HPLC	Serva, Heidelberg, Germany
ECL+plus Western Blotting Detection System	GE Healthcare, Freiburg, Germany
High Pure PCR Product Purification Kit	Promega, Madison, USA
High-Range-molecular weight marker (HMW for SDS-PAGE)	BioRad, München, Germany
Low-Range-molecular weight marker (LMW for SDS-PAGE)	BioRad, München, Germany
Rainbow marker for SDS-PAGE	GE Healthcare, Freiburg, Germany
Wizard® Plus SV Mini-Preps DNA purification kit	Promega, Madison, USA
Wizard® SV Gel and PCR Clean-Up System	Promega, Madison, USA

2.1.3. Proteins and antibodies

Alkaline phosphatase	Roche, Mannheim, Germany
Monoclonal IgG-POD conjugate against rabbit-IgG (goat)	Sigma, St. Louis, USA
Monoclonal IgG-POD conjugate against mouse-IgG (rabbit)	Sigma, St. Louis, USA
Anti-phosphotyrosine-IgG 4G10 (mouse)	Millipore, Bedford, USA
Anti-avian Src-IgG EC10 (mouse)	Millipore, Bedford, USA
Dnase I	Roche, Mannheim, Germany
Enolase (rabbit)	Sigma, St. Louis, USA
Expand High Fidelity PCR System	Roche, Mannheim, Germany
Phusion-DNA polymerase	New Englad Biolabs, Beverly, USA
rAPid alcalic phosphatase	Roche, Mannheim, Germany
Restriction enzymes	New Englad Biolabs, Beverly, USA
T4-DNA-Ligase	Promega, Madison, USA

2.1.4. Chromatographic material

HisTALON™ Superflow Cartridges	Clontech Laboratories, Mountain View, USA
His-Trap™ FF (5 ml)	GE Healthcare, Freiburg, Germany
Resource-S	GE Healthcare, Freiburg, Germany
Resource-Q	GE Healthcare, Freiburg, Germany
HiLoad™ SuperdexTM 75 pg (16/60 and 26/60)	GE Healthcare, Freiburg, Germany
HiLoad™ Superdex™ 200 pg (16/60 and 26/60)	GE Healthcare, Freiburg, Germany

2.1.5. Cell culture material

Binocular DM IL HC	Leica, Solms, Germany
Cryo 1 °C freezing container	Thermo Fischer, Roskilde, Denmark
Serological pipettes (1 ml, 2ml, 5 ml, 10 ml, 25 ml)	Sarstedt, Nürnbrecht, Germany
Sterile bank HERASafe	Heraeus, Hanau, Germany
Cooling incubator KB 115	Binder, Tuttlingen, Germany
Microscope Axiolab	Zeiss, Jena, Germany
Cell culture tissue flask (mono layer cultures; 25 cm^2, 75 cm^2)	Sarstedt, Nürnbrecht, Germany
Cell scraper	Sarstedt, Nürnbrecht, Germany
6-well tissue plates	Sarstedt, Nürnbrecht, Germany

2.1.6. Miscellaneous material

Centricon 3, Centricon 10, Centricon 30	Amicon, Witten, Germany
Dialysis bags Spectra/Pore 6000-8000 Da	Spectrum, Houston, USA
Disposable cuvettes, 1,5 ml, halfmicro	Zefa, München, Germany
Filter paper	Whatman, Maidstone, UK
Immobilon-NC (Nitrocellulose) membrane	Millipore, Bedford, USA
Immobilon-P (PVDF) membrane	Millipore, Bedford, USA
Millipore Ultra device	Millipore, Bedford, USA
PD-10 desalting columns	GE Healthcare, Freiburg, Germany
PE tubes (50/15 ml)	Greiner & Söhne, Nürtingen, Germany
pH-indicator strips	Roth, Karlsruhe, Germany
Phosphor screen	GE Healthcare, Freiburg, Germany
Phosphor screen cassette	GE Healthcare, Freiburg, Germany
Silica glass Suprasil cuvettes	Hellma, Jena, Germany
Sterile filters 0,2 µm	Zefa, München, Germany
Ultrafiltration membranes YM3, YM10, YM30	Millipore, Bedford, USA
X-ray films X-OMAT AR	Eastman Kodak, Rochester, USA

All other materials were purchased from VWR (Darmstadt, Germany).

2.1.7. Equipment

Balances

Analysis balance BP 121 S	Sartorius, Göttingen, Germany
Halfmicro balance BL 310	Sartorius, Göttingen, Germany

Centrifuges

Avanti J 25 with JA-10 and JA-25.50 rotors	Beckman, Wien, Austria
Beckman XL-I analytical ultracentrifuge	Beckman, Wien, Austria
Eppendorf table-top centrifuge 5415 C	Eppendorf, Hamburg, Germany
Rotina 46 R coolable centrifuge	Hettich, Tuttlingen, Germany
Universal 32 R coolable centrifuge	Hettich, Tuttlingen, Germany

Chromatographic machines

Äkta FPLC machine	GE Healthcare, Freiburg, Germany
FP-1520 fluorescence detector	Jasco, Groß-Umstadt, Germany
GradiFrac system	GE Healthcare, Freiburg, Germany
HighLoad system	GE Healthcare, Freiburg, Germany
LG-980-02S gradient unit	Jasco, Groß-Umstadt, Germany
PU-1580 HPLC Pump	Jasco, Groß-Umstadt, Germany
Super loops (5ml, 10 ml, 150 ml)	GE Healthcare, Freiburg, Germany
UV-1575 UV-VIS detector	Jasco, Groß-Umstadt, Germany

Gelelectrophoresis and blotting devices

Fast Blot B44 apparatus	Biometra, Göttingen, Germany
Hoefer Mighty Small II gelelectrophoresis unit	GE Healthcare, Freiburg, Germany
RHU10X	Roth, Karlsruhe, Germany

Phosphoimager

Typhoon Phosphoimager	GE Healthcare, Freiburg, Germany

Spectrofluorimeter

FluoroMax-2 with tempering cuvette holder	Spex, Edison, USA
FluoroMax-3 with tempering cuvette holder	Spex, Edison, USA

Spectrophotometer

Biochrom 4060 UV-VIS Photometer	GE Healthcare, Freiburg, Germany
Cary 50 Bio UV-VIS-spectrophotometer	Varian, Palo Alto, USA
Cary 100 Bio UV-VIS-spectrophotometer	Varian, Palo Alto, USA
J-715 spectropolarimeter with PTC 343 peltier tempering unit	Jasco, Groß-Umstadt, Germany
Nanodrop	Peqlab, Erlangen, Germany
Novaspec II visible	GE Healthcare, Freiburg, Germany

Voltage sources

LKB-GPS 200/400	GE Healthcare, Freiburg, Germany
EPS 3500, 301 und 1001	GE Healthcare, Freiburg, Germany

Proton / Deuterium exchange – Mass Spectrometry equipment

Leap robot (HTS PAL)	Leap Technologies, Carrboro, USA
Immobilized pepsin column	Applied Biosystems, Poroszyme™, Foster City, USA
Synapt® G2-S mass spectrometer	Waters, Milford, USA
Waters ACQUITY UPLC®	Waters, Milford, USA
Waters UPLC® CSH™ C 18 column	Waters, Milford, USA

Further equipment

Air circulation incubator	New Brunswick Scientific, Nürtingen, Germany
Cell disruption machine Basic Z	Constant Systems, Warwick, UK
Culture shaker Certomat S	Braun Biotech, Melsungen, Germany
Digital thermometer with thermosensor	Keithley, Cleveland, USA

Eppendorf thermomixer	Eppendorf, Hamburg, Germany
Ice machine	Ziegra, Isernhagen, Germany
Magnetic stirrer Heidolph MR 2000	Heidolph, Kelheim, Germany
Metal thermo block TB 1	Biometra, Göttingen, Germany
pH-meter	WTW, Weilheim, Germany
Thermocycler Primus	MWG, Ebersberg, Germany
Test tube roller	Heidolph, Kelheim, Germany
Sonic cell disruption device Sonifier B-12	Branson, Danbury, USA
Sonic water bath Sonsorex RK 100H	Bandelin, Berlin, Germany
Varioklav steam autoclave EP-Z	H+P, Oberschleißheim, Germany
Water bath Haake F6-K	Haake, Karlsruhe, Germany

2.1.8. Computer software

Adobe Photoshop CS2	Adobe Inc., San Jose, USA
Adobe Illustrator CS2	Adobe Inc., San Jose, USA
Adobe Reader 8.0	Adobe Inc., San Jose, USA
Borwin	Jasco, Groß-Umstadt, Germany
Corel Photo Paint 8.0	Corel Corporation Ltd., Ontario, Canada
ClustalW sequence alignment (http://www.ebi.ac.uk/Tools/clustalw2/index.html)	Myers & Miller, 1998, Wilbur & Lipman, 1983
Dichroweb CD data deconvolution (http://www.dichroweb.cryst.bkk.ac.uk)	Lobley *et al*., 2002, Whitmore & Wallace, 2004, Whitmore & Wallace, 2008
ImageJ 1.42	National Institutes of Health, USA
ImageQuant	GE Healthcare, Freiburg, Germany
Microsoft Office 7.0	Microsoft, Unterschleißheim, Germany
ProtParamTool (http://expasy.hcuge.ch/)	ExPasy (Gasteiger *et al*., 2003)

ProtScale Tool (http://expasy.hcuge.ch/)	ExPasy
Pymol 0.99	Delano Scientific LLC, Schrödinger
SIM alignment (http://expasy.hcuge.ch/)	ExPasy
OligoCalculator 3.26	Northwestern University, Chicago
Origin 8.0	OriginLab Corp., Northampton, USA
Sedview	Hayes & Stafford, 2010
Molecular dynamics simulations	
CHARMM27 force field	MacKerell *et al*., 1998
NAMD	Phillips *et al*., 2005
Visual Molecular Dynamics	Humphrey *et al*., 1996
Proton / deuterium exchange – mass spectrometry	
HDX manager	Waters, Milford, USA (Zhang *et al*., 2014)
Waters Protein Lynx Global Server PLGS Vers. 2.5.3.	Waters, Milford, USA
DynamX Vers. 2.0	Waters, Milford, USA

2.2. Microorganisms and cultivation

2.2.1. Strains

The bacterial strains used in this work are specified in the following table.

Table 1 List of *E. coli* bacterial strains used in this work.

Strain	Geno-/Phenotype	Origin/Company
E. coli DH10B	F⁻*ara*D 139Δ(*ara leu*) 7697Δ*lac*X74 *gal*U *gal*K *mcr*A Δ(*mrr*⁻ *hsd*RMS- *mcr*BC) *rps*L *dec*R 380 Δ*lac*Z ΔM15 *end*A1 *nup*G *rec*A1	Berthesda Research Laboratories, Berthesda, USA

E. coli One-Shot® Mach1™	F-φ80(*lacZ*)ΔM15 Δ*lac*X74 *hsd*R(r_K^- m_K^-) Δ*rec*A1398 *end*A1 *ton*A	Invitrogen, Carlsbad, USA
E. coli XL1 Blue	Δ(*mcr*A) 183 Δ (*mcr*CB-hsdSMR-mrr) 173 *end*A1 supE44 thi-1 *rec*A1 *gyr*A96 *rel*A1 *lac*[F`*pro*AB $lacI^qZ\Delta M15$ $Tn10\ (Tet^r)$] Su^-	Stratagene, La Jolla, USA
E. coli BL21 (DE3) Codon Plus	F^- *omp*T *hsdSB* (rB^-mB^-) gal *endA* The [argU ileY leuW Cam^R	Stratagene, La Jolla, USA
E. coli DH10Bac™	F^-*ara*D 139Δ(*ara leu*) 7697Δ*lac*X74 *gal*U *gal*K *mcr*A Δ(*mrr*$^-$ *hsd*RMS- *mcr*BC) *rps*L *dec*R 380 Δ*lac*Z ΔM15 *end*A1 *nup*G *rec*A1 pMON14272/pMON7124	Invitrogen, Carlsbad, USA

E. coli DH10B and *E. coli One-Shot® Mach1™* were used for cloning and amplification of plasmids. *E. coli* BL21 (DE3) Codon Plus were used for gene epression in order to obtain recombinant protein. *E. coli* DH10Bac™ were used for the generation of Bacmid DNA for protein expression in *Sf*9 cells.

The yeast strains used in this work are specified in the following table.

Strain	Geno-/Phenotype	Origin/Company
ECU82α	A *can*1-100 *ade2*-1 *his*3-11, 15 *leu*2-3, 12 *trp*1-1 *ura*3-1 hsc82::LEU2 hsp82::LEU2 (pKAT6)	(Nathan & Lindquist, 1995)

2.2.2. Media and solutions

Media used for growth of E. coli

LB_0	20 g/l LB-powder
	For plates: 15 g/l Bacto-Agar
Double YT (2xYT)	16 g/l Bacto Trypton
	10 g/l yeast extract
	5 g/l NaCl

Antibiotic concentrations used for growth of E. coli

Ampicillin	100 mg/l
Kanamycin	35 mg/l
Chloramphenicol	50 mg/l

DH10Bac-Media Plates	10 g/l Bacto Trypton
	5 g/l yeast extract
	10 g/l NaCl
	pH 7.0 (NaOH)
	15 g/l Bacto-Agar

Addition at 50 °C:

	50 mg/l Kanamycin
	7 mg/l Gentanamycin
	10 mg/l Tetracyclin
	100 mg/l X-Gal
	40 mg/l IPTG

Storage at 4 °C, in the dark.

Solutions for Bacmid preparation

Bacmid-solution I	15 mM Tris-HCl (pH 8.0)
	10 mM EDTA
	100 mg/l RNase A

Sterile filtered. Storage at 4 °C.

Bacmid-solution II	0.2 M NaOH
	1 % SDS (w/v)

Media used for growth of yeast

YPD	5 g/l yeast extract
	10 g/l Bacto-Pepton
	20 g/l Glucose
	For plates: 20 g/l Bacto-Agar
CSM	6.7 g/l YNB
	1 g/l amino acid mix (for selection)
	20 g/l sugar source (glucose, raffinose or galactose)
	1 ml/l 1 M NaOH
	For plates: 20 g/l Bacto-Agar

Amino acid mix (for selection of yeast clones)

Adenine	0.5 g
Alanine	2.0 g
Arginine	2.0 g
Asparagine	2.0 g
Aspartic Acid	2.0 g
Cysteine	2.0 g
Glutamine	2.0 g
Glutamic Acid	2.0 g
Glycine	2.0 g
Histidine	2.0 g
Inositol	2.0 g
Isoleucine	2.0 g
Leucine	10.0 g
Lysine	2.0 g
Methionine	2.0 g
Phenylalanine	2.0 g
Proline	2.0 g
Serine	2.0 g
Threonine	2.0 g
Trypthophan	2.0 g
Uracil	2.0 g

Valine	2.0 g
For 5'-FOA-plates:	0.1 % (w/v) 5'-Fluororotic acid (at 50 °C)

Yeast transformation

PLATE Mixture	sterile 45 % PEG 4000	90 ml
	1 M Lithium acetate (Li OAc)	10 ml
	1 M Tris (pH 7.5)	1 ml
	0.5 M EDTA	0.2 ml

2.2.3. Growth and storage of *E. coli*

Streaked cultures of *E. coli* on agar plates were incubated at 37 °C for 16 hours and kept at 4 °C in the fridge for short-time storage. Growth of *E. coli* liquid cultures in LB_0-media was performed upon addition of the according antibiotic in order to select for the respective plasmid. Small volumes were inoculated with a single colony from the plate, larger volumes with an overnight culture. Volumes up to 5 ml were incubated in a test tube roller, volumes larger than 5 ml were incubated in a culture shaker. Growth of *E. coli* was monitored photometrically at a wavelength of 600 nm. An OD_{600} ~ 1 roughly represents 8 x 10^8 cells/ml. For long-term storage of bacterial strains, 700 µl of an exponentially growing culture were mixed with 300 µl of 50% sterile glycerole, shock-frozen in liquid nitrogen and stored at -80 °C.

2.2.4. Growth and storage of *S. cerevisiae*

Streaked cultures of *S. cerevisiae* were incubated on YPD or CSM-plates for 2-3 days at 30°C. Small volumes of liquid cultures, inoculated from a single colony, were incubated in a test tube roller. Bigger volumes, inoculated from stationary overnight cultures, were grown in a culture shaker at 30°C. Growth of the yeast cells was monitored photometrically at a wavelength of 600 nm. An OD_{600} ~ 1 roughly represents 2 x 10^7 cells/ml. For long-term storage of yeast strains, 700 µl of an exponentially growing culture were mixed with 300 µl of 50% sterile glycerole, shock-frozen in liquid nitrogen and stored at -80 °C.

2.3. Working techniques in molecular biology

2.3.1. Plasmids

Table 2 Used and created plasmids during this work.

Insert	Plasmid	Reference/Origin
c-Src (chicken)	pFastBacHTA	L. Reefschläger
c-SrcΔC	pFastBacHTA	L. Reefschläger
c-Src3M	pFastBacHTA	L. Reefschläger
c-Src3MΔC	pFastBacHTA	L. Reefschläger
v-Src (Schmidt-Ruppin strain D)	pFastBacHTA	L. Reefschläger
c-Src	pY413	created in this work
c-SrcΔC	pY413	created in this work
c-Src3M	pY413	created in this work
c-Src3MΔC	pY413	created in this work
v-Src	pY413	created in this work
c-SrcK295R	pFastBacHTA	created in this work
v-SrcK295R	pFastBacHTA	created in this work
v-SrcY416F	pFastBacHTA	created in this work
Hsp90α (human)	pET28b	K. Richter
Hsp90β (human)	pET28b	K. Richter
Cdc37 (human)	pQE30	M. Pandya
Cdc37-S13E (human)	pQE30	M. Pandya
Cdc37-S13E- M164R-L205R (human)	pQE30	created in this work
Hop (human)	pET28	K. Richter
Aha1 (human)	pET28b	K. Richter
Hdj-1 (human)	pET21d	Freeman *et al*., 1995
Hsp70 (human)	n/a	Abravaya *et al*., 1992

2.3.2. Molecular biological solutions

TAE (50 x):	Tris/Acetate pH 8.0	2 M
	EDTA pH 8.0	50 mM
Gel loading buffer (10 x):	Glycerin	50 % (v/v)
	EDTA pH 8.0	10 mM
	Bromphenole blue	0.2 % (w/v)
	Xylencyanole	0.2 % (w/v)
1 % Agarose solution:	Agarose	1 g
	TAE (1 x)	100 ml
	Ethidiumbromide solution	1 µl
dNTP-Mix:	dATP	10 mM
	dGTP	10 mM
	dCTP	10 mM
	dTTP	10 mM

For the growth of microorganisms and for molecular biological work sterile hollow-ware and solutions were used all the time. If not stated otherwise, work was performed at room temperature.

2.3.3. Preparation of plasmid DNA from E. Coli

Plasmid DNA for analytical and preperative purposes was preparated and purified from 5 ml overnight cultures with the Wizard® Plus SV Mini-Prep kit according to the protocol of the manufacturer (Promega, Madison, USA).

2.3.4. Separation of DNA by agarose gel electrophoresis

For the analytical and preparative separation of DNA 1 % (w/v) agarose gels containing 0.4 µg/ml ethidium bromide were used. Electrophoresis was carried out in 1 x TAE running buffer with a constant voltage of 120 V. After running for 50 min,

DNA was detected with a Bio Doc II system. 1 kb DNA-ladder (Peqlab, Erlangen, Germany) was used as molecular weight standard.

2.3.5. DNA isolation from agarose gels

DNA bands were excised from the gel with a scalpel and the DNA was extracted from the agarose piece using the PCR Product Purification kit (Promega, Madison, USA) according to the manufacturer's protocol. Purified DNA was stored at -20 °C.

2.3.6. Purification of PCR products and vectors

PCR products and plasmids were purified with the PCR Product Purification kit (Promega, Madison, USA) according to the manufacturer's protocol. Purified DNA was stored at -20 °C.

2.3.7. DNA sequencing analysis

Every construct was sequenced prior to further use. To this aim, 15 µl DNA derived from a standard mini-prep were mixed with 15 µl of sterile H_2O dd in an Eppendorf cup and sent to GATC Biotech (Konstanz, Germany) or MWG (Ebersberg, Germany) for sequencing.

2.3.8. Transformation of *E. coli* cells

For transformation of *E. coli* cells, 100 µl of competent cells were mixed with 1 µl of the respective plasmid DNA vector or with 10 µl of a ligation reaction and incubated on ice for 20 min. The cells were heat-shocked at 42 °C for 42 sec and cooled on ice for 5 min. After addition of 900 µl LB0 the cells were incubated at 37 °C for 1 hour while shaking rigorously. For retransformation, 100 µl of the culture were plated on the respective selection plates. For transformation of a ligation reaction, the cells were spun down, the supernatant was discarded, the cell pellet was resuspended in the remaining liquid and plated on the respective selection plates.

2.3.9. Transformation of S. cerevisiae cells

For transformation of yeast cells, a modified protocol from Elble, 1992 was applied. Briefly, yeast cells were grown overnight in YPD at 30 °C, after incubation 200 µl of cells spun down (5,000 rpm, room temperature), the supernatant discarded and 0.67 µl of sperm carrier DNA added to the remaining liquid, thereby resuspending the

cells. 1 µl (~ 500 ng) of plasmid DNA was added and the cells were vortexed. 150 µl of PLATE mixture was added and the cells vortexed. 6 µl of 1 M DTT was added, the mix vortexed and incubated overnight at room temperature. The next day, without disturbing the settled cells, a heat shock for 30 min at 42 °C was performed, the settled cells were withdrawn with a pipette (100 µl) and plated onto the respective CSM plate.

2.3.10. PCR amplification

The polymerase chain reaction (PCR) was used to amplify regions of plasmids or linear DNA templates for analysis or for further subcloning of the DNA fragments into other plasmids. Specific introduction of point mutations is discussed in chapter 2.3.11. For the amplification either Phusion DNA-Polymerase (New Englad Biolabs, Beverly, USA) or the Expand High Fidelity PCR System (Roche, Mannheim, Germany) was used. In a 50 µl mixture supplemented with 800 µM of dNTPs (200 µM of dATP, dTTP, dGTP, dCTP each), 2.5 U Polymerase was added as well as 5 µl 10x reaction buffer as recommended by the company. Optionally, 5 % DMSO was added to prevent secondary structure formation. The reaction procedure was mainly dependent on the DNA template and the melting temperature of the DNA primers used. The first step is a denaturing step at 95 °C for 5 min. Following this 20-30 cycles of denaturing, annealing and elongation was performed. The denaturing step was 95 °C for 30-45 sec. For primer-annealing a lower temperature, depending on the base composition of the primers, was set. A rule of thumb is to use an annealing temperature of 5 °C below the lowest primer melting temperature. Annealing temperatures were designed to be similar for both primers and varied between 40 °C and 68 °C. Restrictions sites for restriction enzymes were attached at the 5'-ends of the primers. The calculation of the melting temperature was performed by the internet-based program Oligo Calculator (Northwestern University, Chicago). Elongation took place at 72 °C, the duration of which was dependent on the length of the template, whereby approximately 1 min was allowed for 1 kb of template. The last step is a final elongation for 5 min. The reaction was analyzed by gel electrophoresis. Products were purified using the Wizard® SV Gel and PCR Clean-Up System (Promega, Madison, USA) or by gel extraction, depending on the product purity.

2.3.11. Quik change mutagenesis

For the introduction of point mutations into plasmid DNA, the Quikchange approach was performed. Two primers (around 30 bp in length) were designed to anneal ten base pairs (bps) upstream and twenty bps downstream from the triplet to be changed. These primers were different from the template DNA in one or two positions to introduce the point mutation during subsequent PCR cycles. The temperature during the annealing step of the PCR was above the annealing temperature of the two primers to each other, but below the one of the primers to the template. For PCR 2.5 U Phusion DNA-Polymerase (New Englad Biolabs, Beverly, USA) were used for amplification of the plasmid. Methylated template plasmid was subsequently digested by *Dpn*I (New Englad Biolabs, Beverly, USA, 10 U, 37 °C, 1 h). 10 µl of the reaction were used for transformation of 100 µl competent *E. coli* cells. The introduction of the mutation was analyzed by sequencing and restriction digest if applicable.

2.3.12. DNA digest by restriction enzymes

Type II restriction endonucleases were used as recommended by the company (New Englad Biolabs, Beverly, USA) using the buffers provided along with the enzymes. For digests, usually a five-fold excess of enzyme was used (5 U enzyme per 1 µg of DNA), incubating for 1 h at the recommended temperature. The reaction was analyzed by gel electrophoresis. If the DNA-fragment was required for further cloning, it was extracted from the gel and purified using the Wizard® SV Gel and PCR Clean-Up System (Promega, Madison, USA).

2.3.13. Dephosphorylation of DNA ends

In order to prevent religation, cut vectors were treated with shrimp alkaline phosphatase subsequently to the restriction digest. For this purpose, 1 µl of alkaline phosphatase (0.1 U) was added directly to the restriction digest reaction and further incubated for one hour.

2.3.14. Ligation of DNA fragments

Generally, 1 µg of vector DNA was ligated with the fragment insert DNA in a molar ration of 1 : 3. For this purpose, the respective volumina of DNA were mixed with 10

µl of 2 x Quick ligation buffer and 1 µl of T4 DNA ligase (approx. 1 U) and incubated at room temperature for 15 min.

2.4. Working techniques of protein expression in *Sf*9 cells

All steps were performed using a sterile bank (Heraeus, Hanau, Germany).

2.4.1. Cultivation of Sf9 cells

Cell line and medium

Ovar-cells of *Spodoptera frugiperda* (*Sf*9) (Invitrogen, Carlsbad, USA)

Insect Xpress™ Medium (protein-free) (Lonza, Basel, Switzerland)

Initiation of cultures from frozen Sf9 cells

1 ml of frozen *Sf*9 cells were thawn in a water bath at 37 °C, diluted in 19 ml of 27 °C prewarmed Insect Xpress™ medium and incubated for 3 days at 27 °C.

Cultivation of liquid cultures

The cell number and viability of a mid-exponential growing culture was determined. For that 50 µl of the cell suspension was mixed with 50 µl 0.4 % Trypan-blue solution (Sigma, St. Louis, USA) and mounted onto a Neubauer counting chamber. Dead cells are stained blue by the dye. First, the dead (blue) cells and next the living (unstained) cells were counted according to the manufacturers recommendations.

The living cell number per ml is then calculated by the following formula:

$$living\ cells\ per\ ml\ = \frac{unstained\ cells}{ml} \times 2 \times 10^4$$

The viability of the culture is calculated by the following formula:

$$viability\ (\%) = \frac{unstained\ cells}{unstained\ cells + stained\ cells} \times 100\ \%$$

The culture in mid-exponential growth phase (typically 3-5 x 10^6 living cells/ml) is then diluted 0.5 x 10^6 living cells/ml in order to achieve and maintain a culture viability of over 95 %. The rate of division for *Sf*9 cells is about 24 h at 27 °C. Cultures were

grown in sterilized non-baffled Erlenmeyer flasks with a size of up to 1 l and with a rotational speed of 130 rpm. The maximum size of a liquid culture was 400 ml.

Storage of Sf9 cells

For long-term storage of Sf9 cells, a liquid culture with over 95 % viability in mid-exponential growth phase was centrifuged (100 x g, 5 min) and the pellet was taken up in a 4 °C chilled mixture of 10 % DMSO, 45 % fresh and 45 % used medium to reach a cell number of 1 x 10^7 living cells/ml. 1 ml aliquots were frozen in a cryo-container to reach -80 °C (2 h) and frozen in liquid nitrogen for subsequent storage in liquid nitrogen.

2.4.2. Blue-white selection of DH10Bac™ *E. coli* cells

DH10Bac™ cells were transformed with pFastBacHTA vectors as described. After heat shock, the cells were mixed with 900 µl LB_0 medium and incubated for 4 h at 37 °C. 100 µl or 10 µl of cells were subsequently plated on DH10Bac™ medium plates and incubated for 48 h at 37 °C. Successful transposition of the gene of interest into the Bacmid was indicated by the emergence of white colonies, due to the disruption of the β-Galactosidase gene in these clones. For verification, a number of white colonies were streaked out again on DH10Bac™ medium plates and incubated for another 48 h at 37 °C.

2.4.3. Preparation of Bacmid DNA

5 ml of LB_0 (supplemented with 50 µg/ml Kanamycin, 7 µg/ml Gentanamycin and 10 µg/ml Tetracyclin) were inoculated with a single white colony from a DH10Bac medium plate and incubated overnight at 37 °C in the test tube roller. After reaching the stationary phase, 1.5 ml were pelleted and the pellet resuspended in 300 µl Bacmid solution I. After addition of 300 µl Bacmid solution II, the mixture was incubated for 5 min at room temperature. Subsequently, 0.3 ml of 3 M Kaliumacetate (pH 5.5) was added slowly, the mix was incubated on ice for 10 min and centrifuged for 15 min (14,000 rpm, table centrifuge 5415 C). The supernatant was discarded and the pellet was washed twice with 70 % ethanol by inverting the tube carefully. Finally, after discarding the ethanol, the pellet was dried at room temperature and carefully (partly) dissolved in 40 µl H_2O by inversion. Pipetting was circumvented, due to potential shearing forces applied to the large Bacmid DNA molecules.

2.4.4. Transfection of *Sf*9 cells with Bacmid DNA

For the production of recombinat Baculoviruses, 9 x 10^5 *Sf*9 cells per well were plated in a 6-well plate and incubated for 20 min at 27 °C to settle them onto the surface. 1 µg or 2 µg of Bacmid DNA and 6 µl of Cellfectin (Invitrogen, Carlsbad, USA) were separately dissolved in 100 µl medium, combined and the resulting mix was incubated for 45 min at room temperature. The cell mono-layer was washed twice with 2 ml medium, the Bacmid DNA-Cellfectin-mix was combined with 800 µl medium, subsequently added to the cells and the transfection reaction was incubated at 27 °C. After 5 h of incubation, the supernatant was discarded, the cells covered with 2 ml of fresh medium and incubated for 7 days. In parallel, a negative control was prepared without DNA in the mix. The amount of medium in the plate was checked for evaporation on a daily basis and fresh medium added, when required. A successful transfection and subsequent rounds of infection are indicated by reduced growth, increased size of the cells and their nuclei, detachment and cell lysis. However, also for successful transfections, this could not always be observed. Hence, every transfection reaction was analysed for its infection potential and, when indicated, protein expression even if these signals did not appear. After the tranfection procedure, the supernatant in the well was centrifuged (300 x g, 5 min) to remove cell debris and cells and the supernatant was stored as P1 viral stock at 4 °C in the dark for further amplification.

2.4.5. Baculovirus amplification

A mid-exponential culture (3-5 x 10^6 cells/ml) of > 95 % viability was diluted to 2 x 10^6 cells/ml and infected with P1 viral stock at a ration of 50 : 1 (v/v). The infection process was followed by counting the cells on a daily basis. Successful infection is indicated by a growth arrest and a decline in viability after roughly 3 days. After 7 days, reaching a viability of under 30 %, the cells were centrifuged (300 x g) and the supernatant was stored as P2 viral stock at 4 °C in the dark for further amplification or protein expression.

2.5. Protein expression

2.5.1. Protein expression in *E. coli* using a plasmid DNA vector

For large-scale expression of a construct of interest, 2 x 100 ml of an overnight culture containing *E. coli* cells transformed with the vector of interest were mixed with 4 x 2 l of fresh 2xYT media containing the respective antibiotic in a ratio of 1 : 40 (v/v). The flasks were shaken at 37 °C until an OD_{600} of 0.6 - 0.8 was reached. Subsequently, protein expression was induced with 1 mM IPTG. After cells were grown for 4 h at 37 °C, the cultures were harvested by centrifugation at 5500 rpm at 4 °C for 10 min.

Human Aha1, PP5, Cyp40, FKBP51, FKBP52, Hsp90α and Hsp90β wildtype and mutants as well as the yeast Hsp90-Cys385 mutant were expressed in the *E. coli* strain BL21 (DE3) CodonPlus as a His6 tagged version using a pET28 vector. Human Cdc37 wildtype and Cdc37 mutants were expressed in the *E. coli* strain HB101 as a His6 tagged version using a pQE30 vector containing the respective gene.

For cell lysis, the pellets of the harvested *E. coli* cells were resuspended in IMAC1-buffer supplemented with Serva HP protease inhibitor mix. The resuspended cells were lysed in a Basic Z model cell disruption system (Constant Systems, Warwick, England) at a pressure of 1.8 kbar. In this system, the cell suspension is accelerated with high pressure through a cone against a metal plate. The shearing forces that develop at the exit point of the cone and the intensive turbulences at the metal plate destroy the cell integrity. In order to clear the lysate, the solution was centrifuged (20,000 rpm, 4 °C, 35 min, Avanti J 25, JA-25.50 rotor).

2.5.2. Protein expression in *Sf*9 cells using a Baculovirus vector

A mid-exponential culture (3-5 x 10^6 cells/ml) of > 95 % viability was diluted to 2 x 10^6 cells/ml and infected with the Baculovirus stock of interest at a ratio of 50 : 1 (v/v). The infection process was followed by counting the cells on a daily basis. After 2-3 days the cells were harvested by centrifugation (7,000 rpm, 4 °C, 10 min, Avanti J 25, JA-10 rotor) and immediately used for protein purification. Alternatively, a smaller volume of the infected cells was used for virus amplification.

The cell pellet was resuspended in 100 ml Src-IMAC1-buffer supplemented with 1-2 ml Protease inhbitor cocktail for His-tagged proteins (Sigma, St. Louis, USA) and the cells lysed by ultrasonication (3 x 30 sec, 60 % duty cycle, 50 % output).

Subsequently, the lysate was centrifuged (20,000 rpm, 4 °C, 45 min, Avanti J 25, JA-25.50 rotor), the supernatant analysed by microscopy and used for protein purification.

2.6. Protein purification

The following chromatographic methods were used for protein purification during this work. The purification success was controlled by SDS-PAGE after every step.

2.6.1. Affinity chromatography

The immobilized metal ion affinity *chromatography* (IMAC) was used in this work, which is based on the interaction between a matrix and a His6-tag that is fused to the protein of interest. Either Ni^{2+} ions (His-TrapTM FF, GE Healthcare, Freiburg, Germany) or Co^{2+} ions (HisTALON^{TM} Superflow Cartridge, Clontech Laboratories, Mountain View, USA) are attached to a chelating matrix of sepharose material. Wash steps and elution is performed by increasing the concentration of imidazole in the running buffer which competes with the His6-tag for binding to the matrix. Usually the immobilized protein of interest was washed with 15 mM and eluted with 300 mM imidazole concentrations.

2.6.2. Ion exchange chromatography

The separation of proteins by ion exchange chromatography is based on the differing net surface charge of the macromolecules and their resulting individual interaction with a charged matrix. Depending on the pI of the protein and the pH of the buffer, the proteins interact to a differing extent with the column material. A protein possessing a pI under 7.0 carries a negative net charge and therefore interacts with an anion exchange column at neutral pH. The opposite is true for a protein with a pI over 7.0, which interacts with cation exchange material at pH 7.0. Elution of the protein of interest is achieved by an increasing salt gradient, resulting in competition with the protein molecules and the column. The procedure was performed according to the guidelines of the manufacturer using a Resource-Q or a Resource-S column (GE Healthcare, Freiburg, Germany).

2.6.3. Size exclusion chromatography

During size exclusion chromatography (also called gel filtration chromatography), proteins are separated according to their hydrodynamic radius. The column matrix forms a three-dimensional network of defined pore size. Large proteins (or protein complexes) and soluble aggregates are not capable of penetrating the pores of the matrix and elute with the void volume of the column. Proteins with a hydrodynamic radius lying within the application range of the used column, are able to penetrate the pores, therefore cover a longer distance and elute at higher volumes compared to larger molecules. Usually, buffers with high ionic strength are used to suppress unspecific ionic protein-protein and protein-matrix interactions. The procedure was performed according to the guidelines of the manufacturer using precast columns of the type HiLoad^{TM} SuperdexTM 75 pg (16/60 and 26/60) and HiLoad^{TM} SuperdexTM 200 pg (16/60 and 26/60) (GE Healthcare, Freiburg, Germany), depending on the required range of separation.

2.6.4. Concentration of proteins

For increasing the concentration of a protein solution, Millipore Ultra concentrators were used following the recommendations of the manufacturer (Millipore, Bedford, USA). The solution was centrifuged (4,000 rpm, 4 °C) until the desired protein concentration was reached. During the concentration process, the solution is filtered through a membrane with a pore-size (3 kDa, 10 kDa or 30 kDa) that lies under the size of the protein to be concentrated. For c-Src and c-Src3M kinase, volumina Amicon cells were used that filter protein solutions through filters by nitrogen gas pressure at ~3 bar under continuous stirring. All other kinase variants were not concentrated after size exclusion chromatography, due to their increased aggregation propensity.

2.6.5. Dialysis of proteins

For changing buffers of protein solutions, the protein was dialyzed in a dialysis bag (Spectrum, Houston, USA) against the 1000-fold of the original volume at 4 °C while continuously stirring. Alternatively, the buffer was changed using a PD-10 desalting column (GE Healthcare, Freiburg, Germany) and the manufacturer’s protocol.

2.6.6. Standard purification of His6-tagged proteins

Solutions

IMAC1-buffer:	40 mM phosphate, pH 7.5, 300 mM KCl, 6 mM imidazole
IMAC2-buffer:	40 mM phosphate, pH 7.5, 300 mM KCl, 400 mM imidazole
Res1-buffer:	40 mM HEPES, pH 7.5, 20 mM KCl, 1 mM EDTA
Res2-buffer:	40 mM HEPES, pH 7.5, 1 M KCl, 1 mM EDTA
GF-buffer:	40 mM HEPES, pH 7.5, 300 mM KCl, 1 mM EDTA
Storage buffer:	40 mM HEPES, pH 7.5, 20 mM KCl

Procedure

The cleared lysate was loaded on a His-trap FF column (2.5 ml/min) equilibrated with IMAC1-buffer using a 150 ml superloop. The column was subsequently washed with IMAC1-buffer containing 15 mM imidazole. Elution was achieved by applying a step gradient to 100 % of IMAC2-buffer containing 300 mM imidazole. The fractions containing the protein of interest were combined and diluted in binding buffer for ion exchange chromatography (Res1-buffer) or in water. The protein solution was loaded onto a Resource Q or Resource S column, equilibrated with Res1-buffer. The column was washed and the protein eluted with a linearly increasing salt gradient, by increasing the ratio of Res2-buffer : Res1-buffer. The fractions containing the target protein were pooled, optionally concentrated to 5 ml and loaded onto a size exclusion column using a 5 ml or 10 ml superloop. Depending on the size of the protein, a Superdex 75 pg or Superdex 200 pg was used. GF-buffer served as loading buffer. The fractions of interest were combined and the protein was dialyzed against Storage buffer. Finally, the protein was concentrated and frozen to 100 µl aliquots in liquid nitrogen and stored at -80 °C. If the protein contained cysteines, 1 mM DTT was added to all buffers, except IMAC1- and IMAC2-buffer.

2.6.7. Purification of Src kinase from *Sf*9 cells

For purification of His6 tagged Src kinases, the cleared lysate was loaded onto a HisTALON^{TM} Superflow Cartridge (Clontech Laboratories, Mountain View, USA) preequilibrated in Src-IMAC-buffer (40 mM Tris, 150 mM NaCl, 5 % Glycerine, 5 mM DTT). To remove unspecifically bound proteins, the column was washed with Src-IMAC-buffer and subsequently with Src-IMAC-buffer containing 15 mM imidazole. The kinase was eluted with Src-IMAC-buffer containing 300 mM imidazole. Src kinase containing fractions (5 ml) were pooled, loaded onto a Superdex 75 Prep Grade column for size exclusion chromatography and eluted with Src-IMAC-buffer containing 5 mM DTT (Src-buffer).

2.6.8. Purification of other proteins from *E. coli*

The human proteins Hsp90α, Hsp90β, Cdc37, Hop, Aha1, Hdj1, Hsp70 and mutants therof were purified as described (Atanas *et al*., 2010, Bose *et al*., 1996, Eckl *et al.*, 2013, Peschek *et al*., 2013,). PP5 and PP5ΔTPR were kind gifts from V. Haslbeck, $Hop_{[TPR2A-TPR2B]}$ was a kind gift from A. Röhl, Cyp40, FKBP51 and FKBP52 were kind gifts from O. Lorenz and Atto550-labelled yeast *Hsp90-Cys385 was provided by B. Zierer.

2.7. Protein analytics

2.7.1. Solutions in protein analytics

Running buffer (10 x):	Tris	0,25 M
	Glycin	2 M
	SDS	1 % (w/v)
5x-Laemmli loading buffer:	SDS	10 % (w/v)
	Glycerin	50 % (w/v)
	Tris	300 mM
	Bromphenol blue	0,05 % (w/v)
	2-Mercaptoethanol	5 % (v/v)

Transfer buffer:	Glycine	36 g
	Tris	7,6 g
	Methanol	500 ml
	SDS	0,3% (w/v)
	H_2O	ad 2,5 l
PBS (-T):	NaCl	5,84 g
	Na_2HPO_4	11,5 g
	NaH_2PO_4	2,96 g
	H_2O	ad 1 l
	(Tween-20	1 ml)
TBS (-T)	Tris	6.05 g, pH 7.5
	NaCl	8.76 g
	H_2O	ad 1 l
	(Tween-20	1 ml)

2.7.2. Sodium dodecyl sulfate polyacrylamide gel electrophoresis (SDS-PAGE)

Discontinuous sodium dodecyl sulfate polyacrylamide gelelectrophoresis (SDS-PAGE) was performed to analyze protein purification steps and cell lysates (Fling & Gregerson, 1986). The separation took place in vertical 7.0 x 9.0 x 0,075 cm SDS-PAGE gels in a SDS-PAGE electrophoresis chamber at a constant current of 35 mA per gel for 50 min. Prior to loading the gel, the protein solution or the lysate was mixed with 5 x Laemmli loading buffer and heated at 95 °C for 5 min, followed by centrifugation at 14,000 rpm at room temperature. LMW marker (BioRad, München, Germany) or Rainbow marker (GE Healthcare, Freiburg, Germany) was used for protein size estimation.

2.7.3. Coomassie-staining of SDS-gels

Fairbanks Solutions

Solution A: 25 % (v/v) Isopropanol, 10 % (v/v) technical grade acetic acid, 0,05 % Coomassie Blue R

Solution D: 10 % technical grade acetic acid

Procedure

After SDS-PAGE, gels were stained using a modified protocol by Fairbanks *et al*. (Fairbanks *et al*, 1971). The gel was covered with Fairbanks solution A, the solution shortly heated up in a microwave and incubated for 5 min at room temperature. Subsequently, the staining solution A was discarded and the gel rinsed with water, prior to destaining with warm Fairbanks solution D. The detection limit of this method is approximately 50 ng.

2.7.4. Aggregation assay

100 µg/ml kinase in Src-buffer was incubated at 45 °C for 10 minutes. To remove insoluble aggregates, the proteins were subsequently centrifuged for 60 min (20,000 g, 4 °C). Pellet and supernatant proteins were denatured in Laemmli buffer, boiled at 95 °C. and subsequently analyzed by SDS-PAGE and densitometry.

2.7.5. Immunoblotting (Western Blot)

Proteins that were separated on a gel by SDS-PAGE were electrophoretically transferred on a PVDF or nitrocellulose membrane in a Semi-Dry blotting apparatus (Biometra, Göttingen, Germany). First, the SDS-PAGE gel, six Whatman 3MM filter papers and a methanol activated PVDF or nitrocellulose membrane were incubated in transfer buffer for five minutes. Second, a stack was formed with three Whatman 3MM filter papers at the bottom, the PVDF membrane with the SDS-PAGE gel above in the middle and three Whatman 3MM filter papers on the top. This stack was then placed in the Semi-Dry blotting apparatus and the transfer was started with a current of 72 mA per SDS-PAGE gel (1.5 mA / $cm^{2)}$ for one hour. After transfer, the PVDF membrane was incubated in PBS-T containing 3 % or 5 % milk in PBS-T or TBS-T for 30 min. The membrane was incubated in a solution containing the primary antibody diluted in PBS-T / TBS-T / 1% milk powder for 60 min at room temperature. After three washing steps with PBS-T / TBS-T for 10 min, the membrane was incubated with secondary antibody for 60 min diluted in PBS-T / TBS-T supplemented with 1 % milk. After three washing steps with PBS-T / TBS-T for 10 minutes, the antibody-enzyme conjugate was detected with an ECL detection kit (Amersham, Uppsala, Sweden). The detection method is based on chemoluminescence. In the presence of H_2O_2, peroxidase catalyzes the oxidation of cyclic diacylhydrazineluminol which is accompanied by light emission. To start the

reaction, a mixture of 975 µl of Reaction Buffer 1 (ECL1) and 25 µl of Reaction Substrate (ECL2) was added to the membrane. The membrane was placed between two plastic foils and light emission was detected on an X-Omat X-ray film (Kodak, Rochester, USA) by incubation up to 10 minutes.

2.7.6. Analytical size exclusion chromatography (SEC) – High performance liquid chromatography (HPLC)

Size exclusion chromatography is based on the separation of proteins according to their molecular size. This method can be used in an analytical scale to derive the molecular size of a single protein or a protein complex. In this study, a Jasco HPLC with UV detection was used. Analysis of proteins was carried out on a Superose 6 column at room temperature. A total volume of 50 µl containing 30 µM Hsp90β (15 µM dimer) was injected with or without 15 µM or 30 µM of Cdc37. The retention time was used to reveal the complex formation of the proteins and their stoichiometry.

2.7.7. Fluorescent protein labeling

Proteins were labeled at cysteine residues using Alexa Fluor® 488 (Invitrogen, Carlsbad, USA) or Atto 550 maleimide (Sigma, St. Louis, USA). These dyes react with thiol groups to give tioether-coupled products. Disulfide bonds have to be reduced prior to introducing the dye. This was achieved by supplementing the protein solution with a 10 fold excess of DTT. However, before the labeling reaction was started, the protein was dialyzed against the labeling buffer (40 mM Hepes/KOH, pH 7.3, 20 mM KCl) (alternatively a PD-10 column (GE Healthcare, Freiburg, Germany) was used for this purpose) in order to remove excess DTT. In general, a threefold molar excess of Atto 488 was solved in 20 µl DMSO and added drop wise to 500 µl protein solution. The reaction was allowed to proceed for 2-3 hours at room temperature or overnight at 4 °C protected from light. The reaction was quenched by addition of 10 mM DTT and the protein was separated from free label by applying to a PD-10 desalting column in a buffer containing 40 mM Hepes/KOH, pH 7.5, 300 mM KCl, 1 mM DTT. The labeling efficiency was determined using UV spectroscopy and the extinction coefficients provided by the manufacturer.

2.7.8. Analytical ultra-centrifugation (aUC) assisted with fluorescence detection

In order to analyze protein-protein interactions, aUC equipped with a fluorescence-detection device was used (Kroe & Laue, 2009; MacGregor et al, 2004). To this aim, the protein of interest was labeled at cysteine residues with the fluorescein derivative Alexa Fluor® 488 (Invitrogen, Carlsbad, USA). The labeled protein was diluted in aUC-buffer (20 mM Hepes, 20 mM KCl, 5 mM $MgCl_2$, 1 mM DTT, pH 7.5, if not stated otherwise) and was subjected to aUC in a Beckman XL-A analytical ultracentrifuge equipped with an AVIV-FIS fluorescence detection system (AVIV Biomedical, Lakewood, USA). Sedimentation experiments were performed in standard 2-sector centerpieces in a Ti50 8-hole rotor at 42,000 rpm. Scans at an excitation wavelength of 488 nm were recorded in 90 sec intervals. In order to obtain binding constants, the labeled protein was supplemented with increasing amounts of the potential binding partner. The program SEDVIEW was used to evaluate the data.

For the analysis of the Cdc37-Hsp90 complex formation, peaks in $\Delta c/\Delta t$ profiles were fit to bi-Gaussian functions using the ORIGIN 8G software package in order to determine the corresponding peak amplitude for free *Cdc37 (Peak1, [Cdc37]) and for complexed *Cdc37 (Peak2, [*Cdc37–Hsp90]). Using several different Hsp90 concentrations, the binding constant was determined by fitting the reduction in Peak 1 and the increase in Peak 2 with Michaelis-Menten.

2.7.9. Hydrogen/Deuterium Exchange – Mass spectrometry

Hydrogen/deuterium exchange mass spectrometry (HDX-MS) experiments were performed on a fully automated system equipped with a Leap robot (HTS PAL, Leap Technologies, Carrboro, USA), a Waters ACQUITY UPLC®, a HDX manager and the Synapt® G2-S mass spectrometer as described elsewhere (Waters, Milford, USA) (Zhang *et al*., 2014). Src kinases were vacuum concentrated in the presence of 100 mM Trehalose (Sigma, St. Louis, USA) The protein samples were diluted in a ratio of 1:4 with deuterium oxide-containing Src-buffer (40 mM Tris pH 7.1, 150 mM NaCl, 5 % Glycerin, 5 mM DTT) and incubated at 25 °C for 20, 60, 600, 3600, 7200 s. After the labeling reaction the protein was denatured and the exchange was stopped by diluting the labeled protein 1 : 1 in quenching buffer (50 mM Na_2HPO_4 x 2 H_2O, 50 mM NaH_2PO_4 x 2 H_2O; 35 mM TCEP, 4 M Gua-HCl, pH 2.6, 4 °C). Digestion was performed online by immobilized pepsin column (Applied Biosystems, Poroszyme™,

Foster City, USA). Peptides were trapped and subsequently separated on a Waters UPLC® CSH™ C 18 column (1.7 µm, 1.0 x 100 mm) with a H_2O + 0.1 % formic acid (v/v) and ACN + 0.1 % formic acid (v/v) gradient. Trapping and chromatographic separation were carried out at 0 °C to minimize back-exchange. Eluting peptides were directly subjected to the time-of-flight mass spectrometer by electrospray ionization. Prior to fragmentation by MS^E and mass detection in resolution mode the peptide ions were additionally separated by drift-time within the mobility cell. Data processing was performed using the Waters Protein Lynx Global Server PLGS (Version 2.5.3.) and DynamX (Version 2.0).

2.8. Spectroscopical methods

For all spectroscopical analyzes recorded spectra were corrected for the respective buffer spectra as reference. The reference buffer was either the dialysis buffer or the gel filtration buffer at the last purification step.

2.8.1. UV-absorption spectroscopy

Absorbtion of electromagnetic radiation in the UV/VIS spectrum range occurs when π-electrons are transferred to an excited, high-energy state. The peptide bonds in proteins absorb between 180 nm and 240 nm. Additionally, the aromatic amino acids tyrosine and tryptophan and to a smaller extend also phenylalanine and disulfide bridges absorb between 250 nm and 300 nm. Tyrosine and tryptophan residues thereby mainly contribute to absorbtion within this range, which is reflected in the significantly increased extinction coefficients (Cantor & Schimmel, 1980) that are one order of magnitude higher than the one of phenylalanine and disulfide bridges (**Table 3**).

Table 3 Extinction coefficients of important determinants of protein absorption at the respective wavelength.

Amino acid	λ_{max} (nm)	λ_{max} (M^{-1} cm^{-1})
Tryptophan	280	5600
Tyrosine	274	1400
Phenylalanine	257	200
Disulfid bridge	250	300
Peptide bond	190	~7000

UV spectroscopy was used to determine the protein concentration of protein solutions and of lysates. The protein concentration can easily be calculated if the molar extinction coefficient of the protein is known and the absorbtion of the protein solution at 280 nm is measured. The law of Lambert-Beer describes this relationship:

$$c = \frac{E}{\varepsilon_{280nm} \cdot d}$$

In this equation, E is the extinction at 280 nm, $\varepsilon_{280\ nm}$ is the molar extinction coefficient, d is the thickness of the cuvette and c is the concentration in mol/l. The extinction coefficent for a certain protein can be calculated on the basis of its amino acid composition. For this purpose, the program ProtParam was used which calculates the extinction coefficent based on different methods (Edelhoch, 1967; Gill & von Hippel, 1989; Pace et al, 1995). All UV absorbtion experiments were either carried out with quartz glass cuvettes using the Cary 50 (or 100) Bio UV-VIS-spectrophotometer (Varian, Palo Alto, USA) or by using the Nanodrop (Peqlab, Erlangen, Germany).

2.8.2. Circular dichroism (CD) spectroscopy – thermal transition

Circular dichroism (CD) is the property of optically active molecules to absorb circularly polarized light with different intensity. The optical activity of proteins is the result of asymetric carbon atoms and / or aromatic amino acids. Proteins are composed of a large number of optically active amino acids and form asymmetric secondary structure. The ellipticity Θ (in degrees) describes the intensity of light rotation by an optically active probe and thus is a quantitative measure for circular dichroism. The molar ellipticity i. e. the ellipticity in relation to the average molecular weight of the amino acids of the protein Θ_{MRW} is calculated as follows:

$$\Theta_{MRW} = \frac{\Theta \cdot 100 \cdot M}{c \cdot d \cdot N_{AS}}$$

Θ is the measured ellipticity in mdeg, M the molecular weight of the protein in kDa, c the protein coi.ncentration in mg/ml, d the thickness of the cuvette in centimeter and N_{AS} the number of amino acids of the protein.

In protein biochemistry, CD spectroscopy is widely used to obtain information about the structure of a protein. Depending on the wavelength range, there exist two methods, allowing different structural insights. Within the near-UV region, ranging from 250 nm - 300 nm, asmmetrically arranged aromatic amino acids are responsible for a CD signal. The environment of these amino acids influences the CD signal and is dependent on the proteins tertiary structure. Consequently, the signal in this region represents a fingerprint of an individual protein. Denatured proteins do not exhibit a signal in this region, since the aromatic regions are no longer surrounded by an asymmetric environment. In the far-UV region (170 nm - 250 nm, amide region) the secondary stucture of a protein can be analyzed. α-helices show two adjacent minima at 208 nm and 222 nm, whereas β-sheets show a less intense signal with a single minimum at 218 nm. These phenomena are nicely summarized in a review from Kelly *et al*. (Kelly *et al*., 2005).

Since the molar ellipticity is independent of the temperature of the solution, CD spectroscopy is ideally suited to measure thermal stability of proteins. Measurements were carried out in a 0.1 cm thick sealable quarz cuvette, a thermostatable cuvette holder and a PTC343 peltier unit (Jasco, Groß-Umstadt, Germany). The thermal

unfolding of the proteins was monitored at 222 nm in 30 mM sodium phosphate buffer, 30 mM NaCl, 2 mM DTT, pH 7.5 using a 0.1 cm quartz cuvette and a protein concentration of 100 µg/ml by measuring changes of the CD signal between 20 °C and 80 °C, at a heating rate of 20 °C per hour. The curves were fitted to a sigmoidal transition.

2.8.3. 1-Anilino-8-Naphthalene Sulfonate (ANS) binding assay

1.6 µM of the respective kinase variant was incubated with 30 µM of 1-Anilino-8-Naphthalene Sulfonate (Sigma, St. Louis, USA) in Src-buffer for 20 min at room temperature and subsequently analyzed in a FluoroMax-3 fluorescence spectrometer (Spex, Edison, USA) with an excitation wavelength of 380 nm and an emission wavelength of 470 nm. The obtained emission spectra of the proteins were normalized against the Src-buffer blank.

2.8.4. Tryptophan quenching

5 M acrylamide was titrated to a 500 nM Src kinase in Src-buffer at 25 °C. Tryptophan fluorescence emission quenching upon excitation at 295 nm was recorded using a FluoroMax-3 fluorescence spectrometer (Spex, Edison, USA). The slit widths were set to 3 nm and 5 nm for excitation and emission, respectively. The changes in fluorescence intensity were plotted against the acrylamide concentration according to a modified Stern–Volmer equation (Lakowicz, 1999).

2.8.5. Fluorescence resonance energy transfer (FRET) measurements

For the optimization of the FRET observed between randomly Alexa488-labeled Cdc37 (*Cdc37, donor) and specifically Atto550-labeled yeast Hsp90-C385 (B. Zierer) (*Hsp90, acceptor), increasing concentrations of *Cdc37 were added to 150 nM *Hsp90 at 25 °C in aUC-buffer (20 mM Hepes, 20 mM KCl, 5 mM $MgCl_2$, 1 mM DTT, pH 7.5). Fluorescence spectra from 475 nm - 625 nm were recorded upon excitation at 504 nm using a FluoroMax-3 fluorescence spectrometer (Spex, Edison, USA). The slit widths were set to 1 nm and 3 nm for excitation and emission, respectively. For the displacement of *Cdc37 from *Hsp90, 75 nM *Cdc37 was mixed with 300 nM *Hsp90 and a time course of the acceptor channel at 577 nm was recorded. After comlex formation, 2 µM Aha1, 2 mM ATP or both was added to observe the effect on the *Cdc37-*Hsp90 complex.

2.9. Src kinase activity assay *in vivo*

2.9.1. Yeast viability assay

The Hsp90 double-knock out strain ECU82α containing yeast Hsp82 on a plasmid (yHsp82 in pRS426) was transformed with plasmids containing the Src variants under a galactose promoter (Src in pY413). After growing in glucose-containing URA/LEU/HIS selection medium to stationary phase, cells were diluted in a ten-fold dilution series and 3 µl of each dilution were spotted on an agar plates containing galactose as sole sugar source. Cells were grown at 30 °C for 3 days. In a second approach, the Hsp90 inhibitor Radicicol (Sigma, St. Louis, USA) was added at a final concentration of 5 µM to the plates for determining the Hsp90-dependence of the expressed Src variants.

2.9.2. Analysis of transphosphorylation activity in *S. cerevisiae*

Src-plasmid transformed yeast cells were grown at 30 °C in raffinose-containing URA/LEU/HIS selection medium to stationary phase, spun down and resuspended in glucose-free URA/LEU/HIS medium containing galactose for induction of Src-expression. The cells were grown for six hours at 30 °C, spun down and the pellet resuspended in 250 µl extraction buffer (8 M urea, 5 % SDS, 40 mM Tris, 0.1 M EDTA, pH 7.5) and additionally lysed with glass beads. After centrifugation at 14,000 rpm for 5 min the protein concentration of the supernatant was measured using a Nanodrop (Peqlab, Erlangen, Germany) and normalized by dilution. After SDS-buffer addition and incubation at 95 °C for 5 min a 10 % SDS-PAGE was run for Western blotting. The blotted membrane was blocked with 5 % milk in TBS-T (0.1 % Tween-20) for 30 min and subsequently treated with mouse anti-phosphotyrosine antibody clone 4G10 (1:1000 in TBS-T, 1 % milk) (Merck Millipore, Darmstadt, Germany). After three 10 min washing steps with TBS-T, the membrane was treated with the secondary rabbit POD-conjugated anti-mouse antibody (1 : 10,000 in TBS-T, 1 % milk) (Sigma, St. Louis, USA). The blot was washed with TBS-T, POD-reaction performed using ECLplus Western Detection System (GE Healthcare, München, Germany) and the chemiluminescence was visualized by exposing the blot to Kodak X-OMAT.

2.9.3. Analysis of Src expression in *S. cerevisiae*

For detection of Src kinase in the yeast lysates, after blocking with 3 % milk in PBS-T (0.1 % Tween-20) for 30 min the membrane was treated with mouse anti-avian Src antibody clone EC10 (1:1000) in PBS-T, 1 % milk) (Merck Millipore, Darmstadt, Germany). After washing in PBS-T the membrane was treated with the secondary rabbit POD-conjugated anti-mouse antibody and developed as described.

2.10. Src kinase activity assay *in vitro*

2.10.1. Kinase activity assay

For activity measurements of Src variants, 320 nM of the respective kinase variant were incubated at 30 °C for 30 minutes in Src-buffer supplemented with 10 mM $MgCl_2$, 1 mM $MnCl_2$ and 40 µM [γ-^{32}P]-ATP with an activity of 0.5 µCi. A tenfold molar excess of acid-denatured enolase (Sigma, St. Louis, USA) was used as a substrate. The reaction was stopped by adding Laemmli buffer and boiling the sample. The samples were separated by SDS-PAGE and transphosphorylation was detected by applying a phosphor image screen onto the gel. The screen was subsequently analyzed using a Typhoon 9200 phosphoimager, revealing a luminescence signal, and evaluation was performed using the program Image Quant (GE Healthcare, München, Germany). The kinase reaction was performed either in the absence or presence of different amounts of chaperones.

2.10.2. Temperature dependence of Src kinase activation and stabilization

To investigate the influence of the temperature on the activity of Src variants and the influence of chaperones on this process, the kinases were first pre-incubated on ice in the presence of absence of chaperones in Src-buffer with 5 mM $MgCl_2$ for 10 min, subsequently incubated at increasing temperatures for ten minutes and cooled down on ice for 10 min. Then enolase and [γ-^{32}P]-ATP were added and the activity was measured as described above.

2.11. Molecular dynamics simulations (by Prof. V. Kaila)

The structure of wild type c-Src (PDB ID:1Y57, Cowan-Jacob *et al.*, 2005) was obtained from Brookhaven Databank and employed for constructing the c-Src3MΔC variant by introducing point mutations (R95W, D117Q, R318Q) *in silico* and by removing the C-terminal tail (ΔC) or replacing the tail with the v-Src sequence (in c-Src3MΔV), respectively. The models were solvated in a water box using a 100 mM sodium chloride concentration. The systems were simulated for 250 ns with a 2 fs integration time step at T = 310 K, and by using the CHARMM27 force field (MacKerell *et al.*, 1998). The simulations were performed using NAMD (Phillips *et al*., 2005), and Visual Molecular Dynamics (Humphrey *et al*., 1996) was used for analysis.

3. Results

3.1. Integration of the cochaperone Cdc37 into the Hsp90-cycle

3.1.1. Characterization of the Cdc37-Hsp90 complex

We aimed to understand the interaction between the chaperone Hsp90 and its kinase specific cochaperone Cdc37. To this end, human Cdc37 was unspecifically fluorescently labelled using the dye Alexa488 (yielding *Cdc37) and the binding to human Hsp90 was tested using fluorescence-assisted analytical ultracentrifugation (aUC) (**Figure 24**).

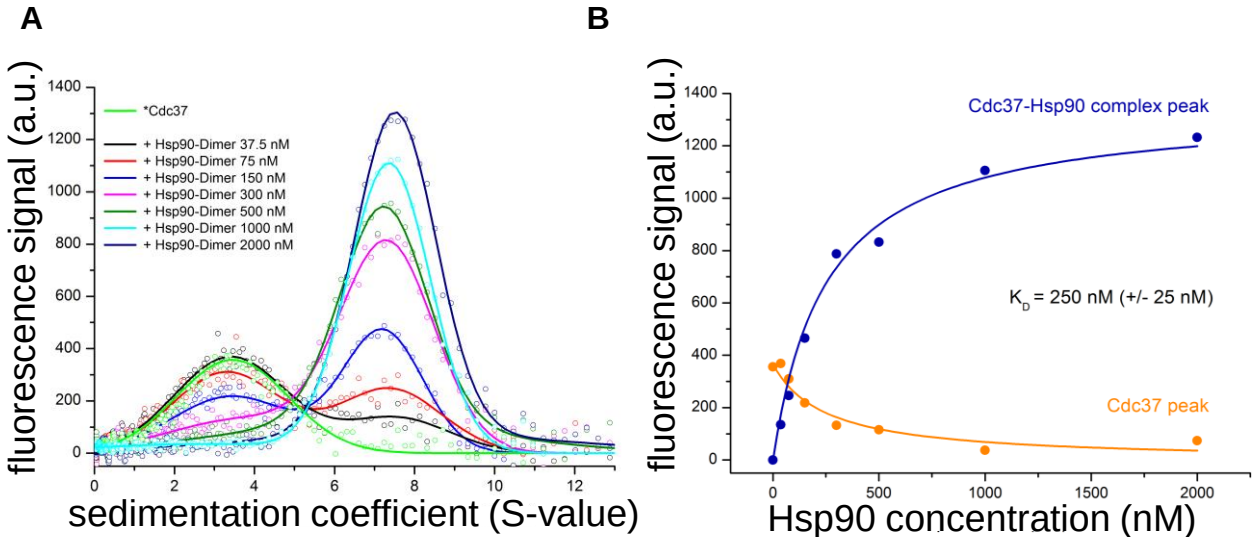

Figure 24

Determining the binding affinity of the Cdc37-Hsp90 complex by aUC.

(A) Titration of Hsp90 to *Cdc37. *Cdc37 shows a signal at 3.5 S, whereas the binding of Hsp90 shifts the peak to 7.1 S (B) The amplitudes of the decreasing labelled human *Cdc37-peak (orange) and increasing *Cdc37-Hsp90-peak (deep blue) derived from the aUC titration shown in (A) were plotted and analyzed by a Michaelis-Menten fit.

Confirming previous results (Eckl *et al*., 2013), *Cdc37 alone exhibited a S-value of 3.5 S, while the complex with Hsp90 showed a S-value of 7.1 S (**Figure 24a, Table 4**). By titrating Hsp90 to *Cdc37 the K_D could be determined by plotting the amplitudes of the increasing *Cdc37-Hsp90-peak and the decreasing *Cdc37-peak against Hsp90 concentrations (**Figure 24b**). The K_D was determined to be 250 nM for the formation of the Cdc37-Hsp90 complex.

Next, we were interested whether Cdc37 would bind to the Hsp90-dimer as a monomer or as a dimer. To this end, the proteins were subjected to analytical size exclusion chromatography (SEC).

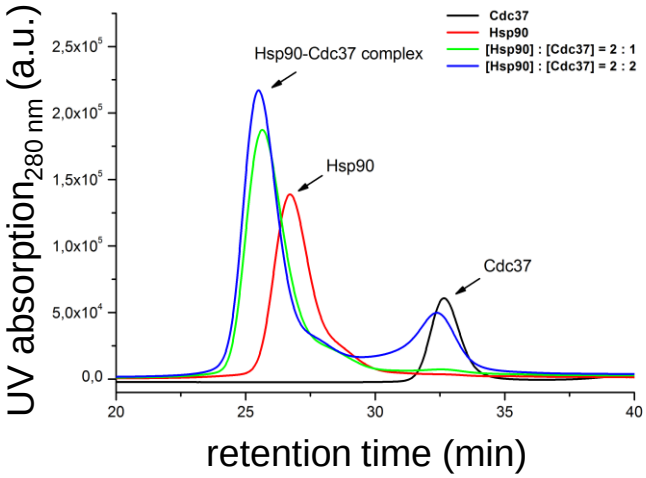

Figure 25

Determining the stoichiometry of the Cdc37-Hsp90 complex.

(A) A SEC run on a Superose 6 column of 15 uM Cdc37 (black) and 15 uM Hsp90-dimer (red) is shown either alone or in combination at a ratio of 2 : 1 ratio (green) and 2 : 2 (blue), respectively.

Cdc37 alone showed a peak at 31.7 min, whereas the Hsp90-dimer gave a peak at 27 min. At equimolar concentrations of Cdc37-monomer and Hsp90-dimer (1 : 2), a complex peak appeared at around 25.5 min. We then assessed, whether an equal additional amount of Cdc37 would be incorporated into the complex with Hsp90, resulting in a potential 2 : 2 stoichiometry ($[Hsp90]_2$: $[Cdc37]_1$ = 1 : 2). This however, was not the case as addition of additional Cdc37, resulted in uncomplexed Cdc37, revealing that the Hsp90-dimer was saturated at a stoichiometry of 1 : 1 (Hsp90 dimer : Cdc37 monomer).

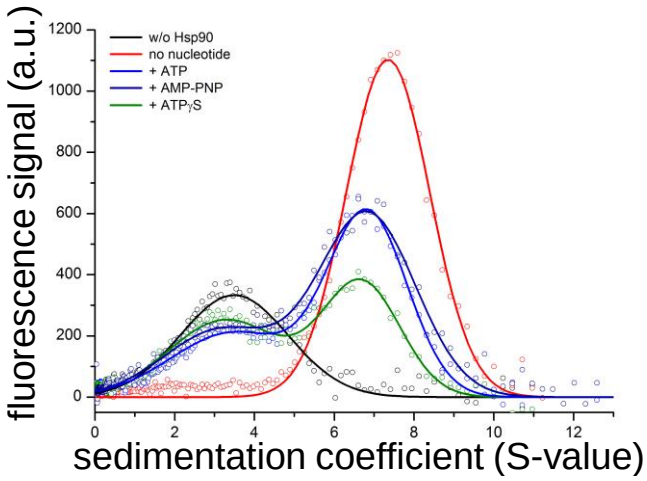

Figure 26

The influence of nucleotides on the Cdc37-Hsp90 complex.

aUC of 150 nM *Cdc37 (black) and 2 µM Hsp90 in the absence (red) or presence of 2 mM of various nucleotide analogues: ATP (blue), AMP-PNP (marine) and ATPγS (green).

Using the aUC set up, we then tested the influence of different nucleotides and their analogues on the interaction of the two proteins (**Figure 26**). Surprisingly distinct from Cdc37 from other organisms, human Cdc37 preferentially bound to apo-Hsp90. When ATP was present, 50 % of *Cdc37 is expelled from Hsp90. Similarly, AMP-PNP released half of the *Cdc37 molecules from the complex. Increased displacement was observed in the presence of ATPγS. 70 % of the cochaperone resided in the unbound form in the presence of ATPγS. Consequently, within the human Hsp90 kinase maturation cycle, Cdc37 seems to play an important role in an early stage during client entry, before ATP binding to Hsp90 occurs.

3.1.2. A ternary complex of Cdc37-Hsp90-Hop is preferentially formed

It has been shown previously that the Hsp70 cycle is involved during the initial folding of kinases (Dey *et al*., 1996). In this context, Hop/Sti1, the cochaperone connecting the Hsp70 and the Hsp90 cycles is of special importance (Lee *et al.*, 2004). In *S. cerevisiae*, Hop/Sti1 is essential for the maturation of v-Src (Schmid *et al.,* 2012). This necessity was further demonstrated for the checkpoint regulatory kinase 1 (Chk1) using *in vitro* reconstitution assays (Arlander *et al*., 2006, Felts *et al*., 2007). In this context, an increase in kinase activation could be observed linearly correlating with the amount of Hop added to the reaction (Arlander *et al*., 2006). It has been proposed that Cdc37 and Hop/Sti1 have functional overlap in stabilizing Hsp90-kinase complexes (Lee *et al*., 2004). Similar to human Cdc37, Hop binds the open conformation of Hsp90 (Richter *et al*., 2003). However, it has been observed that Hop expels Cdc37 from Hsp90 in *C. elegans* studies (Gaiser *et al.*, 2010).

To understand the interplay of human Cdc37 and human Hop, we tested their complex formation with Hsp90 applying aUC.

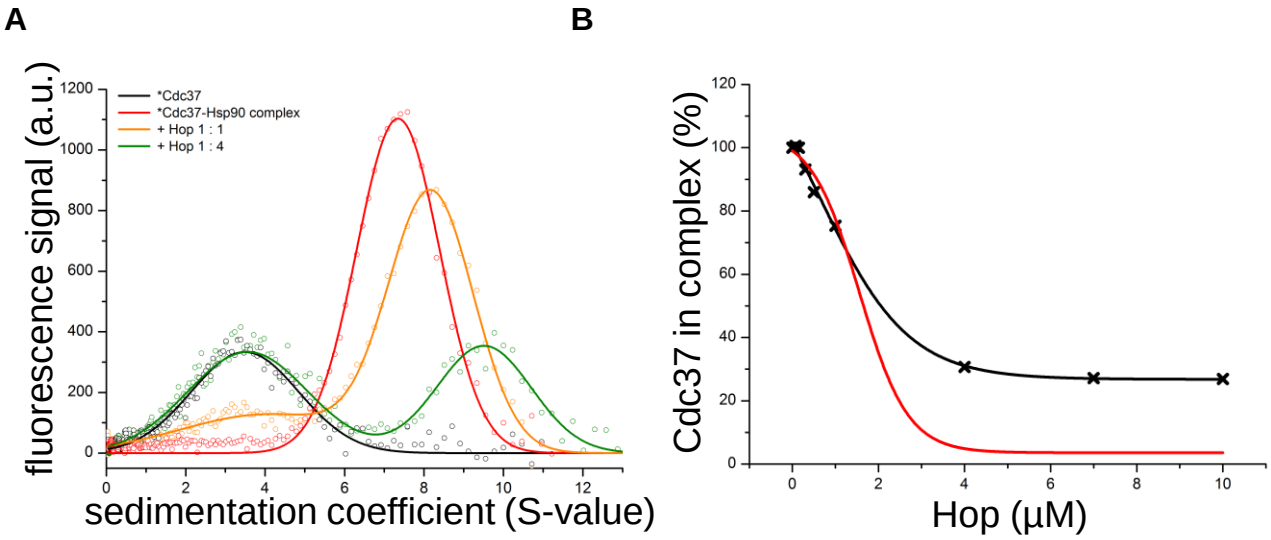

Figure 27

Interaction of Hop with the Cdc37-Hsp90 complex.

(A) Hop was added either in equimolar amounts (orange) or in 4-fold excess (green) to the complex of 150 nM *Cdc37 and 2 µM Hsp90 (red). *Cdc37 alone in black. (B) quantitative evaluation of the Hop–Cdc37–Hsp90 complex formation. Raw sedimentation-velocity runs were evaluated by UltraScan to obtain the complexed and free concentrations of Cdc37 in the presence of Hsp90 at different concentrations of Hop, and the complexed fraction of Cdc37 was

plotted. Separately, we simulated random binding using the binding constant for Cdc37 that best matched the initial decrease in the complexed Cdc37 fraction (red line).

In contrast to *C. elegans*, in the human chaperone system, addition of Hop to *Cdc37-Hsp90 in equimolar concentrations resulted in a displacement of only 25 % of bound *Cdc37 from the complex. The three components formed a complex with a S-value of 8.0 S (**Figure 27a**). Surprisingly, further increased amounts of Hop shifted the peak to 9.4 S, thereby expelling a major fraction of *Cdc37 from the complex. However, even at a Hop concentration of 10 µM (10-fold excess over the Hsp90-dimer) only 75 % of Cdc37 were displaced from the complex (**Figure 27b**). The red line in **Figure 27b** represents the expected curve of Cdc37 displacement from the complex for the assumption that Hop would compete with Cdc37 to bind to Hsp90, demonstrating a preference of a ternary complex formation.

To specify the findings on Cdc37-displacement by Hop, we analyzed the complex formation using a Hop truncation variant in which only the two central TPR-domains of Hop are present ($Hop_{[TPR2A-TPR2B]}$) (**Figure 28**). This Hop construct is nevertheless able to promote survival and client folding in yeast as well as ATPase-inhibition of Hsp90 (Schmid *et al*., 2012).

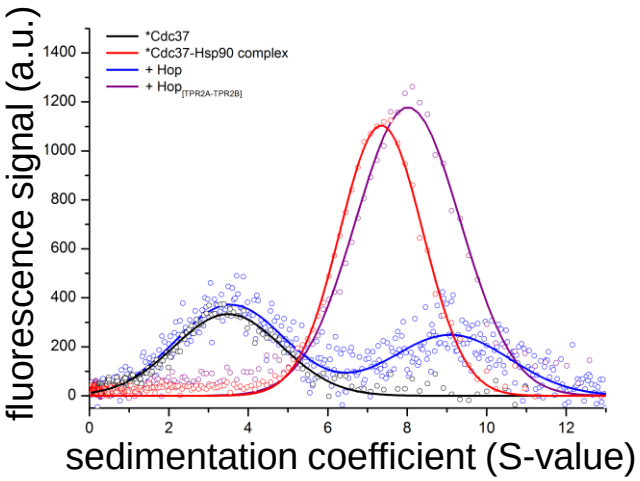

Figure 28

Binding of $Hop_{[TPR2A-TPR2B]}$ to the Cdc37-Hsp90 complex.

Addition of 2 µM $Hop_{[TPR2A-TPR2B]}$ does not expell Cdc37 from Hsp90 and a ternary complex is formed with a S value of 8.0 S.

Addition of $Hop_{[TPR2A-TPR2B]}$ to the *Cdc37-Hsp90 complex in 2-fold excess resulted in a peak shift from 7.1 S to 8.0 S, with no displacement of Cdc37 from the complex,

indicating that the TPR1-, DP1- and/or the DP2-domain of Hop mediates Cdc37-displacement from Hsp90 at high concentrations.

Summarizing, the results suggest that Hop is able to form a ternary complex with Cdc37 and Hsp90 at equimolar concentrations. However, at higher concentrations, a TPR1-, DP1- and/or DP2-domain-dependent partial displacement of Cdc37 is observed. Nevertheless, even at a 10-fold excess of Hop, the cochaperone does not fully displace Cdc37 from Hsp90 and the formation of a ternary complex is possible. In fact, similar to previous studies on the formation of asymmetric yeast Hsp90 complexes with Sti1 and the PPIase Cpr6 (Li *et al.*, 2011), we observe a preference for a ternary complex consisting of Hop, Cdc37 and Hsp90.

3.1.3. Cdc37 and the phosphatase PP5 closely cooperate during an intermediate stage of the kinase maturation cycle

PP5 is a TPR-domain containing phosphatase specifically dephosphorylating Cdc37 (Vaughan *et al*., 2008). Hsp90 is needed for PP5 to facilitate Cdc37-dephosphorylation (Vaughan *et al*., 2008). Furthermore, deletion of the corresponding gene in yeast led to compromised maturation of v-Src kinase (Vaughan *et al.*, 2008*)*. Hence, PP5 seems to represent a key module within the Hsp90 kinase maturation cycle. It has been described previously that PP5 can bind to Hsp90 complexes containing Cdc37 and heme-regulated eIF2α kinase (HRI) in rabbit reticulocyte lysates (Shao *et al*., 2001) and ternary complexes consisting of Cdc37, Hsp90 and Pph5 (a PP5 homologue) were found analyzing the *C. elegans* system (Gaiser *et al*., 2010). To investigate this complex formation, we performed aUC (**Figure 29**) using a PP5 homologue derived from rat, which shares 98 % sequence with human PP5.

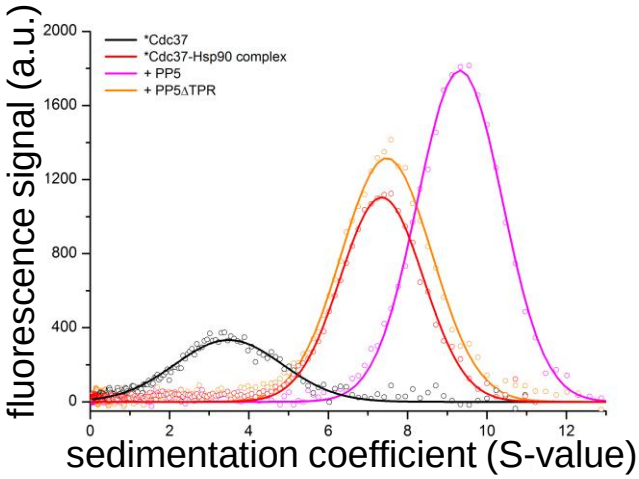

Figure 29

Binding of PP5 to the Cdc37-Hsp90 complex.

150 nM *Cdc37 (black) was mixed with 2 µM Hsp90 in the absence (red) or presence of 2 µM rat PP5 (magenta) or a PP5-construct missing the TPR-domain (PP5ΔTPR, orange).

Addition of PP5 to the Cdc37-Hsp90 complex shifted the peak from 7.1 S to a S-value of 9.3 S (**Figure 29**). Most probably, the revealing complex included the three components *Cdc37, Hsp90 and PP5. Thus, exhaustive binding of *Cdc37 took place, arguing for a preference of the kinase cochaperone to enter the Hsp90-PP5 complex. The complete loss of interaction between PP5 and the Cdc37-Hsp90 complex upon deletion of PP5's TPR-domain indicates that this domain may bind to the MEEVD-motif of Hsp90 (**Figure 29**).

Next, we were interested whether PP5 would be able to displace Hop from the Cdc37-Hsp90 complex and from Hsp90 alone. By using labelled Hop (*Hop), we were able to observe by aUC that PP5 weakens the binding of Hop to Hsp90 and to the Cdc37-Hsp90 complex at equimolar concentrations (**Figure 30**).

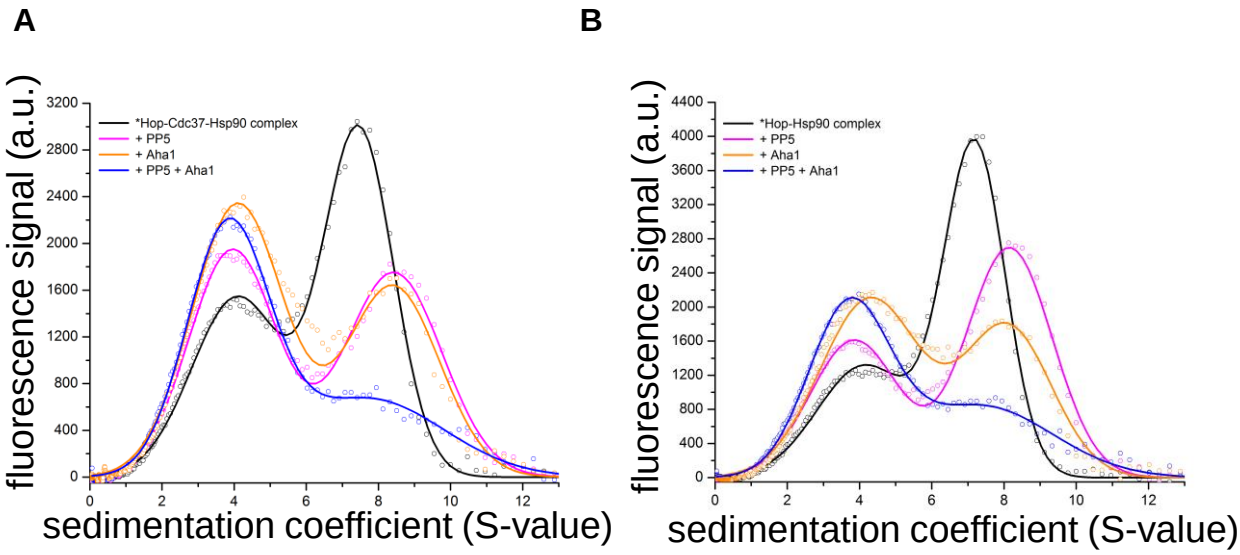

Figure 30

Hop is synergistically displaced from Hsp90 complexes by Aha1 and PP5.

(A) 150 nM labelled human Hop (*Hop) was mixed with 2 µM Hsp90 and 2 µM Cdc37 (black) in the presence of either 2 µM PP5 (magenta) or 2 µM human Aha1 (orange) and with both 2 µM PP5 and 2 µM Aha1 (blue). The same experiment was conducted in the absence of Cdc37 (B)

Interestingly, a mixed complex consisting of Hsp90, Cdc37, Hop and PP5 is formed with an S-value of 8.5 S (**Figure 30a**). Similar to previous results analyzing mixed Hsp90 complexes using yeast Hop/Sti1 and Cpr6 (Li *et al*., 2011), we found here that Aha1 is needed to displace Hop from the human Hsp90 complex. Neither PP5 nor Aha1 alone were able to displace Hop from the complex completely, but only the combination of both cochaperones expelled the Hsp70-connector Hop from the Hsp90-Cdc37-complex (**Figure 30**). Interestingly, the displacement of Hop from Hsp90 by Aha1 and PP5 could also be observed in the absence of Cdc37 (**Figure 30b**).

It has been shown previously that Cdc37 co-purified with exogenously expressed Cpr7, a PPIase from yeast (Abbas-Terki *et al*., 2002). Hence, we were interested if human PPIases could also bind to the Cdc37-Hsp90 complex. To investigate this potential interaction, we performed aUC combining *Cdc37-Hsp90 and the human PPIases Cyp40, FKBP51 and FKBP52 (**Figure 31**).

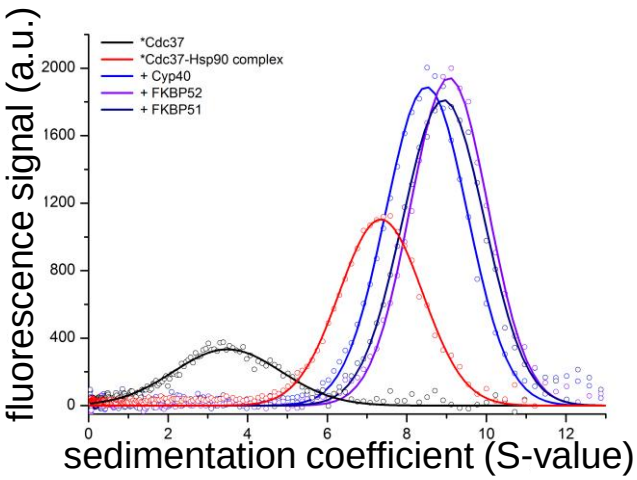

Figure 31

Human PPIases bind to the Cdc37-Hsp90 complex.

150 nM *Cdc37 (black) was mixed with 2 µM Hsp90 in the absence (red) or presence of 2 µM Cyp40 (blue), FKBP51 (deep blue) or FKBP52 (violet).

All tested PPIases were able to bind to the Cdc37-Hsp90 complex. Thereby the addition of of Cyp40 shifted the peak of the Cdc37-Hsp90 complex with a S-value of 7.1 S to a peak with a S-value of 8.5 S. FKBP51 and FKBP52 both bound to the Cdc37-Hsp90 complex yielding S-values of 8.9 S and 9.1 S, respectively (**Figure 31**, **Table 4**).

3.1.4. Cdc37 is displaced from Hsp90 by the combination of Aha1 and ATP-binding

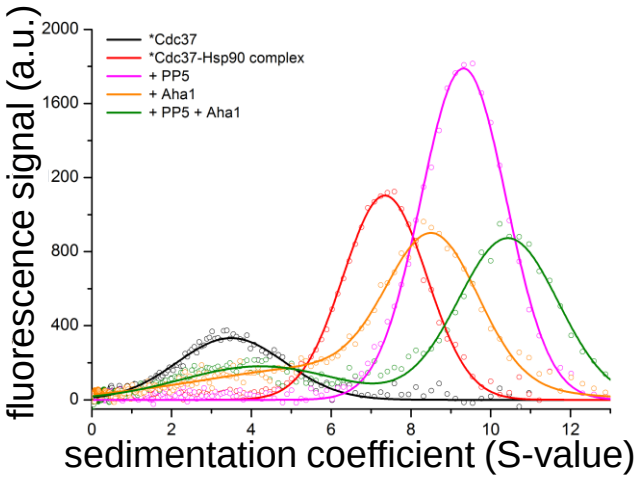

Figure 32

A quaternary complex is formed between Cdc37, Hsp90, PP5 and Aha1.

aUC runs of 150 nM *Cdc37 in the absence (black) or presence of 2µM Hsp90 (red). 2 µM PP5 (magenta) and 2 µM Aha1 (orange) were added to the *Cdc37-Hsp90 complex either alone or in combination (green).

It is known that Aha1 plays an important role for the maturation of kinases in *S. cerevisiae* (Panaretou *et al., 2002,* Meyer *et al*., 2004) and human cells (Xu *et al*., 2012) and has been shown to bind Cdc37-Hsp90 complexes in *S. cerevisiae* and *C. elegans* (Panaretou *et al.,* 2002, Gaiser *et al.*, 2010). Hence, we aimed to investigate the complex formation with Aha1 in the human context (**Figure 32**). To this end, we added Aha1 to *Cdc37-Hsp90. We found a ternary complex with a S-value of 8.5 S. Similar to characteristics of components derived from *C. elegans* (Eckl *et al.*, 2013), Aha1 bound to the complex, only moderately reducing the affinity of Cdc37 for Hsp90. Furthermore, we were interested if Aha1 could bind to a complex consisting of Cdc37, Hsp90 and PP5. Remarkably, addition of Aha1 to *Cdc37, Hsp90 and PP5 yielded a quarternary complex with a S-value of 10.5 S (**Figure 32**).

Since during this stage of the Hsp90 cycle, ATP is believed to bind to the chaperone (Li *et al.,* 2013), we were interested how the nucleotide would influence this complex. When ATP was added to the *Cdc37-Hsp90-Aha1 complex, displacement of Cdc37 from Hsp90 took place (**Figure 33**).

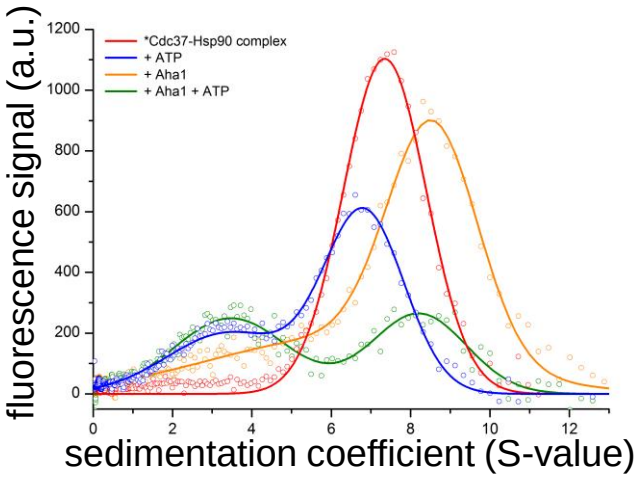

Figure 33

Cdc37 is expelled from Hsp90 by Aha1 and ATP.

aUC runs of 150 nM *Cdc37 in the presence of 2 µM Hsp90 (red). 2 µM Aha1 (orange) or 2 mM ATP (blue) were added either alone or in combination (green).

Surprisingly, this effect differs from observed nucleotide effects in *C. elegans*. Notably, in the nematode displacement of Cdc37 from an Aha1-Hsp90 complex takes place at the ATP hydrolysis stage mimicked by the nucleotide analogue AMP-PNP (Gaiser *et al.*, 2010) and not in the presence of ATP, emphasizing the evolutionary differences of the two Hsp90-machineries.

To analyze the observed expulsion of Cdc37 from Hsp90 in a kinetic manner, we developed a FRET system. For that, in lack of a human system, we used the established platform of a single cysteine variant of yeast Hsp90 (Hessling *et al*., 2009). By titrating randomly Alexa488-labelled human *Cdc37 to M-domain (Cys385) Atto550-labelled yeast *Hsp90, an energy transfer between the two chromophores could be observed (**Figure 34**).

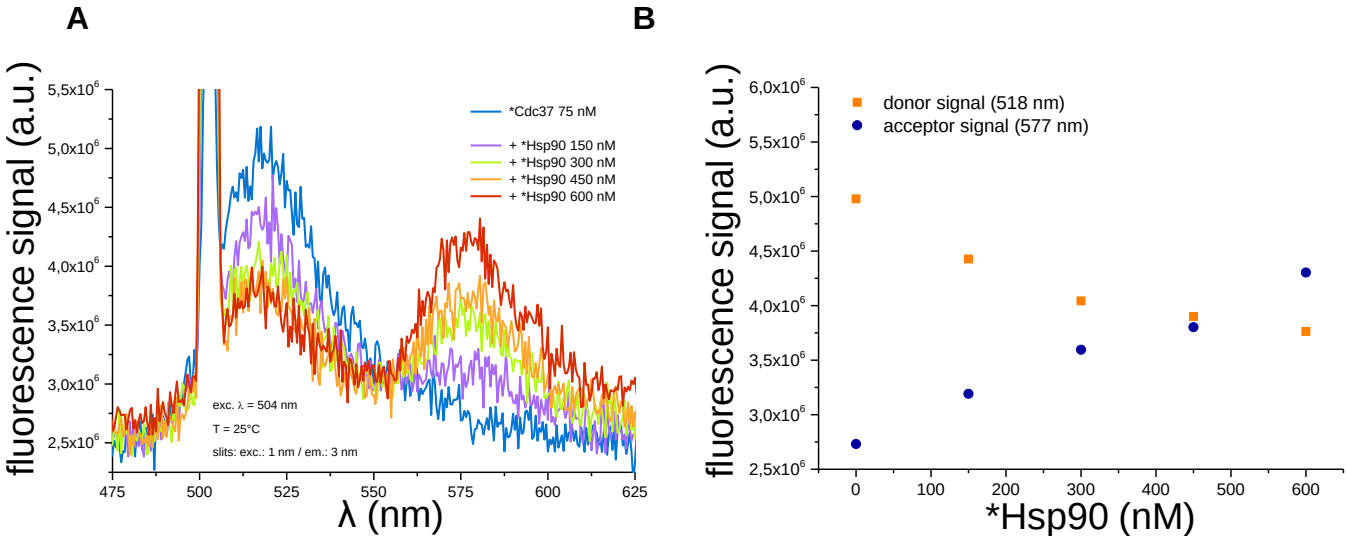

Figure 34

Concentration dependent FRET between *Cdc37 and *yHsp90.

Titration of *Cdc37 to M-domain labelled yeast *Hsp90. The FRET pair was excited at 504 nm. In (A) the spectra from 475 nm to 625 nm and in (B) the maximum peak intensities at 518 nm and 577 nm at increasing *Hsp90 concentrations are shown.

We used this FRET system further to monitor the expulsion of human Cdc37 from yeast Hsp90 by Aha1 and ATP (**Figure 35**).

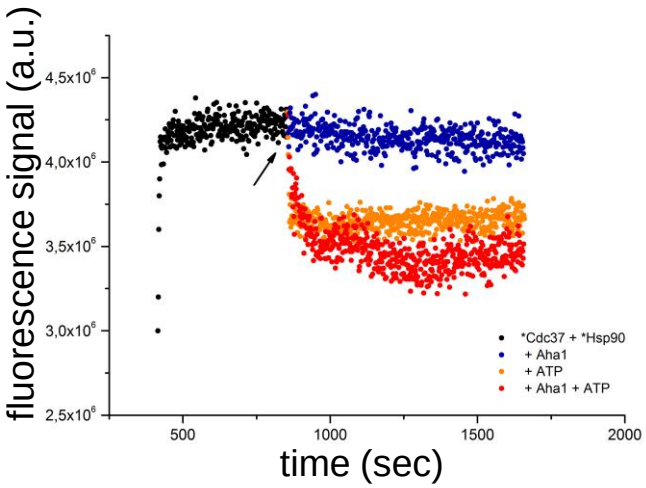

Figure 35

FRET measurements using randomly labelled human *Cdc37 and M-domain specifically labelled yeast *Hsp90.

After association of 75 nM *Cdc37 to 300 nM *Hsp90 (black) 2 µM Aha1 (blue) and 2 mM ATP (orange) were added either alone or in combination (red). The time point of addition is indicated by a black arrow.

Interestingly, Aha1 alone did only moderately contribute to a displacement of Cdc37 from the complex. Only in the presence of ATP, the main fraction of Cdc37 was expelled from Hsp90 (**Figure 35**). Thus, ATP and Aha1 cooperated during Cdc37 release. Partial Cdc37 dissociation by ATP alone could be observed and was very fast ($t_{1/2}$ ~ 3 sec), whereas full dissociation of Cdc37 from Hsp90 by the addition of ATP and Aha1 seems to be a slower process, only completed after roughly 300 sec ($t_{1/2}$ ~ 30 sec), indicating the involvement of slow rate-limiting steps, such as ATP-hydrolysis.

Given the aUC results revealing the existence of a quaternary *Cdc37-Hsp90-PP5-Aha1 complex, we asked whether displacement of Cdc37 by ATP would also be possible in the presence of PP5. Fluorescence detection of *Cdc37 in an aUC experiment revealed that displacement of Cdc37 via ATP took place in the presence of PP5, similarly to the effect of ATP in the absence of PP5 (**Figure 36**).

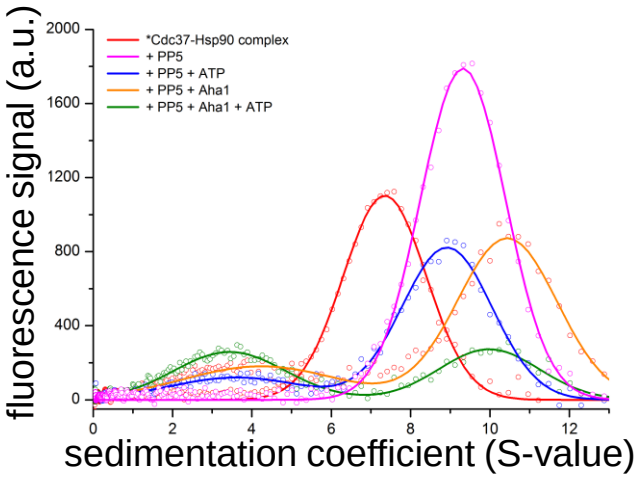

Figure 36

Aha1-ATP mediated Cdc37 displacement takes place in the presence of PP5.

aUC runs of 150 nM *Cdc37 in the presence of 2 µM Hsp90 (black) and 2 µM PP5 (marine). 2 µM Aha1 (red) and 2 mM ATP (magenta) were added either alone or in combination (blue).

Displacement of the kinase cochaperone by Aha1 and ATP is not increased in the presence of the phosphatase in comparison to Aha1 and ATP alone, suggesting that Aha1-ATP mediated Cdc37 displacement is PP5 independent.

After displacement of Cdc37 from the quaternary complex consisting of Cdc37, Hsp90, PP5 and Aha1, we wondered whether a ternary complex with all the components, but without Cdc37 would be able to remain. To observe such a potentially existing complex consisting of Hsp90, PP5 and Aha1, we fluorescently labelled human Aha1 and analyzed its binding to Hsp90 in the presence and absence of PP5 (**Figure 37**).

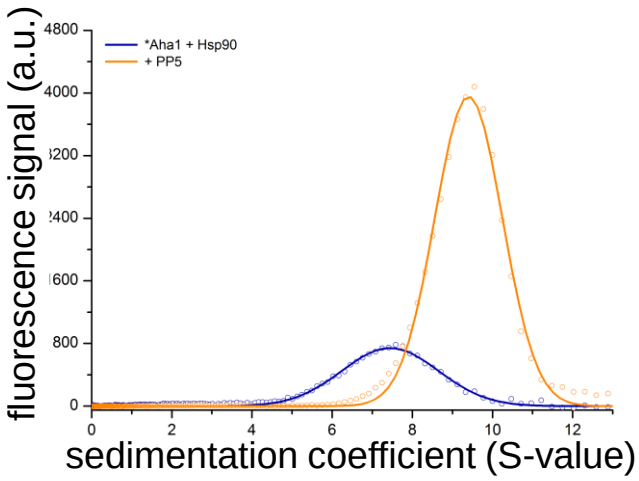

Figure 37

PP5 binds to the Aha1-Hsp90 complex.

150 nM of labelled Aha1 (*Aha1) was mixed with 2 µM Hsp90 (blue) and 2 µM PP5 (orange).

The complex consisting of Aha1 and Hsp90 revealed a single peak with a S-value of 7.5 S, indicating exhaustive binding of Aha1 to Hsp90 under these conditions (**Figure 37**). Addition of PP5 to this complex resulted in a peak shift to a S-value of 9.4 S (**Figure 37**). This indicates that all Aha1 molecules are interacting with Hsp90-PP5 complexes and that this ternary complex formation is possible.

All S-values of the observed complexes are summarized in **Table 4**.

Table 4 S-values for Hsp90 complexes.

Species	S-value (S)
*Cdc37	3.5
*Cdc37-Hsp90	7.1
*Cdc37-Hsp90-Hop (1 : 1)	8.0
*Cdc37-Hsp90-Hop (1 : 2)	9.4
*Cdc37-Hsp90-$Hop_{TPR2A2B}$	8.0
*Cdc37-Hsp90-PP5	9.3
*Cdc37-Hsp90-Aha1	8.5
*Cdc37-Hsp90-PP5-Aha1	10.5
*Cdc37-Hsp90-Cyp40	8.5
*Cdc37-Hsp90-FKBP51	8.9
*Cdc37-Hsp90-FKBP52	9.1
*Hop	3.9
*Hop-Hsp90-Cdc37	7.4
*Hop-Hsp90-Cdc37-PP5	8.5
*Aha1-Hsp90	7.5
*Aha1-Hsp90-PP5	9.4

The S-values were obtained from the aUC experiments. The concentration of the fluorescently labeled component was 150 nM, of the unlabeled components 2 uM and of nucleotides 2 mM, if not stated otherwise. The aUC was performed in a Beckman XL A analytical ultracentrifuge equipped with an AVIV-FIS fluorescence detection system (AVIV Biomedical, Lakewood, USA) at 42,000 rpm.

3.2. Chaperoning of v-Src kinase in vitro

3.2.1. Hsp90-dependent chaperoning of v-Src in vitro

It is well established that v-Src kinase activity is strictly Hsp90-dependent *in vivo* (Nathan & Lindquist, 1995, Taipale *et al*., 2012). Furthermore, v-Src requires the Hsp90 co-chaperone Cdc37 to reach full activity in the cell (Brugge, 1986, Xu & Lindquist, 1993). Strikingly however, Hsp90 does not affect the highly homologous cellular form of v-Src, c-Src (Xu & Lindquist, 1993). We aimed to reconstitute the effects of Hsp90 on v-Src activity *in vitro*. To this end, we purified the v-Src and c-Src kinases from insect cells (*S. frugiperda*, *Sf*9) and determined the influence of Hsp90 on Src activity (**Figure 38a**). When we tested the effect of Hsp90 on c-Src kinase we could not observe a significant change in its activity (**Figure 38b**). In contrast, for v-Src in the presence of Hsp90 this resulted in a 3-fold increase in activity (**Figure 38b**).

A

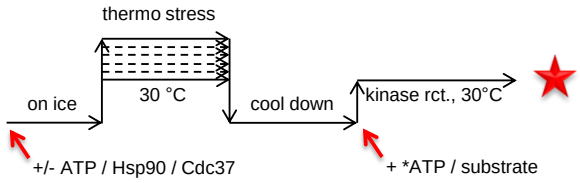

B

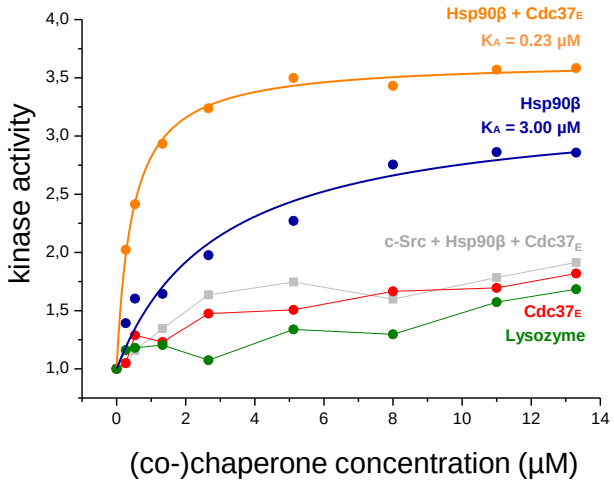

Figure 38

***In vitro* influence of Hsp90 on Src kinase.**

(A) Assay-scheme for the *in vitro* stabilization and activation of Src kinase by chaperones. Prior to transphosphorylation Src was preincubated for 10 min on ice in the presence or absence of

Hsp90 (and / or Cdc37 variants) and 20 µM ATP, followed by 10 min at increasing temperatures (stabilization) or 30 °C (activation) and 10 min incubation on ice. (B) v-Src kinase activation by chaperones *in vitro*. Hsp90β (blue) and Cdc37-S13E ($Cdc37_E$) (red) were titrated either alone or in combination (orange) to v-Src kinase and compared to a lysozyme control (green). Hsp90β together with $Cdc37_E$ had no significant effect on c-Src (grey).

In vivo experiments had suggested that phosphorylation of Cdc37 at Ser13 is involved in the regulation of its function (Shao *et al*., 2003, Vaughan *et al*., 2008). Therefore we used a Cdc37 variant in which the phosphorylation was mimicked by a glutamate substitution (Cdc37-Ser13Glu yielding $Cdc37_E$). This variant alone had no significant influence on v-Src (**Figure 38b**). However together with Hsp90, we observed an almost 4-fold increase in its activity. Importantly, the combination of Hsp90 and $Cdc37_E$ increased the apparent affinity towards the kinase by roughly 15-fold, reflected by the activation constants, K_A, obtained from a Michaelis-Menten fit. For Hsp90β, we obtain a K_A value of 3.0 µM, whereas for the combination of Hsp90β and $Cdc37_E$, the K_A value decreased to 0.23 µM (**Figure 38b**).

This activating effect of Hsp90 and Cdc37 is ATP-dependent as shown by the addition of the Hsp90 inhibitor Radicicol during the reaction (**Figure 39**), in which the activity of v-Src decreased to its basal, Hsp90-independent level.

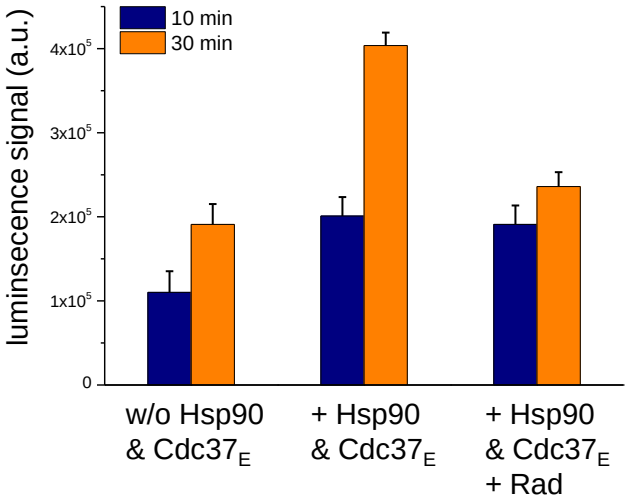

Figure 39

Effect of Radicicol on the ability of Hsp90 to activate v-Src.

10 min after starting the kinase reaction, 250 µM Radicol was added and kinase activity was analyzed after 30 min.

This shows that v-Src kinase activation is constantly dependent on Hsp90.

To gain more insight into the kinase activating mechanism, facilitated by Hsp90 and Cdc37, we tested additional combinations of Hsp90 and Cdc37 variants and other chaperones on their influence on v-Src kinase activity. **Figure 40** shows a summary of the observed effects.

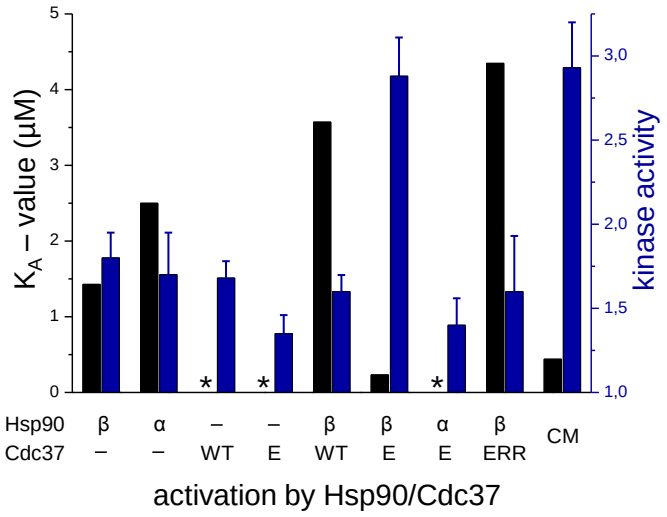

Figure 40

Effects of different chaperone combinations on v-Src activity.

Activation of v-Src by different combinations of Hsp90β (β) or Hsp90α (α) and $Cdc37_E$ (E), $Cdc37_{WT}$ (WT), a non-Hsp90-binding Cdc37 mutant (Cdc37-S13E-M164R-L205R, $Cdc37_{ERR}$ (ERR)) and a chaperone-mix including Hsp90β, $Cdc37_E$, Hdj-1 (Hsp40), Hsp70 and Hop (CM). Depicted are the activation constants K_A (black bars) and the kinase activity at a (co-)chaperone concentration of 1.3 µM (blue bars). A black asterisk indicates activation curves for which no activation constant was calculable.

Surprisingly, only the human Hsp90 isoform, Hsp90ß, but not the Hsp90-α isoform, was active in chaperoning v-Src kinase (**Figure 40**).

Consistent with the literature, only the phospho-mimicking mutant of Cdc37 ($Cdc37_E$) and not $Cdc37_{WT}$ was able to increase the activation of v-Src by Hsp90.

To test whether the interaction between $Cdc37_E$ and Hsp90 is required for the increase in apparent affinity towards v-Src, we made use of a $Cdc37_E$ mutant defective in Hsp90 binding ($Cdc37_{ERR}$; Smith *et al*., 2013). We found that this variant was incapable of kinase activation in the presence of Hsp90, suggesting that the formation of a complex between Cdc37 and Hsp90 is important for activating v-Src (**Figure 40**).

Further, we could not observe a significant increase in kinase activation by the addition of Cdc37-Hsp90 together with the Hsp70 chaperone system (Hsp70, Hsp40 and Hop) to v-Src (**Figure 40**), indicating that after purification from *Sf*9 cells, the kinase might have undergone folding and resides in a folded, but not yet activated state.

These findings suggest that Hsp90β together with phosphorylated Cdc37 are the key players responsible for activating the client kinase.

To analyze how Hsp90 couples ATP-binding and -hydrolysis to v-Src activation and stabilization, we used two well-characterized ATPase-deficient variants of human Hsp90β and tested them for activation of Src kinase (**Figure 41**).

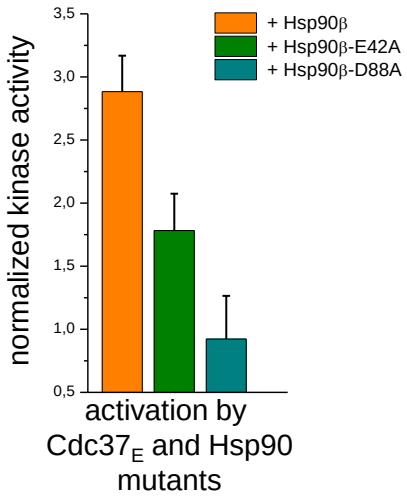

Figure 41

Involvement of the ATPase activity of Hsp90 in the activation process.

Influence of the Hsp90β ATPase-deficient mutants Hsp90β-E42A and Hsp90β-D88A with $Cdc37_E$ on v-Src activation at 1.3 µM chaperone concentration.

Hsp90-E42A binds ATP but does not hydrolize it. Hsp90-D88A on the other hand neither binds nor hydrolizes ATP (Obermann *et al.*, 1998, Panaretou *et al*. 1998). Analysis of these Hsp90 mutants showed that Hsp90-D88A in combination with $Cdc37_E$ did not affect v-Src activity, whereas Hsp90-E42A was able to activate v-Src about 2-fold (**Figure 41**). ATP binding by Hsp90 is thus mandatory and hydrolysis increases the performance of Hsp90.

It has been reported that in addition to prohibit ATP-hydrolysis, the E42A-mutation in Hsp90 would also lead to a lower affinity for Cdc37 (Jiang et al., 2010). To exclude that the observed effects of Hsp90 and Cdc37 on v-Src kinase activity are due to a lower concentration of chaperone-cochaperone complexes, we determined the K_D of Cdc37 and Hsp90-E42A and compared this to the interaction with wildtype Hsp90.
For that we titrated Hsp90-mutant or -wildtype to fluorescently labelled *Cdc37 and subjected the complex to aUC (**Figure 42**).

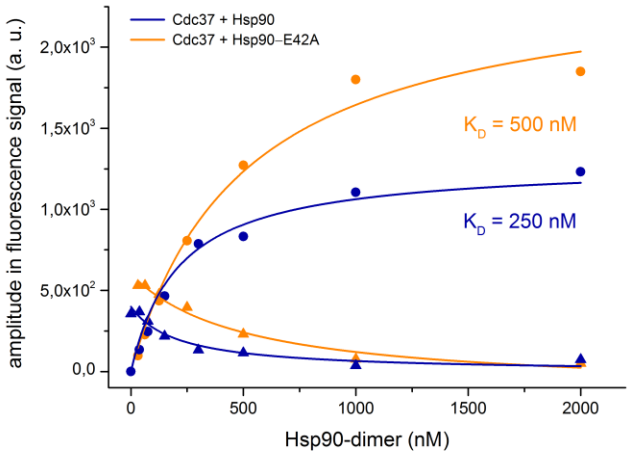

Figure 42

Determination of the K_D of complex formation of Cdc37 and Hsp90 and Hsp90-E42A.
150 nM *$Cdc37_E$ and increasing amounts of Hsp90 (blue) and Hsp90-E42A (orange) were mixed and subjected to aUC. The amplitude fluorescence signals of the observed monomer- and complex-peak of the aUC runs were plotted and fit with the Michealis-Menten model to reveal the respective K_D.

Consistent with the results from Jiang *et al*. (2010), we observe a weakened binding of the Hsp90-E42A mutant to Cdc37 in comparison to wildtype Hsp90. However, the observed effects on the activation of v-Src kinase are not due to this lower affinity of Hsp90-E42A for Cdc37, since the used concentrations of Hsp90 and Cdc37 in the v-Src activation assay (1.3 µM) lie within the saturation of the Cdc37-Hsp90 complex.

It is established that v-Src is less stable than c-Src against thermal unfolding (Falsone *et al*., 2004). We thus asked whether Hsp90 could stabilize v-Src kinase at elevated temperatures. To this end, we incubated v-Src at different temperatures with Hsp90 or in the presence of both Hsp90 and $Cdc37_E$ (**Figure 43**).

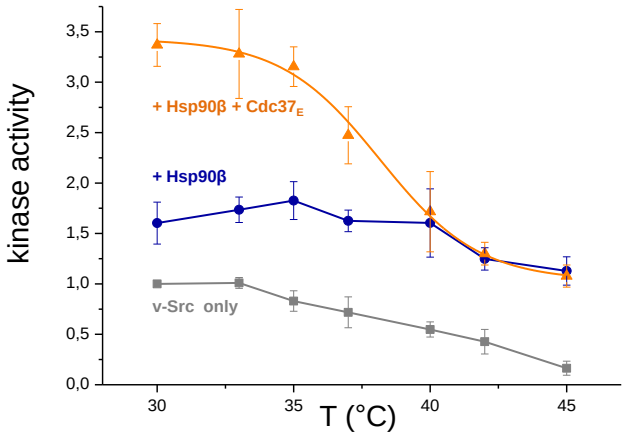

Figure 43

Influence of Hsp90 and $Cdc37_E$ on v-Src during exposure to elevated temperatures.
v-Src was incubated at different temperatures with 20 µM ATP in the absence (grey) or presence of 1.3 µM Hsp90 (blue) or 1.3 µM Hsp90 and 1.3 µM Cdc37 (orange).

With increasing temperatures, v-Src alone rapidly lost its activity compared to c-Src (**Figure 43**). However, in the presence of Hsp90β, the loss of kinase activity was prevented. Remarkably, this stabilizing effect became Cdc37-independent at higher temperatures (**Figure 43**) as two curves representing the Cdc37-Hsp90 and Hsp90-only effects converge at around 40 °C.

We next sought to analyze this Hsp90-dependent stabilization effect in more detail (**Figure 44**).

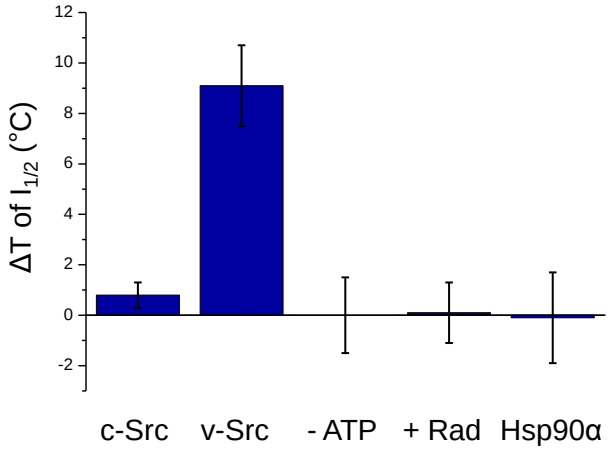

Figure 44

Stabilization of c-Src and v-Src by Hsp90 and ATPase-dependence of the process.
Plotted are the changes in the temperature (ΔT) of half-maximal inactivation ($I_{1/2}$). Leaving out ATP or addition of the Hsp90 inhibitor Radicicol during the preincubation steps of v-Src compromised the ability of Hsp90 to rescue v-Src from inactivation. Unlike Hsp90β, Hsp90α was not able to stabilize v-Src.

Interestingly, in the presence of Hsp90 the temperature of half-maximal inactivation $I_{1/2}$ was shifted by 9 °C (**Figure 44**). Thus, the apparent stability corresponded to that of c-Src. For c-Src the presence of Hsp90 did not affect the inactivation process (**Figure 44**). The stabilizing effect of Hsp90ß (but not Hsp90α) on v-Src was dependent on its ATPase activity as the effect required the presence of ATP and could be suppressed by the addition of Radicicol (**Figure 44**).

To correlate conformational changes and ATP-hydrolysis of Hsp90 to this process, we tested the influence of ATPase-deficient Hsp90 mutants.

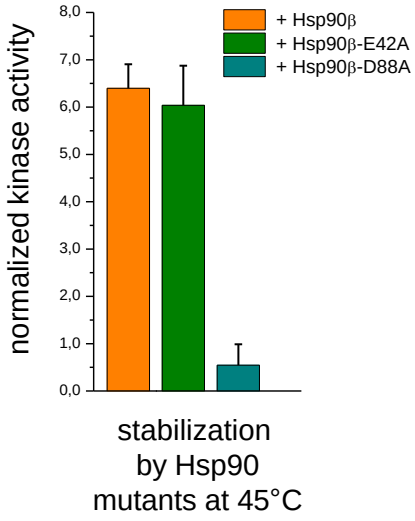

Figure 45

Stabilization of v-Src by Hsp90 ATPase-deficient mutants.

Influence of the Hsp90β ATPase-deficient mutants Hsp90β-E42A and Hsp90β-D88A at 1.3 µM on v-Src stabilization at 45 °C.

We found that Hsp90-D88A could not stabilize v-Src, which is in agreement with the necessity of ATP for this reaction (**Figure 45**). Intriguingly however, Hsp90-E42A was able to stabilize v-Src similar to wildtype Hsp90 (**Figure 45**), implying that ATP-binding is sufficient for this effect.

3.2.2. Src chimera reveal client features of v-Src

Having reconstituted the Hsp90-dependent chaperoning of v-Src kinase *in vitro*, we probed factors that render v-Src a chaperone client but leave c-Src unaffected.

Viral Src kinase differs from its cellular isoform c-Src in only a few amino acids and in the absence of the C-terminal tail (**Figure 46**).

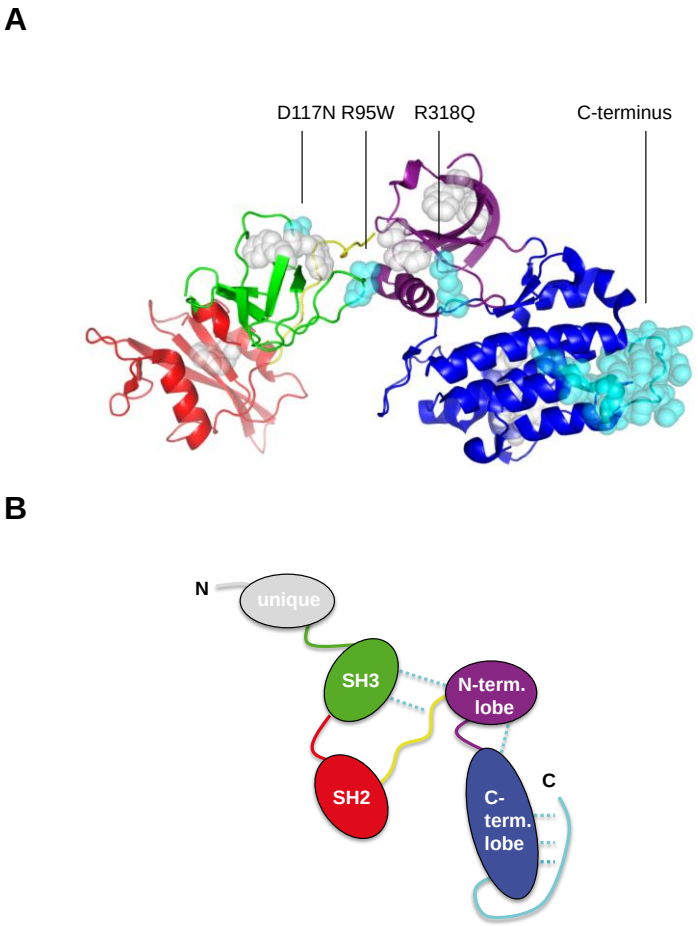

Figure 46

Design of a Hsp90 client kinase by alteration of specific elements.

(A) Structure of c-Src (PDB: 1Y57). Coloring from N- to C-terminus: SH3-domain in green, SH2-domain in red, linker connecting SH2-domain and N-lobe of the kinase domain in yellow, kinase domain N-lobe in violet and C-lobe in blue. Tryptophan residues are depicted as white spheres. The mutated or deleted residues in the c-Src variants are depicted as blue spheres. (B) Schematic representation of c-Src. Colors are the same as in the crystal structure. The unique domain, which is missing in the crystal structure, is shown in grey. Intramolecular contacts made by the mutated residues are represented by dotted light blue lines.

Specifically, three mutations have been shown to be responsible for the transforming potential of v-Src (Iba *et al.*, 1984, Kato *et al.*, 1986, Miyazaki *et al.*, 1999). These

point mutations are located in the SH3–linker–kinase domain interface. To determine how these changes affect the function of the kinase as well as its structure and Hsp90-dependence, we created chimera of c-Src. In the c-Src variant c-Src3M, three residues were exchanged for their respective residues in v-Src (R95W, D117N and R318Q). Furthermore, we created a c-Src variant, in which the C-terminal tail of c-Src was deleted (c-SrcΔC) and finally we combined both elements in the variant c-Src3MΔC.

To test the activity of the generated c-Src mutants *in vivo*, we expressed these variants in *S. cerevisiae.* v-Src is known to be highly toxic for yeast, whereas c-Src does not affect yeast growth (Xu & Lindquist, 1993).

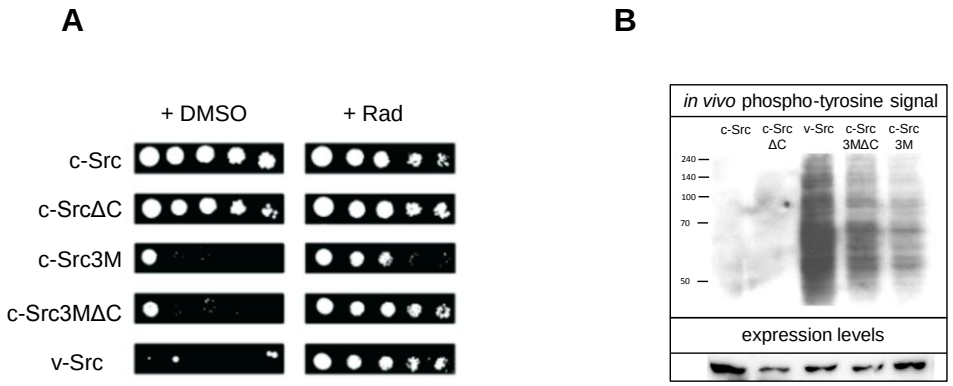

Figure 47

Activity and expression levels of Src variants *in vivo.*

(A) Serial dilutions of *S. cerevisiae* expressing different Src variants in the absence or presence of the Hsp90 inhibitor Radicicol in the medium. (B) *In vivo* activity of Src was tested by detecting phospho-tyrosines in yeast lysates. In addition, Src expression levels were determined by a Src specific antibody.

We were able to reproduce these findings and also show that the expression of c-Src3M and c-Src3MΔC led to a reduced growth of yeast, though to a lesser extent as compared to v-Src (**Figure 47a**). c-SrcΔC did not affect yeast viability. Apparently, the three introduced point mutations are responsible for the compromised growth observed in yeast. To test for a possible Hsp90-dependence of the Src variants, cells were analyzed in the presence of the Hsp90 inhibitor Radicicol (**Figure 47a**). Upon Hsp90 inhibition, yeast cells exhibited less pronounced lethality in the case of c-Src3M and normal growth upon expression of v-Src and c-Src3MΔC. Thus, the

toxic effect of c-Src3MΔC and v-Src was much more Hsp90-dependent than that of c-Src3M and the Hsp90-dependence is largely caused by the missing regulatory C-terminal tail in v-Src. To further investigate Src kinase activity *in vivo*, we analyzed the presence of phospho-tyrosines in yeast proteins (**Figure 47b**). For c-Src and c-SrcΔC, no phospho-tyrosines were detectable. However, for c-Src3M, c-Src3MΔC and v-Src, a distinct phosphorylation pattern appeared. The intensity increased from c-Src3M to c-Src3MΔC with v-Src exhibiting the most pronounced effects. Interestingly, *in vivo* activity did not seem to correlate with protein abundance (**Figure 47b**). The expression of the toxic c-Src3M mutant was increased, although this kinase showed less activity relative to the c-Src3MΔC and v-Src variants. Furthermore, the mutants with a deleted C-terminal tail were less abundantly expressed, indicating a lower stability of these constructs (**Figure 47b**).

Next, we tested the different Src variants for their potential to be activated by Hsp90 and $Cdc37_E$ *in vitro*.

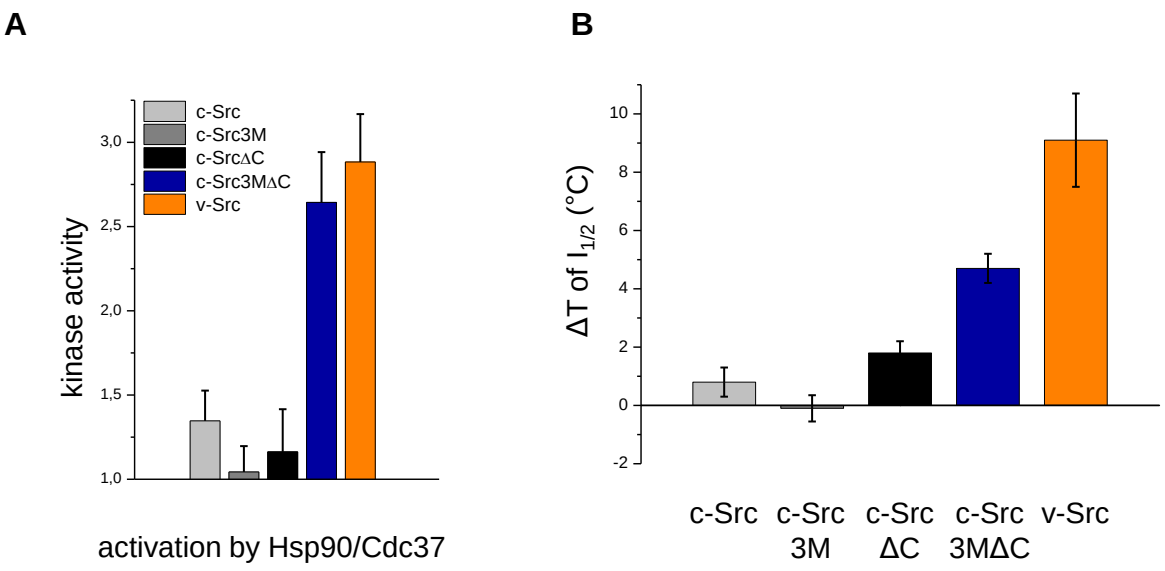

Figure 48

Activation and stabilization of Src variants *in vitro.*

(A) Activation of Src variants by 1.3 µM Hsp90β and $Cdc37_E$. (B) Stabilization of Src variants by 1.3 µM Hsp90β is represented as the increase in the temperature of half-maximal inactivation.

We found that v-Src and c-Src3MΔC were readily activated whereas, in accordance with the *in vivo* results on their Hsp90-dependence, c-Src, c-SrcΔC and c-Src3M

showed only low activation potential (**Figure 48a**). This was consistent with the observation of a lower *in vivo* activity of c-Src3M regardless of its robust expression. A similar picture emerged under heat shock conditions: c-Src3M and c-SrcΔC were not significantly stabilized and, in contrast, the inactivation of c-Src3MΔC and v-Src was strongly affected by Hsp90 (**Figure 48b**).

3.2.3. What renders a kinase Hsp90-dependent?

The set of mutants allowed defining characteristics which correlate with differences in Hsp90-dependence. When comparing the activity of the different Src variants, we found that isolated v-Src has a 4-fold higher activity than c-Src (**Figure 49**).

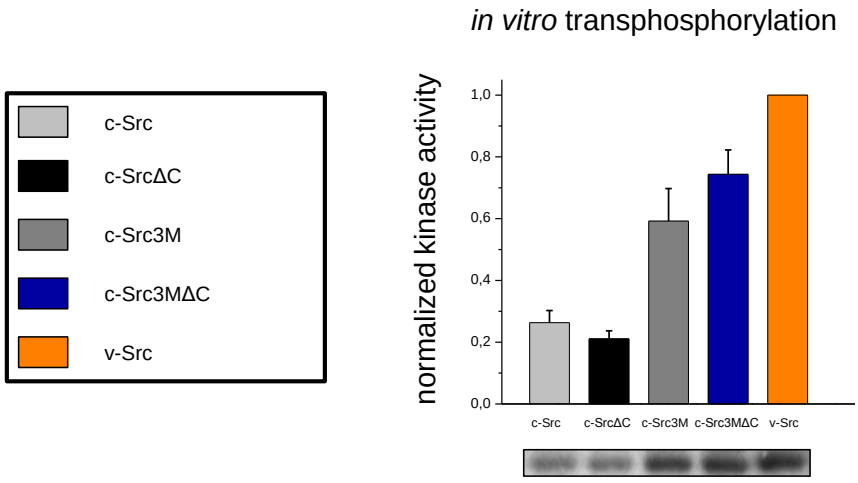

Figure 49

***In vitro* kinase activity of Src variants.**

Kinase activity was determined as decribed and normalized to v-Src.

In agreement with results from the *in vivo* activity (**Figure 47**), deletion of the C-terminal tail in c-Src did not significantly alter the activity of the kinase. Introduction of the three point mutations (c-Src3M) however, led to a nearly 2.5-fold activation of c-Src, while the combination of the amino acid substitutions and the C-terminal deletion (c-Src3MΔC) gave rise to a 3-fold increase (**Figure 49**). It is noteworthy that c-Src and c-SrcΔC did not show detectable activity in yeast, but were active as purified proteins *in vitro*. Overall, the activities of the three toxic kinase variants were comparably increased *in vitro*.

To gain more insight in the meachnism by which c-Src and v-Src are activated upon autophosphorylation, we designed a catalytically inactive variant of c-Src and v-Src by introducing a point mutation (K295R) within the active center (Snyder *et al.*, 1985). We then used these variants to determine whether autophosphorylation in c-Src and v-Src occurs in *cis* or in *trans* (**Figure 50**).

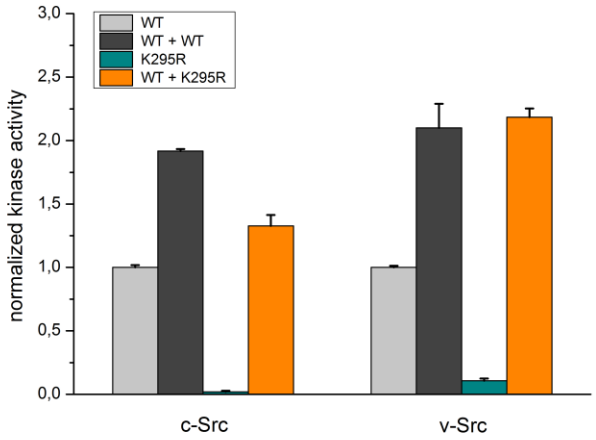

Figure 50

***In vitro* autophosphorylation of c-Src and v-Src and their inactive counterparts c-SrcK295R and v-SrcK295R.**

Kinase activities of wildtype c-Src and v-Src were determined either at 320 nM (grey) or 640 nM (dark grey) and normalized to the respective activity at 320 nM. 320 nM of the corresponding inactive K295R-mutant was added to 320 nM of active c-Src and v-Src, respectively (orange). The activities of 320 nM of inactive mutants alone are shown in green.

Figure 50 shows that for c-Src as well as for v-Src, the catalytically inactive variant of the respective kinase serves as a substrate for the active wildtype kinase. Thus, Src autophosphorylation takes place in *trans*. The increased activity of v-Src compared to c-Src is reflected in the increased amount of phosphorylated kinase during incubation.

Next, we determined the K_M for the five different designed Src kinase variants for ATP (**Figure 51**).

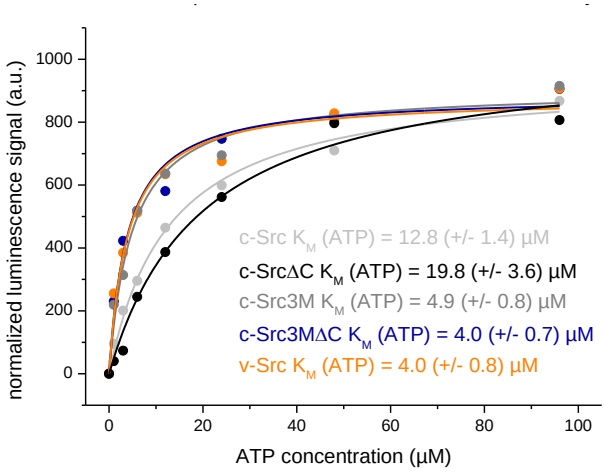

Figure 51

K_M determination of Src variants for ATP measured by radioactive kinase assay.

The different Src variants were subjected to the standard kinase activity assay with increasing amounts of ATP, keeping the ratio of not radioactive ATP and radioactive ATP constant.

Consistent with the literature, the K_M of c-Src for ATP was in the ~13 µM range (Meyn *et al.*, 2005) (**Figure 51**, **Table 5**). We found that the K_M of c-SrcΔC was slightly increased to about ~20 µM. Notably, all Src variants carrying the three point mutations showed a 3- to 5-fold increase in the ATP affinity with K_M values of ~4 µM.

To determine the stability of the Src variants, we incubated each of them at elevated temperatures and measured their activities (**Figure 52**).

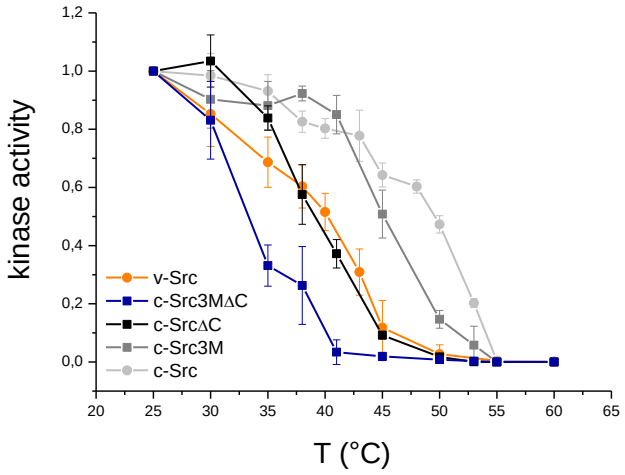

Figure 52

Inactivation patterns of Src constructs under various conditions.

Thermal inactivation of 320 nM of kinase variants. Prior to the transphosphorylation reaction, Src variants were preincubated for 10 min at increasing temperatures. The values are averages of at least three independent experiments.

In agreement with previous results (Falsone *et al.*, 2004), c-Src lost its activity at higher temperatures compared to v-Src (**Figure 52**). The temperature of half-maximal kinase activity ($I_{1/2}$) was 49.5 °C for c-Src and 40.2 °C for v-Src (**Table 5**). The C-terminal tail contributes significantly to the loss of activity of v-Src already at moderate temperatures. The additional three single amino acid substitutions (c-Src3MΔC) destabilized the protein even further with an $I_{1/2}$ of 33.3 °C. In summary, grafting of v-Src elements onto c-Src kinase generally decreased kinase activity at elevated temperatures. In this context, the C-terminal tail deletion seems to play a pivotal role, with a loss of activity at a temperature at least 10 °C observed for all C-terminally deleted kinase variants.

The structural changes of the Src variants during thermal unfolding were monitored by circular dichroism (CD) spectroscopy (**Figure 53, Table 5**).

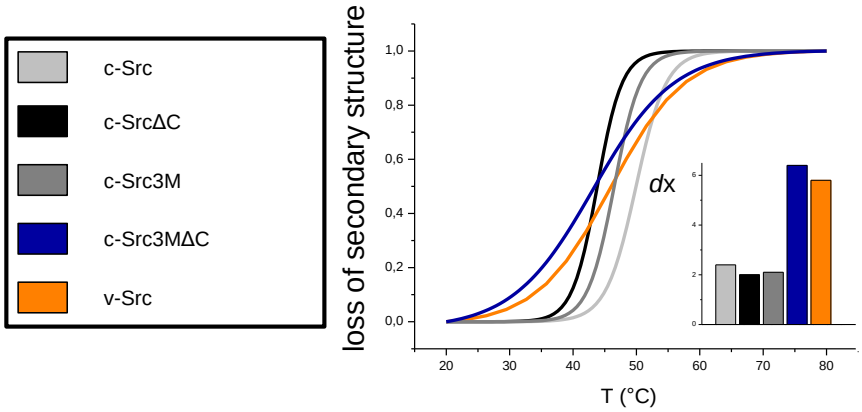

Figure 53

Stability and unfolding cooperativity of Src variants measured by CD spectroscopy.
Thermal transitions were recorded at 222 nm. The inset shows the *d*x values of the Boltzmann-plot.

We found that c-Src was most stable with a melting temperature (T_M) of 50 °C, whereas the T_M for v-Src was 46 °C. The c-SrcΔC mutant showed a T_M of 44 °C and the c-Src3M mutant exhibited an unfolding behavior in between those observed for c-Src and c-SrcΔC. v-Src and the mutant c-Src3MΔC showed remarkably low cooperativities, as indicated by the less sigmoidal melting curves, and had already begun to unfold around 20 °C. Interestingly, the unfolding process was completed only above 70 °C. In conclusion, deletion of the C-terminal tail in v-Src contributes mainly to the observed instability at lower temperatures, whereas the combination of the point mutations and the C-terminal deletion strongly decreased the cooperativity of unfolding. This revealed a correlation between the unfolding cooperativity of the kinases and their respective *in vivo* Hsp90-dependence: the two stringent client kinases v-Src and c-Src3MΔC unfolded over a broad temperature range. This is reflected in the high *d*x values of the Boltzmann-fits for these constructs, which can be described as a scaling factor, determining the steepness of the fit. These values could be calculated to be 6.4 and 5.8 for c-Src3MΔC and v-Src, respectively. However, for the less Hsp90-dependent constructs c-Src, c-SrcΔC and c-Src3M this value was in the range of 2.0, resulting in steeper curves for these constructs

compared to the two strong client kinases and indicating increased cooperativity of the unfolding process (**Figure 53, inset, Table 5**).

Given the pronounced effects of the C-terminal tail on Src stability and inactivation, we tested its influence on aggregation. The heated proteins were separated in soluble and insoluble fractions and analyzed by SDS-PAGE (**Figure 54**).

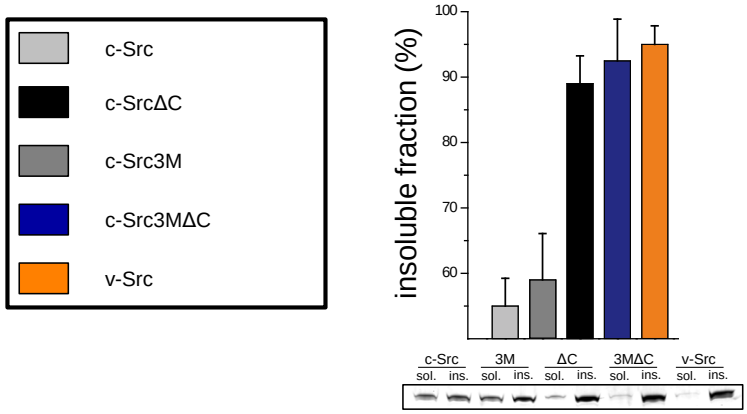

Figure 54

Analysis of aggregation propensity of Src variants.

Src variants were incubated for 10 min at 45 °C and soluble and insoluble fractions were analyzed by SDS-PAGE after centrifugation at 20,000 g for 1 h and quantified by densitometry.

After heat treatment, half of the c-Src protein was still soluble, whereas 95 % of v-Src was found in the insoluble fraction (**Figure 54**). The two Src variants missing the C-terminal tail both resembled the aggregation behaviour of v-Src. Analogous to c-Src, for c-Src3M 58 % of the protein was found in the insoluble fraction. Thus, deletion of the C-terminal tail led to increased aggregation propensity, suggesting that the point mutations alone did not influence the aggregation of c-Src.

The structural reasons for this difference remained enigmatic. To gain further insight into conformational changes, we monitored the accessibility of tryptophan residues in the Src variants. Solvent accessibility of tryptophans is a sensitive measure of conformational changes. Usually, tryptophan residues are buried in the core of a protein. Higher molecular flexibility will result in an increased exposure of these hydrophobic residues to added quenchers like acrylamide (Lakowicz, 1999). To

analyze the tryptophan accessibility of the Src variants, acrylamide was titrated to the proteins and the decrease of fluorescence signal was recorded (**Figure 55**).

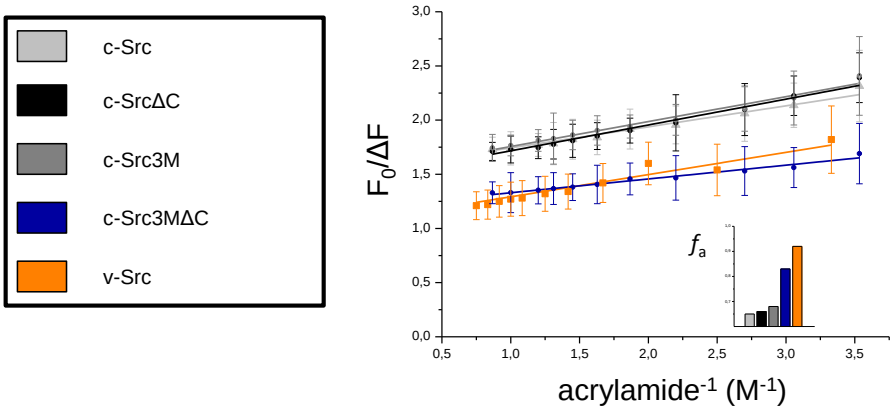

Figure 55

Quenching of tryptophan fluorescence of Src variants.

Acrylamide was titrated to the proteins and fluorescence emission monitored at 340 nm. Shown are modifed Stern-Volmer plots for the different Src mutants. In the inset the f_a values representing the accessibility of tryptophans are plotted for the different proteins.

Modified Stern-Volmer plots revealed the corresponding accessibility factors, f_a, of the analyzed Src variants (**Figure 55**). v-Src and c-Src3MΔC both showed a f_a value of 0.9. This indicates that most of the tryptophan residues were readily accessible for the quenching molecules. For c-Src and the mutants c-Src3M and c-SrcΔC the f_a value was 0.6. Hence, in these proteins not all tryptophan residues were accessible for the quencher, suggesting the tryptophan residues were more buried.

To further characterize the conformation of the variants, we determined their hydrophobic surfaces by the fluorescent probe 1-Anilinonaphthalene-8-sulfonic acid (ANS).

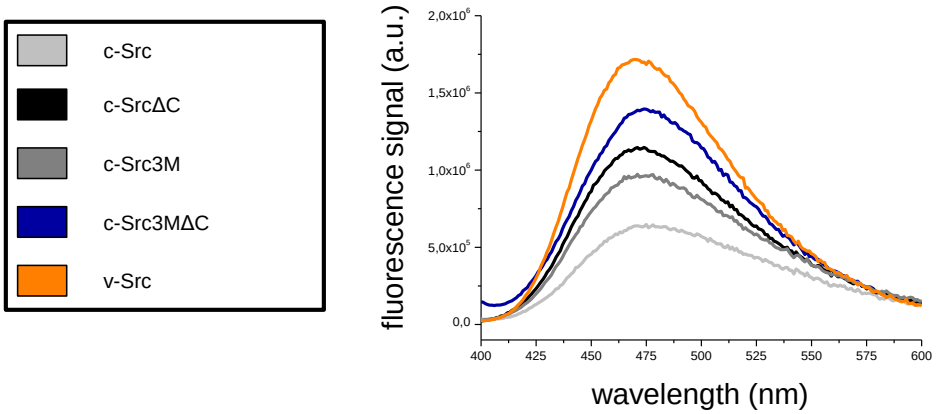

Figure 56

Analysis of ANS binding to hydrophobic protein patches.

Fluorescence spectra after excitation at 380 nm were recorded and buffer corrected.

Figure 56 shows that the three point mutations led to a moderate increase in ANS binding. However, in accordance with the aggregation behaviour, the kinase variants lacking the C-terminal tail exhibited considerably stronger ANS-binding, arguing for an increased exposure of hydrophobic patches.

Taken together, our results suggest that the point mutations together with the C-terminal tail deletion in v-Src destabilize the protein, reduce its molecular rigidity, increase surface hydrophobicity and aggregation propensity.

Since it has been suggested that kinase activity determines the degree of Hsp90-dependence (Len Neckers, oral communication), we asked whether the mutation of the catalytic lysine would lead to altered biophysical properties in c-Src and v-Src. For that we used our established set of assays to investigate the qualities of c-SrcK295R and v-SrcK295R (**Figure 57**).

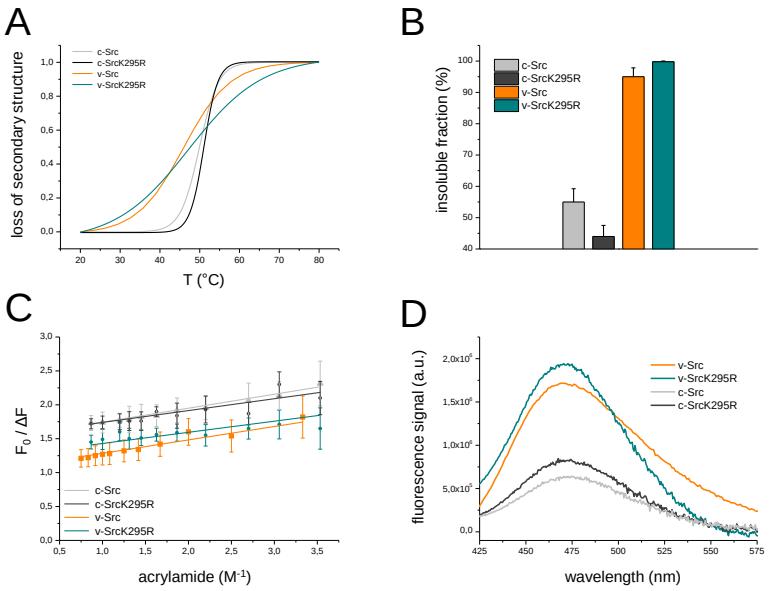

Figure 57

Biophysical characterization of c-SrcK295R and v-SrcK295R.

(A) Stability and unfolding cooperativity measured by CD. Thermal transitions were recorded at 222 nm. (B) Analysis of aggregation propensity. Src variants were incubated for 10 min at 45 °C and soluble and insoluble fraction quantified by SDS-PAGE. (C) Quenching of tryptophan fluorescence. Acrylamide was titrated to the proteins and fluorescence emission monitored at 340 nm. Shown are modifed Stern-Volmer plots for the different Src mutants. (D) Analysis of ANS binding to hydrophobic protein patches. Fluorescence spectra after excitation at 380 nm were recorded and buffer corrected.

The characterization of c-Src in comparison to c-SrcK295R and v-SrcK295R in comparison to v-Src by our established set of methods revealed similar behaviour of both enzymatically inactive K295R-mutants to their wildtype counterparts (**Figure 57, Table 5**). These findings indicate that sole kinase activity may not serve as exclusive criterion to determine Hsp90-dependence.

The major characteristics of the different Src kinase variants determined in this study are summarized in **Table 5**.

Table 5 Characteristics of investigated Src kinase variants.

	$I_{1/2}$ (° C)	T_M (° C)	*d*x - value of unfolding	aggregation (%)	tryptophan accessibility (f_a)	ANS-fluorescence (10^5 a.u.)	K_M for ATP (µM)
c-Src	49.5	50	2.4	55	0.65	6.48	12.8 (+/- 1.4)
c-Src3M	45.1	46.5	2.1	59	0.68	9.73	4.9 (+/- 0.8)
c-SrcΔC	38.8	44	2.0	89	0.66	11.46	19.8 (+/- 3.6)
c-Src3MΔC	33.3	43.5	6.4	92.5	0.83	13.91	4.0 (+/- 0.7)
v-Src	40.2	46	5.8	95	0.92	17.17	4.0 (+/- 0.8)
c-Src-K295R	-	51	1.7	44	0.64	8.35	-
v-Src-K295R	-	32.6	9.2	99.8	0.79	19.34	-

3.2.4. Assigning exposed regions in Hsp90 client Src kinases by hydrogen / deuterium (H/D) exchange in collaboration with Marco Dehling

To intimately compare Hsp90 client and non-client kinase conformations, we employed hydrogen/deuterium (H/D) exchange experiments. For this, a time course of two or three kinase variants was recorded in parallel in a side-by-side analysis revealing relative increase and/or decrease in backbone-proton exchange. **Figure 58** shows representative plots of four different peptides taken from a comparison between the non-client c-Src, the weak client c-Src3M and the strong client v-SrcK295R. We used the catalytically inactive v-Src mutant v-SrcK295R, due to significantly increased protein yields compared to v-Src.

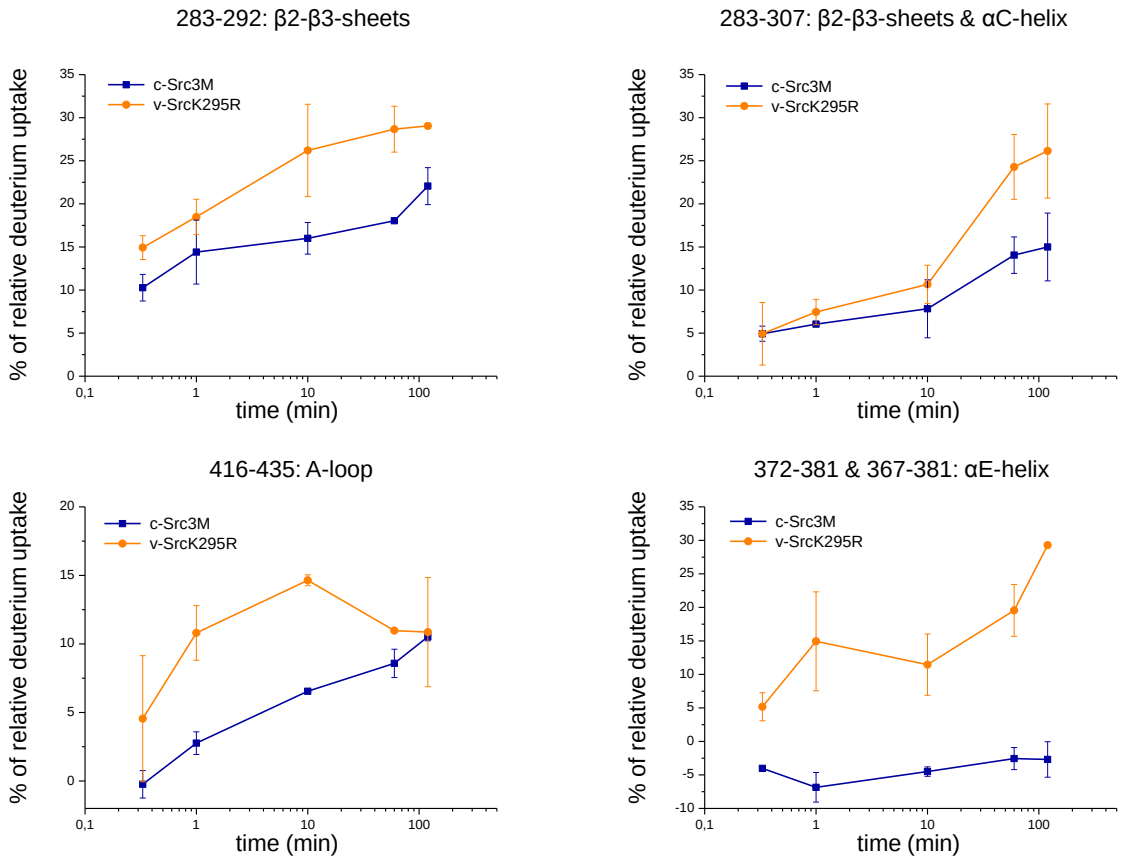

Figure 58

Representative deuterium uptake of c-Src3M- and v-SrcK295R-peptides relative to the respective c-Src peptides.

Relative uptake plots of the peptides [283-292], [283-307] and [416-435], all located in key regions, are shown. Due to differing pepsin-cleavage patterns, the αE-helix is represented by the peptide [367-381] for c-Src3M and by [372-381] for v-SrcK295R.

The investigated peptides of c-Src3M and v-SrcK295R shown in **Figure 58** exhibited significantly increased backbone-proton exchange compared to c-Src as indicated by the increased masses. Thereby, 1 Da of mass-increase reflects the exchange of one proton in the backbone for a deuterium from the solvent. By measuring the increase of peptide-mass over time, the solvent exposure of the peptides could be quantified. **Figure 58** shows that in these four peptides, v-SrcK295R showed higher solvent exposure compared to c-Src3M and that c-Src3M showed higher solvent exposure compared to c-Src. For a detailed analysis the identified peptides showing increased exposure were plotted onto the crystal structure of c-Src (PDB: 1Y57) in **Figure 59**.

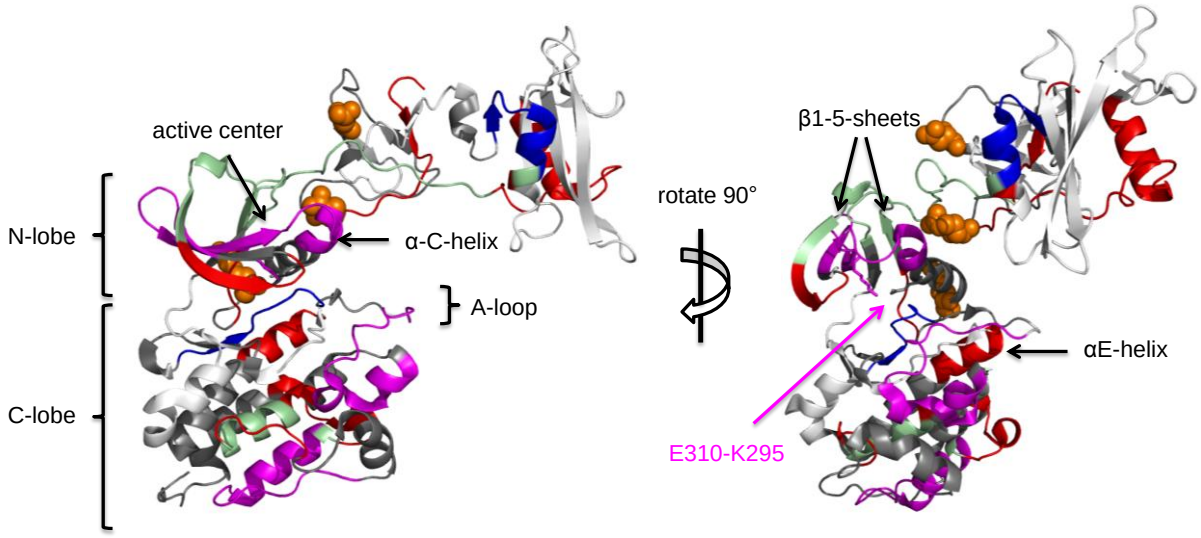

Figure 59

H/D exchange of v-SrcK295R in comparison to c-Src and c-Src3M.

Increased exchange in c-Src3M compared to c-Src in pale green and blue, increased exchange in v-SrcK295R compared to c-Src in red and regions overlapping with c-Src3M in pale green, increased exchange in v-SrcK295R compared to c-Src3M in magenta. The Glu310-Lys295 ion pair is depicted as stick model. The three point mutations in c-Src3M and v-Src are depicted as orange spheres.

For c-Src3M, the regions with more exchange in comparison to c-Src are located in the SH2-domain, in the kinase linker and around the active center, including the active site residues as well as the αC-helix, the αC-β4-loop, the β-1, β-2 and β-3-sheets and the β4-β5-sheets (**Figure 59**). Moreover, we observed an increased exchange in the A-loop region, including the site of autophosphorylation Tyr416, and around the C-terminal part of the kinase domain.

Strikingly, the exposed regions in v-Src almost completely overlap with those of c-Src3M (**Figure 59**). However, we observe additional exposed parts in v-Src and even higher solvent accessibility in the regions that are crucial for kinase activation, which include the active center region containing the αC-helix, the P-loop and the β1- to β3-sheets of the kinase domain N-lobe. The accessibility of the A-loop and of the C-terminal part of the kinase domain is increased in v-Src over c-Src3M. In addition, in v-Src also the αE-helix is more accessible (**Figure 59**).

Next, we determined the relative exchange comparing the two non-client Src variants c-Src and c-SrcΔC (**Figure 60**).

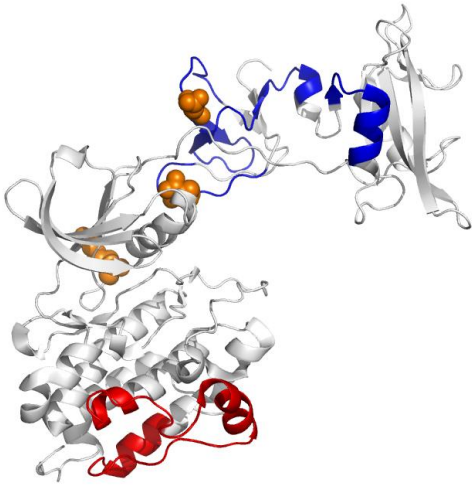

Figure 60

H/D exchange of c-SrcΔC in comparison to c-Src.

Increased exchange in c-SrcΔC compared to c-Src in red, decreased exchange in c-SrcΔC compared to c-Src in blue and regions with no significant change in white. For orientation, the three mutated residues in the other variants are depicted as orange spheres.

The deletion of the C-terminal tail in c-SrcΔC caused increased H/D exchange in the respective region. Additionally however, the alteration at the C-terminal end of the kinase also resulted in significantly decreased H/D exchange in the distant SH3- and SH2-domains (**Figure 60**), arguing for a global conformational change and/or for an alteration of the interdomain communication within the kinase.

3.2.5. Analyzing protein flexibility of Src variants by molecular dynamics (MD) simulations in collaboration with Prof. V. Kaila

To probe intrinsic dynamics of the kinases, we performed classical atomistic molecular dynamics (MD) simulations on the *in silico* mutated Src variant c-Src3MΔC and compared these to MD simulations of wild type c-Src.

The X-ray structures of the active (PDB: 1Y57) and inactive (PDB: 2SRC) states of c-Src, suggest that the Glu310-Lys295 ion pair remains closed in the active state, and inactivation is triggered by dissociation of the ion pair and formation of a new contact between Glu310 and Arg409. The active state is also characterized by a partially unfolded A-loop region (residues 404-424) with a solvent-exposed outward conformation of Tyr-416 that allows another c-Src to phosphorylate the residue, further stabilizing the active state. The unfolding of the A-loop is assisted by tilting the αC-helix (residues 305-316), which contains the active site residue Glu310. The activation process is thus highly cooperative, and most likely requires several transient switching events between intermediate states (Ozkirimli *et al*., 2009, Ozkirimli & Post, 2009). The dynamics of the central Glu310-Lys295 ion pair, and the Arg409-Tyr416 interaction in the A-loop region thus represent indicators of the kinase activation process, which we used to address the underlying molecular mechanism for the remarkable increase in activity and loss of stability in Src variants.

Figure 61 shows the snapshots of the MD relaxed structures obtained after the 250 ns simulations.

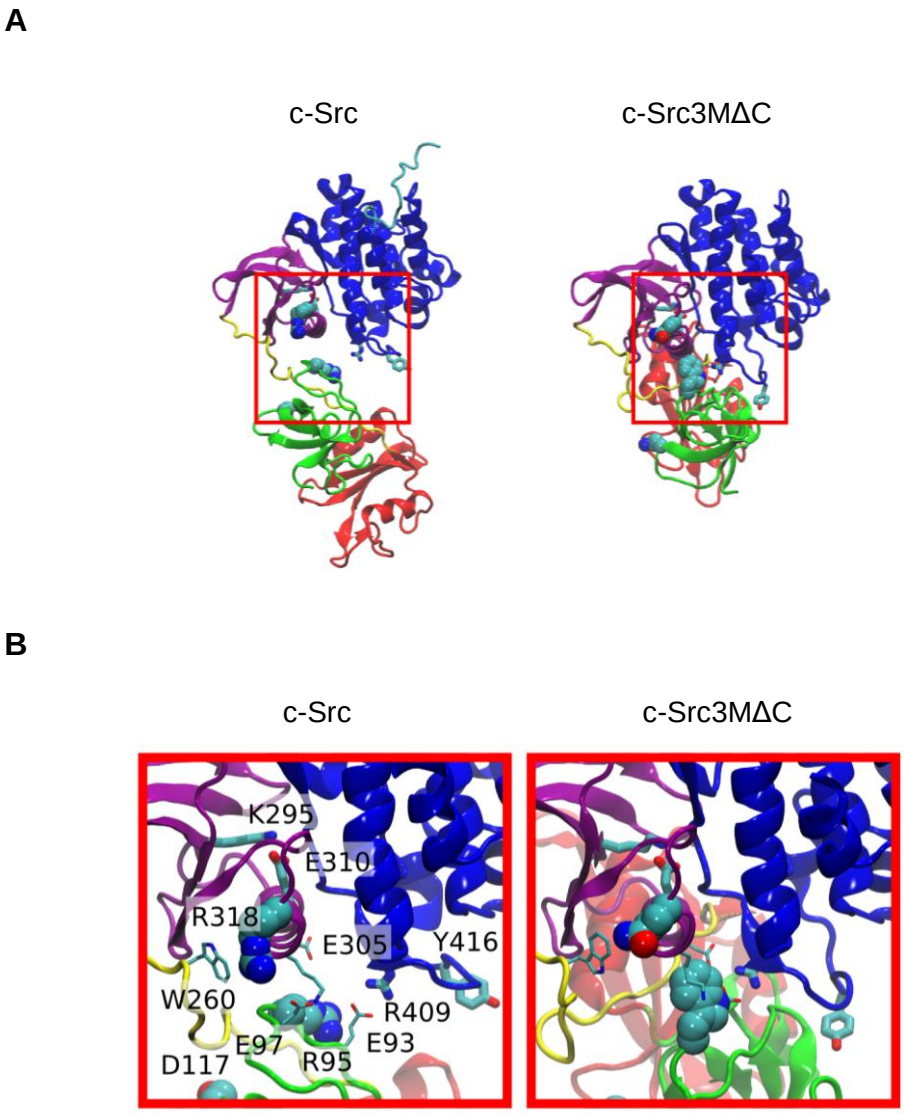

Figure 61

Snapshots of the structures of c-Src and c-Src3MΔC models obtained after 250 ns MD simulations.

(A) The three mutated residues (R95W, D117Q, R318Q) are shown in van der Waals representation and the active site residues (Lys295, Glu310, Arg409, Tyr416) in licorice. The SH2-domain is shown in red, the SH3-domain in green, the P-loop in yellow, the N-terminal domain in purple, and the kinase domain in blue, with the C-terminal tail in cyan. (B) Conformation of the central active site residues, αC-helix and the A-loop region.

We observe large-scale conformational changes in the regulatory SH2- and SH3-domain relative to the kinase domain (**Figure 61**). In c-Src3MΔC, the SH2- and SH3-

domain move closer to the catalytic domain, making the structure, at least transiently, more compact. Interestingly, the X-ray structure of the inactive state of c-Src is also more compact, with the SH2/SH3-domains folded around the kinase domain (PDB: 2SRC). Although the structural importance of this conformational change remains unclear, we find that the introduced neutral residues (Trp95, Asn117 and Gln318) are likely to trigger the structural rearrangement by electrostatic destabilization, and re-formation of several ion-pairs, which is consistent with the previously suggested long-range electrostatic switching model of c-Src (Ozkirimli *et al*., 2009, Ozkirimli & Post, 2009).

To explain the striking differences in stability between full length and C-terminally deleted kinase variants, we additionally simulated a kinase construct carrying the three point mutations and the shortened v-Src C-tail: c-Src3MΔV and plotted the dynamics of the C-terminal tail of both, c-Src and c-Src3MΔV onto the crystal structure of c-Src (**Figure 62**).

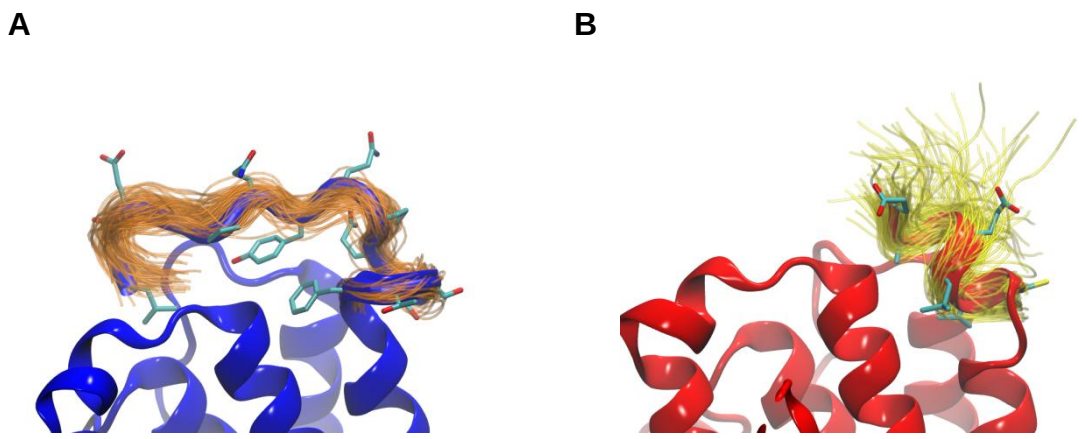

Figure 62

The dynamics of the C-terminal region in c-Src and c-Src3MΔV.

Plotted here are all 150 conformations of the C-terminal tail, shown in orange for c-Src (A) and yellow for c-Src3MΔV (B) over a simulation of 150 ns.

This revealed significantly increased dynamics and number of conformations of this part in the c-Src3MΔV variant compared to c-Src, indicating an at least locally increased flexibility.

To investigate the conformational changes upon c-Src mutation in more detail, we analyzed the local dynamics of the active site residues Glu310, Lys295, Arg409 and Tyr416 (**Figure 63**).

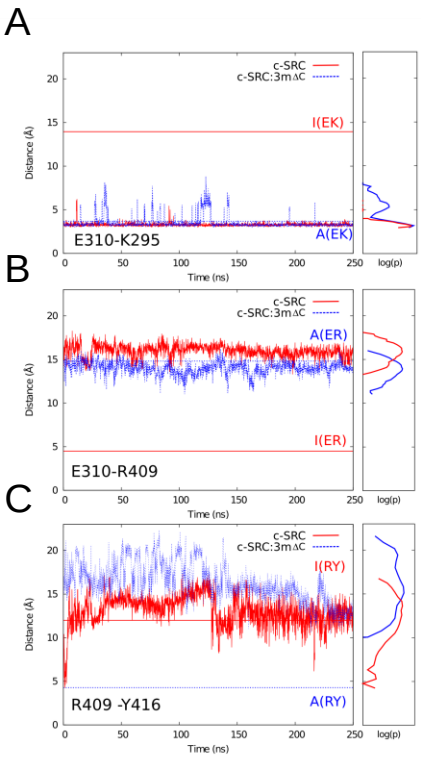

Figure 63

The dynamics of key residue interactions in c-Src and c-Src3MΔC.

(A) The dynamics of Glu310-Lys295, (B) Glu310-Arg409 distances, and (C) the Arg409-Tyr416 distance of c-Src (red lines), and c-Src3MΔC (blue lines). The Glu310-Lys295 distances are 3.4 Å and 14.0 Å in the active (A(EK)) and inactive (I(EK)) states of c-Src, respectively. The Glu310-Arg409 distances are 14.8 Å in the active state (A(ER)), and 4.5 Å in the inactive state (I(ER)), and the Arg409-Tyr316 distances are 4.3 Å and 12.0 Å in the active and inactive state, respectively.

For the c-Src model, we find that the Glu310-Lys295 ion pair remains closed for most of the 250 ns simulation, suggesting that the structure is trapped in the active state, consistent with the 4 kcal mol^{-1} activation barrier recently estimated by Shukla *et al*. (2014) based on Markov state models and large-scale molecular simulations. In contrast, for c-Src3MΔC, we observe several transient dissociation events of the Glu310-Lys295 ion pair, and a consistent shortening of the Glu310-Arg409 distance (**Figure 63**).

To compare these conformational and dynamic changes on a more global level, a plot illustrating the displacement and the solvent accessible surface area (SASA) of the kinase domain is shown (**Figure 64**).

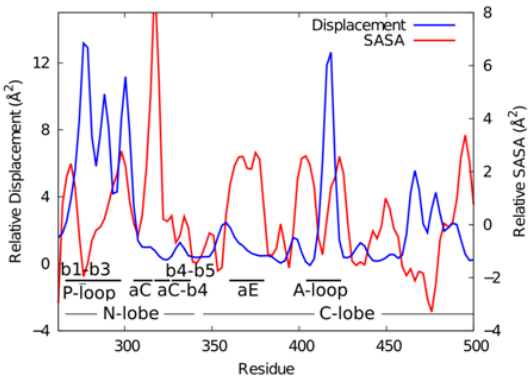

Figure 64

Difference in c-Src3MΔC vs. c-Src displacement and solvent-accessible surface area (SASA) for the kinase domain.

The SASA was calculated as the average over the 250 ns runs for the complete residues. The displacement was calculated from the displacement of the C-α position obtained from end point structures at 250 ns.

Here, the conformational changes in the A-loop region in c-Src3MΔC relative to c-Src, indicating significant displacement and partial unfolding become obvious (**Figure 64 & Figure 59**). Moreover, we observe a subtle outward tilting of the αC-helix and an increase in the solvent accessibility and residue flexibility of the active site and the A-loop regions (**Figure 64**), which may affect the accessibility for substrate binding. We do not observe a large-scale structural shift in the stacking of hydrophobic R-spine residues (His384, Phe405, Met314, Leu325), which has also been suggested to be play a central role in the activation process (Taylor & Kornev, 2011). However, the β-1-β-2-β-3-sheets show increased displacement and surface exposure and, consistent with our H/D exchange data, the αE-helix seems to be more flexible compared to c-Src (**Figure 64**).

The increased *active-to-inactive*-like transitions in c-Src3MΔC suggest that the kinetic barrier for activation is effectively lowered, which might explain the experimentally observed increased activity of this variant. The MD simulations can reveal possible reasons for the distinct behavior of the c-Src3MΔC variant relative to c-Src. In the c-Src simulation, Arg95 forms an ion pairs with two glutamate residues

(Glu305 and Glu93), which are involved in stabilizing the αC-helix and Arg409 of the A-loop (**Figure 61**). The R95W mutation leads to the formation of a π-cation interaction between Arg409 and Trp95, and partial dissociation of the Arg95-Glu305/Glu93 ion pairs, thus destabilizing the αC-helix and the A-loop region. We also observe that the interaction between Arg318, at the end of the αC-helix, with Trp260 is weakened by replacement with Gln318, which is also likely to contribute to the flexibility of the helix. The increase in the solvent accessibility of these both central regions may affect the accessibility for substrate binding, and explain the higher H/D exchange rates.

4. Discussion

4.1. Integration of the kinase cochaperone Cdc37 into the Hsp90 cycle

The cochaperone Cdc37 is thought to provide specificity for the Hsp90 machinery (Hunter & Poon, 1997). In fact, Cdc37 is one of the most specific partners of the chaperone, almost exclusively being involved in the stabilization and maturation of kinase clients (Mandal *et al.*, 2007, Taipale *et al*., 2012). However, cochaperones not only function as adapters, but also play an important role in the regulation of the folding machinery itself. Many drive the Hsp90 cycle as their entry and exit during the progression of the cycle influences ATP-hydrolysis, conformational change and the maturation of the client (Li & Buchner, 2013).

In this study, we analyzed the formation of Hsp90-cochaperone complexes with the intention to reconstitute the complete kinase-specific chaperone cycle. The final goal was to integrate previously identified components and to explain their complex interplay with the chaperone and its conformational, ATPase-dependent cycle. We aimed to achieve this by exploiting the unique ability of analytical ultracentrifugation assisted with a fluorescence detection system (aUC) to track the distribution of a single protein component in different complexes at the same time. Due to the high sensitivity of this technique, it is possible to observe the formation of protein complexes in solution at much lower concentrations compared to other biophysical methods such as analytical size exclusion chromatography or analytical ultracentrifugation using UV-absorbance for detection. During the experiment, the fluorescently labeled component (*Cdc37 in this case) is typically concentrated to 150 nM, which corresponds to the concentration of this cochaperone in a living cell (Ghaemmaghami *et al*., 2003, Jorgensen *et al*., 2002). Since Hsp90 is present at much higher concentrations *in vivo*, the aUC measurements conducted under these conditions (2 µM of Hsp90 dimer) accurately reflect the physiological conditions in the cell cytoplasm.

4.1.1. Characterization of the Cdc37-Hsp90 interaction

By using aUC we found that Cdc37 binds to Hsp90 with a K_D of 250 nM. Of note, this value is one order of magnitude lower than previously determined affinities of the same complex measured by intrinsic tryptophan fluorescence and CD-spectroscopy (Zhang *et al*., 2004, Siligardi *et al*. 2002). Notably, using our aUC set up, we were able to observe Cdc37-Hsp90 complex formation at a Cdc37-concentration at which

the cochaperone is present as a monomer. The K_D for the Cdc37-dimerization has been determined to lie between 5.5 µM and 80 µM (Zhang *et al*., 2004, Siligardi *et al*., 2002). Previously, the interaction between Cdc37 and Hsp90 was measured at Cdc37-concentrations at which the cochaperone starts to form a monomer-dimer equilibrium (Zhang *et al*., 2004, Siligardi *et al*., 2002). It is well possible that a Cdc37-dimer exhibits an altered binding mode for Hsp90 than a Cdc37-monomer.

To clarify the stoichiometry of the Cdc37-Hsp90 complex, the binding of Cdc37 to Hsp90 was followed by size exclusion chromatography. Notably, even at high concentrations of Cdc37 and Hsp90 (30 µM), we were not able to observe a $[Hsp90]_2$::$[Cdc37]_2$ complex. Only one Cdc37-monomer bound to the Hsp90-dimer under these conditions. Although previous studies also found two Cdc37 molecules binding to the Hsp90-dimer (Zhang *et al*., 2004, Siligardi *et al*., 2002, Roe *et al*., 2004), our results are consistent with the notion that only one molecule of Cdc37 was found in complex with dimeric Hsp90 and one kinase molecule (Vaughan *et al*., 2006) and with the finding that Cdc37 did not influence the rate of subunit exchange in the Hsp90-dimer (Eckl et al., 2013), suggesting that Cdc37 does not bridge the Hsp90-dimer in solution.

Since Hsp90 undergoes large conformational rearrangements upon ATP-binding and -hydrolysis, we asked how the presence of different nucleotide-analogues would influence the binding of Cdc37 to the chaperone. We found that the presence of different nucleotides including ATP, ATPγS and AMP-PNP decreased the affinity of Cdc37 for Hsp90, suggesting that strong binding of Cdc37 to Hsp90 is important during an early phase of the conformational cycle, when Hsp90 is present in its apo-form. Cdc37 fixes the lid segment of Hsp90 to an open state, inserts an arginine side chain into the ATP-binding pocket and prevents dimerization of the N-domains (Roe *et al*., 2004). However, it has been shown that the nucleotide binding pocket is still fully accessible in the Cdc37-Hsp90 complex (Eckl *et al*., 2013). Furthermore, binding of the Hsp90-inhibitor Geldanamycin to the ATP-binding site does not displace Cdc37 from the chaperone (Siligardi *et al*., 2002). This indicates that not a direct competition between nucleotides and the cochaperone takes place, but rather conformational changes associated with ATP-binding to Hsp90 cause the altered affinity of the cochaperone towards the Hsp90-dimer. This notion is also supported by the observation that the presence of human Cdc37 decreases the dimer-closure rate of yeast Hsp90 (Eckl *et al*., 2013). Surprisingly, the response of the human

Cdc37-Hsp90 complex to the presence of nucleotides seems to strongly differ in comparison to other species, as in the *C. elegans* system, ATP-binding in fact increases the affinity of Cdc37 towards Hsp90 (Eckl et al., 2013).

4.1.2. The effect of Hop/Sti1 on the Cdc37-Hsp90 complex

During the *de novo* folding of proteins Hsp90 takes over the pre-folded client from Hsp70. This step is facilitated by the Hsp70-Hsp90-connecting cochaperone Hop/Sti1. It has been suggested that a Cdc37-pathway would represent an alternative alley for a client to enter the Hsp90 folding machinery, thereby bypassing Hop/Sti1. Further, Cdc37 and Hop/Sti1 have been proposed to functionally overlap in Hsp90-kinase complexes (Lee *et al*., 2004). Analysis of the *C. elegans* components revealed that Cdc37 and Hop/Sti1 exclude each other during the binding to Hsp90 (Gaiser *et al*., 2010). Here, we asked how the presence of Hop/Sti1 would influence the Cdc37-Hsp90 complex in the human context using our aUC set up.

Interestingly, we found that Hop/Sti1 forms a ternary complex with Cdc37 and Hsp90 at equimolar concentrations and that Cdc37 is partly, but not completely displaced from Hsp90 even at saturating concentrations of Hop/Sti1. The TPR1-, DP1- and/or the DP2-domain of Hop/Sti1 are essential for Cdc37-expulsion, since a construct lacking these domains does not decrease Cdc37-Hsp90 affinity. Interestingly, the same construct promotes full viability and efficient kinase maturation in *S. cerevisiae* (Schmid et al., 2012), suggesting that the displacement of Cdc37 by full length Hop/Sti1 is not essential for kinase maturation.

From these results, we conclude that Hop/Sti1 in complex with Cdc37 and Hsp90 plays a central role in the initial step of kinase chaperoning by Hsp90. The inability of Hop/Sti1 to fully displace Cdc37 from Hsp90 speaks for a preferation of Hsp90 to bind to Cdc37 and Hop/Sti1 at the same time, which has been similarly observed for other Hsp90-cochaperone complexes (Li *et al*., 2011). We propose that, within this complex, the client kinase is handed over from Hsp70 to the Cdc37-Hsp90 complex. These results are in line with previous findings on the necessity of Hop/Sti1 during *in vitro de novo* chaperoning of Chk1 kinase (Arlander et al., 2006, Felts et al., 2007) and the dramatic negative effect of a Hop/Sti1 gene deletion on v-Src kinase maturation in yeast (Schmid et al., 2012). A possible role of Hop/Sti1 during this process is shown in **Figure 65** passing the pre-folded client over from Hsp70 to

the Cdc37-Hsp90 complex. As the next step, within this complex Cdc37 could stabilize the kinase via interaction with the kinase domain (Polier *et al.,* 2013).

4.1.3. Binding of TPR-domain containing cochaperones to the Cdc37-Hsp90 complex

Since Cdc37 binds to the N-domain of Hsp90, it is expected that the MEEVD-motifs on its C-terminal domains would be accessible for recognition by TPR-domain-containing cochaperones. However, it has been suggested that the binding of Cpr6, a PPIase from yeast, would interfere with Cdc37 binding to Hsp90, as Cpr6 partly restored the Cdc37-dependent inhibition of Hsp90's ATPase activity (Siligardi et al., 2002). Thus, we asked how TPR-containing cochaperones would influence the Cdc37-Hsp90 complex.

PP5, an Hsp90-dependent phosphatase responsible for the specific dephosphorylation of Cdc37, is known to play an important role during kinase chaperoning (Vaughan *et al*., 2008). Hence, we aimed to analyze its influence on the Cdc37-Hsp90 complex formation. We found that PP5 binds with high affinity to the Cdc37-Hsp90 complex via its TPR-domain. This is consistent with the notion that PP5 has been observed to interact with an Hsp90-kinase complex (Shao *et al*., 2001) and with a Cdc37-Hsp90 complex in *C. elegans* (Gaiser *et al*., 2010).

Next, we analyzed complex formation of the three human TPR-containing PPIases Cyp40, FKBP51 and FKBP52 with Cdc37 and Hsp90 and found that all PPIases tested were able to form a ternary complex with Cdc37 and Hsp90. Since it is well possible that the inhibiting effect of Cdc37 is lowered within a PPIase-Cdc37-Hsp90 complex, our results do not contradict these previous results (Siligardi et al., 2002). Moreover, our findings are notably consistent with a former study on the co-purification of Cdc37 with the exogenously expressed PPIase Cpr7 (Abbas-Terki et al., 2002). The interactions of the TPR-domain-containing cochaperones with the Cdc37-Hsp90 complex are summarized in **Figure 65**.

4.1.4. The role of Aha1 within the kinase chaperoning cycle of Hsp90

Aha1 is the only cochaperone known to accelerate the ATPase activity of human Hsp90. Furthermore, it has been implicated to play an important role during *de novo* kinase maturation in yeast and in man (Panaretou *et al*., 2002, Meyer *et al*., 2004, Xu *et al*., 2012). It has been found to physically interact with the Cdc37-Hsp90 complex

in *S. cerevisiae* and *C. elegans* (Panaretou *et al*., 2002, Gaiser *et al*., 2010). When testing its interaction with Cdc37 and Hsp90 in the human context, we found that Aha1 forms a ternary complex with Cdc37 and Hsp90 and moreover is also able to form a quarternary complex with PP5, Cdc37 and Hsp90.

When testing the effect of Aha1 on the binding of Hop/Sti1 to Hsp90, we found that, similar to previous results analyzing mixed yeast Hsp90 complexes (Li *et al*., 2011), the two cochaperones Aha1 and PP5 synergistically displace Hop/Sti1 from the complex. Neither PP5 nor Aha1 alone were able to displace Hop/Sti1 from the complex completely, but only the combination of both cochaperones expelled Hop/Sti1 from Hsp90. The expulsion of Hop/Sti1 was driven by the combined interaction of Aha1 and PP5 with Hsp90 both in the presence and in the absence of Cdc37. This suggests that although Hop/Sti1 partly competes with Cdc37 binding to Hsp90 at high Hop/Sti1 concentrations, Cdc37 does not play a crucial role in Hop/Sti1 displacement during the progression of the Hsp90-cycle.

Next, we wondered whether Aha1 would also have an influence on the binding of Cdc37 to Hsp90. Since it is believed that Aha1- and nucleotide-binding to Hsp90 take place during the same stage of the chaperone cycle (Li *et al*., 2013), we analyzed Cdc37 binding in the presence of Aha1 and ATP. Interestingly, Cdc37 was displaced from Hsp90 in the presence of Aha1 and ATP. This process was independent of the presence or absence of PP5. Of note, in this point the kinase maturation cycles of Hsp90 in the human and in the *C. elegans* system dramatically differ as in the nematode ATP does not lead to Cdc37-displacement in the presence of Aha1 (Gaiser *et al*., 2010). To further investigate the kinetics of the Cdc37-expulsion process, we developed a FRET system between Cdc37 and Hsp90. This revealed that the displacement of Cdc37 by ATP and Aha1 is a process with a $t_{1/2}$ of about 30 sec, indicating the involvement of slow rate-limiting steps such as ATP-hydrolysis. Hence, the presence of ATP repels Cdc37 from Hsp90 only to a certain extent, but the binding of Aha1 is needed to reach full performance during this process. As Cdc37-binding does not compete with the binding of nucleotides (Eckl *et al*., 2013), this process is likely to be due to conformational changes in the Hsp90-dimer, whereas Aha1 stabilizes the closed conformation in which Cdc37 is expelled from the chaperone complex.

Taken together, we propose that Aha1 plays a key role for the progression of the Hsp90 cycle during kinase maturation as this cochaperone in companion with PP5 leads to Hop-displacement and beyond that to the expulsion of Cdc37 as soon as ATP binds to the complex. Aha1 seems to be involved in the last stage of Hsp90's kinase maturation cycle forming a complex with Hsp90 and potentially with PP5.

The results are summarized in **Figure 65**.

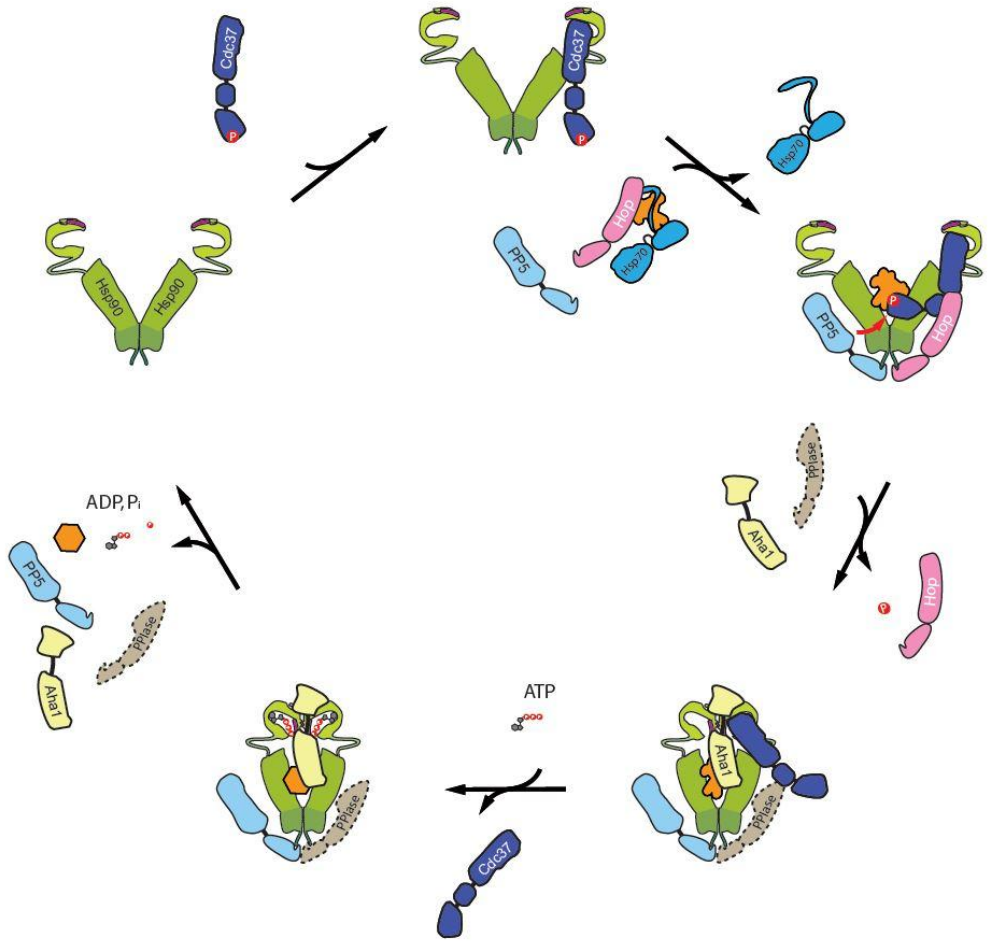

Figure 65

Model of entry and exit of the kinase cochaperone Cdc37 within the human Hsp90 reaction cycle. Cdc37 enters the chaperone cycle by binding to the open Hsp90-dimer. Hop/Sti1 hands over the pre-folded client kinase (orange) from Hsp70 and binds to the Cdc37-Hsp90 complex. PP5 may interact with this complex via its TPR-domain and dephosphorylate Cdc37. In the next step Aha1 displaces Hop/Sti1 and forms a complex with Hsp90, PP5, Cdc37 and potentially with a PPIase. Binding of ATP leads to Cdc37 displacement upon closure of the Hsp90-dimer, which is stabilized by Aha1. ATP-hydrolysis leads to the dissociation of the complex and the release of the folded kinase.

We reconstituted the kinase maturation cycle of Hsp90 *in vitro*, thereby gaining further insight into the mechanism that drives the cycle during kinase maturation.

We observe that Cdc37 preferentially binds to the open form of Hsp90. Hop/Sti1 interacts with the Cdc37-Hsp90 complex handing over the pre-folded client from Hsp70. PP5 may join this complex and dephosphorylate Cdc37 at pSer13. Binding of PP5 and Aha1 displaces Hop/Sti1 from the complex, which may be accompanied by the interaction of a PPIase with the remaining MEEVD-motif of one Hsp90-subunit. Thereby, Cdc37 remains bound to Hsp90. Binding of ATP to the complex displaces Cdc37 by conformational rearrangements within the Hsp90-dimer, which may in turn lead to the maturation of the client kinase, being released upon ATP-hydrolysis.

Continuative studies would include the presence of a client kinase during the reconstitution of the Hsp90-cycle. For this purpose, the isolation of a client kinase in milligram quantities would be necessary. This approach would reveal how a client kinase itself influences the chaperone machinery.

4.2. What makes a client a client: Conformational processing of v-Src kinase by Hsp90

4.2.1. The conformational activation of v-Src kinase

It could be shown that *in vivo*, the Hsp90 machinery activates the chimera c-Src3MΔC and v-Src kinase. Reconstitution of these chaperone-effects *in vitro* showed that although Hsp90 alone is able to increase Src activity, Cdc37 strongly enhances this effect. The affinity of Hsp90 towards the kinase is increased in the presence of Cdc37 about 15-fold with a K_A of 0.23 µM. We assume the physiological concentration of Hsp90 to be in the low micromolar range and the concentration of Cdc37 mid nanomolar (Ghaemmaghami *et al*., 2003, Jorgensen *et al*., 2002). Thus, Cdc37 allows Hsp90 to interact with kinases in the cell under normal growth conditions. This notion was falsified by using a $Cdc37_E$ version with impaired binding to Hsp90 ($Cdc37_{ERR}$). $Cdc37_{ERR}$ was not able to increase the affinity of Hsp90 towards v-Src, indicating that formation of the Cdc37-Hsp90 complex is mandatory for kinase activation. This finding confirms a previous study showing that Hsp90 binding of Cdc37 is needed for client kinase mediated cell proliferation and survival in human prostate epithelial cells (Schwarze *et al*., 2003). However, a recent study showing that a non-Hsp90-binding Cdc37 variant exhibits a Hsp90-dependent stabilization ability, suggests an alternative pathway for certain kinases to reach the chaperone (Smith *et al*., 2013), which seems not be true for v-Src in our reconstitution assay.

Consistent with the literature, the active form of Cdc37 is the phosphorylated one (Vaughan *et al*., 2008). For efficient activation of v-Src, this form of Cdc37 was sufficient and no dynamic cycling through phosphorylation and dephosphorylation was necessary.

Interestingly, our results suggest that strong kinase clients and weak ones seem to be differently modulated by chaperones. When testing the influence of Cdc37 on v-Src, we could not detect kinase inhibition. It remains to be seen whether this is a specific characteristic of v-Src, as for another kinase, B-Raf, it was reported that Cdc37 would inhibit its kinase activity (Polier *et al*., 2013) via direct competition with ATP for binding to the active center. In this context, it has been proposed that the K_M of kinases for ATP would determine the rate of association with Cdc37 and Hsp90, whereupon a higher affinity of the kinase towards ATP would result in stronger competition with the chaperones and lead to less kinase-chaperone

interaction. This however, is not the case for the Src kinase pair, as the strong client v-Src shows a ten-fold lower K_M for ATP than the non-client c-Src. As B-Raf was previously determined to be a very weak client of Hsp90 (Taipale *et al*., 2012), our results suggest a distinct mechanism by which chaperones may act either on weak or on strong client kinases.

4.2.2. Chaperoning of v-Src during heat shock

Under stress conditions, a different picture emerges for the effect of Hsp90 on Src kinase. At elevated temperatures Hsp90 stabilizes v-Src. The stabilization is ATP-dependent and can be inhibited by Radicicol. Notably, Cdc37 does not seem to be important for Hsp90 to stabilize Src. At a transition point of 38°C we observe a shift from Hsp90-Cdc37-mediated activation towards a Hsp90-dependent stabilization. Thus, it should be tested, whether Cdc37 is still functional under these conditions. The observed stabilization effect might require different interactions with Hsp90 for which Cdc37 is dispensable. It is tempting to speculate that thermal destabilization of Src kinase leads to the accumulation of a kinase conformation with increased affinity for Hsp90 and thus the initial step of Cdc37-association is bypassed. In yeast, only Hsp90, Sti1 and and Cpr6 but not Cdc37 are upregulated under heat shock conditions (Gasch *et al*., 2000). Also, Cdc37-independent association of Hsp90 with kinases has been observed previously (Polier *et al*., 2013). Furthermore, Cdc37 is not present in all organisms, suggesting a distinct role of Hsp90 in client kinase maturation (Johnson & Brown, 2009). Consistent with the notion that under heat shock conditions only part of the chaperone cycle may be required (Gasch *et al*., 2000), we find that under these conditions ATP-binding by Hsp90 is necessary, whereas ATP-hydrolysis is not. It has beend proposed that ATP-hydolysis is not mandatory for client binding (Millson *et al*., 2005). Furthermore, it has recently been shown that another stringent Hsp90 client associates with Hsp90 in the presence of ATP and is released in the presence of ADP (Lorenz *et al*., 2014).

4.2.3. Dissecting the kinase maturation process of Hsp90 and Cdc37

During kinase activation, ATP-binding and -hydrolysis by Hsp90 is a prerequisite. Our results imply that the kinase molecules are constantly activated by the chaperone. An initial activation of a subset of kinase molecules activating the remaining molecules by autophosphorylation would be in conflict with these findings. Since inhibition of

Hsp90 during the reaction leads to a decrease in kinase activity to its basal Hsp90-independent level, we conclude that the activated state of v-Src is strictly dependent on the continued ATPase cycle of the chaperone. However, based on our data, we propose that the chaperones shift the conformational ensemble of different states towards the more active one. Due to the interaction and ATP-dependent action of Hsp90, these states are concomitantly modulated towards a stabilized conformation that exhibits increased kinase activity. Upon inhibition of Hsp90's ATPase, v-Src shifts back to a low-activity state. Thus, this process is reversible.

Summarizing, our findings imply two specific tasks of Hsp90: (1) it assists in the maturation of a broad spectrum of kinases, including c-Src, during initial folding via a transient interaction. (2) In the case of v-Src it seems that the kinase reaches higher levels of activity on the expense of stability and, importantly, structural cooperativity. This results in an equilibrium of a meta-stable high-activity and low-activity states. This in turn seems to render the kinase to be a Hsp90 client. Hsp90 shifts the kinase equilibrium by stabilizing the high activity-state and stabilizing client kinases throughout their lifetimes, protecting the kinase from unfolding under stress conditions. Without the chaperone, the equilibrium of v-Src is clearly shifted towards a less active state. The balance of the equilibrium may determine the degree of the dependence on Hsp90. For strong clients, their intrinsic instability is sufficient to trigger Hsp90 association via Cdc37.

4.2.4. Revealing the characteristics of a Hsp90-client

We identified the properties of a kinase, which render it a client for the molecular chaperone Hsp90. For that, we made use of the highly homologous pair of v-Src and c-Src kinase. As they differ only in a few positions grafting of client elements onto the scaffold of the non-client c-Src kinase was possible. By analyzing and comparing the characteristics of different versions of Src kinase that stepwise varied in their dependence on Hsp90, we could correlate the structural properties of the proteins with their chaperone dependence. Interestingly, the deletion of the regulatory C-terminal tail in c-SrcΔC, which is the primary reason for the conversion of c-Src to a transforming protein in mammals (Frame, 2002), did not show increased Hsp90-dependence. Nevertheless, c-SrcΔC showed a significantly decreased stability compared to the wildtype c-Src kinase as well as a high aggregation propensity.

Another c-Src variant carried three point mutations that are relevant for the development of transforming properties in cancer. These mutations are sufficient for the toxic effect of v-Src in yeast. The combination of the C-terminal tail deletion and the three point mutations in c-Src3MΔC and wildtype v-Src significantly increase the activity of the kinase. Of note, the deletion generally leads to decreased expression, suggesting a destabilizing role *in vivo*.

Notably, c-Src3M shows similar expression levels like wildtype c-Src and increased expression compared to c-Src3MΔC and v-Src, but it is less active. This finding implicates an activating mechanism specific for c-Src3MΔC and v-Src *in vivo* and thus supports our results on the activation of c-Src3MΔC and v-Src by Hsp90 and Cdc37 *in vitro*.

In summary, we found that the introduction of the three point mutations into c-Src created a weak Hsp90 client and this Hsp90-dependence could be strongly increased by the truncation of the C-terminal tail. The non-client c-SrcΔC was similarly instable and aggregation-prone as the strong clients c-Src3MΔC and v-Src. Thus, against common beliefe, these characteristics do not seem to be sufficient to render a kinase Hsp90-dependent. To resolve this conundrum, we aimed to define the structural differences between the variants. We found that the introduction of a v-Src element into c-Src leads to a general decrease in stability. However, only the two strong Hsp90 clients c-Src3MΔC and v-Src show remarkable low folding cooperativity. This indicates that the protein is flexible and may exist as an ensemble of folded structures. Furthermore, Hsp90-dependence is correlated with increased hydrophobicity, especially when testing for elevated tryptophan accessibility, since this residue is normally buried in the interior of the protein. This finding is in agreement with the notion that in Hsp90 clients partially folded structures and increased dynamics are important. This reveals a correlation between Hsp90-dependence of a kinase and its molecular compactness.

In summary, a combination of qualities seems to cause Hsp90-dependence: client kinases are destabilized, aggregation-prone, partially unfolded, hydrophobic, structurally less compact and can hence be designated as meta-stable proteins.

4.2.5. Exposure of key regions determine Hsp90-dependence

We found that, in Hsp90 clients backbone hydrogen exchange is significantly increased in regions crucial for kinase activation. Notably, these regions lie within

chaperone binding sites previously suggested. These studies revealed that the glycine-rich P-loop, the αC-helix, the adjacent loop as well as β4- and β5-sheets, all located in the N-lobe of the kinase domain, may be potential binding sites for Cdc37 (Prince & Matts, 2004, Prince *et al*., 2005, Citri *et al*., 2006). Hsp90-binding, may additionally include the αE-helix in the kinase C-lobe (Miyata *et al*., 2001).

Our H/D exchange experiments show that the accessibility of the central region surrounding the active center is significantly increased. This includes the αC-helix, the αC-β4-loop and the β1- to β5-sheets. Additionally, the P-loop and the aE-helix is more accessible in v-Src compared to c-Src and c-Src3M, which could account for the differences in response to Hsp90.

Molecular dynamics simulations confirm these notions and extend the picture. The increased *active-to-inactive* transitions in c-Src3MΔC suggest that the kinetic barrier for activation is effectively lowered. This might explain the experimentally observed increased activity and conformational flexibility in this variant. Additionally, for c-Src3MΔC, we observed a transition state-like structure with partial structural features from both the active and inactive states. Together with our results on their unfolding cooperativity, observed by CD, this might be an indication that there exist more native-like structures in v-Src, which could potentially be stabilized by the interaction with Hsp90. Thermodynamically, the native-like structures would result in an entropy gain, which render the activation process more efficient.

In our simulations, specific regions show increased exposure and/or flexibility including the αC-helix, the proximal portion of the αC-β4-loop and the αE-helix. Since the P-loop is rich in glycines, the overall SASA (surface accessible surface area) is small for this region. Nevertheless, there seems to be a structural difference, as indicated by the increase in displacement, which describes the relative movement of this part of the protein to its former position.

The finding of a general increase in conformational flexibility corroborates previous suggestions of a correlation between chaperone binding and the openness of the kinase fold (Grbovic *et al*., 2006). Additionally, the A-loop region shows higher mobility, suggesting an increased activation potential of the v-Src-like variant.

Given the high similarities between chaperone-dependent and -independent kinases, the idea has been raised that intrinsically instable kinases would frequently expose Hsp90 binding sites, whereas stable kinases only do so during initial folding and therefore only transiently interact with chaperones during maturation (Falsone *et al*.,

2004, Caplan *et al*., 2007). Our results substantiate this interpretation and other findings on the kinase regions involved in chaperone interaction. We found that previously suggested binding sites are frequently exposed in v-Src, thereby potentially serving as recognition sites that are buried in the non-client kinase c-Src. The degree of exposition of these sites correlates with the strength of the dependence on Hsp90, rising from c-Src, over c-Src3M to v-Src. Furthermore, our study extends the view due to the fact that, with the point mutations, the deletion of the C-terminal tail strongly elevates the accessibility of the distant active center and the A-loop. A comparison of the T_M values obtained by CD spectroscopy and the $I_{1/2}$ of thermal inactivation for the Src variants lacking the C-terminal tail reveals that at a temperature where still half of the secondary structure is retained, yet these kinases show no detectable activity. This indicates a crucial role of the C-terminal tail in supporting a kinase domain with an active fold.

Based on our results, we propose that Src may exist in multiple native-like states. We suggest that the activated state of the kinase is instable and reverts to the less active state unless Hsp90 is present which may induce or select this state. This, leads to an apparent higher activity of v-Src in the presence of Hsp90.

4.2.6. Hsp90 and cancer

Hsp90 has been shown to be upregulated in many cancer types (Ciocca & Calderwood, 2005). Thus, Hsp90 plays a pivotal role in cancer development and progression, which makes it a promising drug target (Trepel *et al.*, 2010). To date, there are 17 different Hsp90 inhibitors in clinical trials (Barrot & Haystead, 2013). Cdc37 and its interaction with Hsp90 have also been proposed as a target (Pearl, 2005). Indeed, overexpression of Cdc37 renders the co-chaperone to be an oncogene itself (Pearl, 2005). Src kinase plays a critical role in cell survival, proliferation and metastasis. Increased Src activity and expression has been observed for a variety of cancers (Belsches-Jablonski *et al*., 2005). Thereby, oncogenic v-Src-imitating mutations increase Src kinase activity and Hsp90-dependence in parallel. In this study, we established a model that can explain this correlation, which is crucial to understand the relationship between Hsp90 and cancer development. We found that v-Src shows a strict specificity towards the β-isoform of human Hsp90. This finding correlates with Hsp90β overexpression in gastric cancer together with Src kinase activity (Liu *et al*., 1999, Yang *et al*., 2014).

The newly identified isoform specificity may have important implications for future drug development. Furthermore, our study suggests that Hsp90 may act on different oncogenic kinases in distinct ways, introducing another level of complexity to the chaperoning process of Hsp90. Our findings on the Hsp90-dependence of the prototype of an oncogene, v-Src kinase, represent an important step to understand the complex Hsp90-client connection.

5. Summary

In this work, the chaperone cycle of Hsp90 with a focus on the kinase specific cochaperone Cdc37 could be reconstituted *in vitro*. Using fluorescence-assisted analytical ultracentrifugation (aUC) and fluorescence resonance energy transfer (FRET), the entry and exit point of Cdc37 in and out of the conformational cycle of Hsp90 could be determined. In the context of preliminary studies, the new insights provided by the present analysis deliver profound knowledge on the mechanism by which kinases are matured in the cell by this complex network of chaperones and cochaperones. This first part of the present study focused on the part of the Hsp90 chaperone cycle taking over a prefolded kinase client from Hsp70 for final maturation.

During the second part of the research project, the influence of Hsp90 and Cdc37 on the activity of the most stringent client kinase v-Src was studied. For that we used recombinantly expressed Src kinases purified from *Sf*9 cells, which were enzymatically active *in vitro*. This indicated that the purified kinase had already undergone folding within the expression host and was present in an at least partly folded state after isolation. Consistent with this oberservation, it was found that early-folding chaperones such as Hsp40, Hsp70 and Hop did not influence the activity of the (pre-)folded kinase. However, Hsp90 was in fact able to activate the client kinase v-Src, whereas its non-client homologue c-Src kinase remained unaffected. Cdc37 significantly increased the performance of this process, suggesting a role for elevating the specificity and affinity during the Hsp90-kinase maturation cycle. The apparent affinity for the v-Src activation process could be determined to be 3.0 µM for Hsp90 and 230 nM for the Hsp90-Cdc37 complex, respectively. Exposure of the Hsp90-Cdc37-kinase complex to heat stress surprisingly revealed a Cdc37-independent kinase stabilization at elevated temperatures. This is a novel finding that suggests the accumulation of kinase conformations with increased affinity for Hsp90 at elevated temperatures. Notably, a previously unknown Hsp90-isoform specificity of v-Src was identified that may have implications for cancer drug development.

Furthermore, by designing chimera of v-Src and c-Src, the characteristics that determine the dependence of a kinase on the Hsp90 chaperone could be identified. By applying CD- and UV-spectroscopy, H/D exchange and MD simulations, it was found that low stability, low folding cooperativity, aggregation propensity, molecular flexibility and exposure of specific regions in the client kinase cause the addiction of

client kinases on the molecular chaperones. Notably, these exposed parts consistently match regions formerly found to be important for kinase–chaperone interaction.

The fact that destabilized oncogenic kinase mutants like v-Src show dramatically increased chaperone dependence, emphasizes the importance to understand the action of molecular chaperones in general and Hsp90 in particular as they may facilitate the formation and progression of diseases.

6. Abbreviations

A_{280}	absorption at 280 nm
activation loop	A-loop
Aha1	activator of heat shock 90kDa protein ATPase homolog 1
ANS	1-Anilino-8-Naphthalene Sulfonate
APS	ammoniumpersulfate
AR	androgen receptor
ATPase	ATP-Hydrolase
aUC	analytical ultracentrifugation
bp(s)	base pair(s)
c-Src	cellular Src kinase
CD	circular dichroism
Cdc37	cell division cycle 37
*Cdc37	Alexa488-labelled human Cdc37
$Cdc37_E$	Cdc37-S13E
$Cdc37_{ERR}$	Cdc37-S13E-M164R-L205R
Cdk	cyclin-dependent kinases
C. elegans	*Caenorhabditis elegans*
Chk1	checkpoint kinase 1
CK2	casein kinase 2
CSK	C-terminal Src kinase
CSM	Complete Supplement Mixture (yeast selective medium)
Cyp40	cyclophilin 40
DMSO	Dimethyl sulfoxide
DNA	Deoxyribonucleic acid
DTT	Dithiothreitol
ε	molar extinction coefficient
E. coli	*Escherichia coli*
EDTA	Ethylenediamine-tetraecetic acid
e. g.	exempli gratia (for example)
EGFR	epidermal growth factor receptor
ER	endoplasmic reticulum
ErbB	epidermal growth factor receptor
ERK	extracellular-signal regulated kinase
FAK	focal adhesion kinase

FKBP	FK506 binding protein
FPLC	Fast Protein Liquid Chromatography
FRET	Fluorescence Resonance Energy Transfer
Grp94	glucose-regulated protein 94
Gua-HCl	Guanidinhydrochlorid
HDX-MS	Hydrogen/deuterium exchange mass spectrometry
HEPES	N-(2-Hydroxyethyl)-piperazin-N'-2-ethansulfonsäure
H_2O dd	double-distilled water
Hop/Sti1	Hsp70-Hsp90 organizing protein / stress inducible phosphoprotein 1
HPLC	High Performance Liquid Chromatography
*Hsp90	Atto550-labelled yeast Hsp90-Cys385
Hsp(s)	heat shock proteins (s)
HtpG	high temperature protein G
$I_{1/2}$	half-maximal kinase activity
i. e.	id est (that is)
IgG	immunoglobulin G
IMAC	immobilized metal ion affinity chromatography
IPTG	Isopropyl-β-D-thiogalactopyranosid
JNK	c-Jun N-terminal kinase
kb	kilo base pairs (1000 bps)
K_M	Michaelis-Menten constant
LB_0	Luria Broth medium
λ	wavelength
MAP	mitogen-activated protein
MD	molecular dynamics
MS^E	time-of-flight mass spectrometry with electrospray ionization
MW	molecular weight
n. a.	not available
NAC	nascent polypeptide-associated complex
n.d.	not determined
OD	optical density
p190RhoGAP	p190Rho-GTPase-activating protein
p.a.	pro analysis

PAGE	Polyacrylamide gel electrophoresis
PBS	Phosphate buffered saline
PCR	Polymerase chain reaction
PDGFR	platelet derived growth factor receptor
PDI	protein disulfide isomerase
pg	prep grade
pH	Potentia Hydrogenii
PH-domain	Pleckstrin homology domain
pI	Isoelectric point
PI3	phosphoinositid-3-kinase
PKA	cyclic AMP-dependent protein kinase
POD	ß-peroxidase
PP5	protein phosphatase 5
Pph1	protein phosphatase 1
PPIase	peptidyl-prolyl-isomerase
PTPB1	protein-tyrosine-phosphatase B1
PVDF	Polyvinylidenfluorid
Rad	Radicicol
RT	room temperature
RTK	receptor tyrosine kinases
SASA	solvent accessible surface area
S. cerevisiae	*Saccharomyces cerevisiae*
SDS	Sodium dodecyl sulfate
*Sf*9	*Spodoptora frugiperda* 9 ovary cells
SH-domain	Src homology domain
sHsp(s)	small heat shock proteins
TAE	Tris-Acetate buffer (containing EDTA)
TBS	Tris buffered saline
TCEP	Tris(2-chlorethyl)phosphat
TEMED	N, N, N', N'-Tetramethylethylendiamine
T_M	melting temperature
TPR	tetratricopeptide repeat
TRAP1	tumour necrosis factor receptor associated protein 1
o/n.	Over night
rpm	revolutions per minute

UV	ultraviolet
v-Src	viral Src kinase
v/v	volume per volume
w/v	weight per volume
x g	centrifugal force
YPD	yeast extract peptone dextrose (yeast full medium)

7. Literature

Abbas-Terki, T., Briand, P.A., Donzé, O., Picard, D. (2002). The Hsp90 co-chaperones Cdc37 and Sti1 interact physically and genetically. Biol. Chem. 383, 1335-42.

Abravaja, K., Myers, M., Murphy, S., Morimoto, R. (1992). The human heat shock protein hsp70 interacts with HSF, the transcription factor that regulates heat shock gene expression. Genes Dev. 6, 1153-1164.

Ali Khan, H., Mutus, B. (2014). Protein disulfide isomerase a multifunctional protein with multiple physiological roles. Front Chem. 2: 70.

Ali, M.M.U., Roe, S.M., Vaughan, C.K., Meyer, P., Panaretou, B., Piper, P.W. (2006). Crystal structure of an Hsp90-nucleotide-p23/Sba1 closed chaperone complex. Nature. 440, 1013-7.

Anfinsen, C.B., Haber, E., Sela, M., White, F.H. Jr. (1961). The kinetics of formation of native ribonuclease during oxidation of the reduced polypeptide chain. Proc. Natl. Acad. Sci. U S A. 47: 1309-14.

Argon, Y., Simen, B. (1999). GRP94, an ER chaperone with protein and peptide binding properties. Semin Cell Dev. Biol. 10, 495-505.

Arlander, S.J., Felts, S.J., Wagner, J.M., Stensgard, B., Toft, D.O., Karnitz, L.M. (2006). Chaperoning checkpoint kinase 1 (Chk1), an Hsp90 client, with purified chaperones. J. Biol. Chem. 281, 2989-2998.

Bates, G. Huntingtin aggregation and toxicity in Huntington’s disease. (2003). Lancet. 361, 1642-4.

Bergman, L.W., Kuehl, W.M. (1979). Formation of intermolecular disulfide bonds on nascent immunoglobulin polypeptides. J. Biol. Chem. 254, 5690-4.

Beyreuther, K., Masters, C.L. (1991). Amyloid precursor protein (APP) and beta A4 amyloid in the etiology of Alzheimer's disease: precursor-product relationships in the derangement of neuronal function. Brain Pathol. 1, 241-51.

Bjorge, J., Pang, A., Fujita, D. (2000). Identification of protein-tyrosine phosphatase 1B as the major tyrosine phosphatase activity capable of dephosphorylating and activating c-Src in several human breast cancer cell lines. J. Biol. Chem. 275, 41439-41446.

Borkovich, K.A., Farrelly, F.W., Finkelstein, D.B., Taulien, J., Lindquist, S. (1989). hsp82 is an essential protein that is required in higher concentrations for growth of cells at higher temperatures. Mol. Cell. Biol. 9, 3919-3930.

Bose, S., Weikl, T., Bügl, H., Buchner, J. (1996). Chaperone function of Hsp90-associated proteins. Science. 274, 1715-7.

Braakman, I., Hoover-Litty, H., Wagner, K.R., Helenius, A. (1991). Folding of influenza hemagglutinin in the endoplasmic reticulum. J. Cell Biol. 114, 401-11.

Broome, M., Hunter, T. (1996). Requirement for c-Src catalytic activity and the SH3 domain in plateletderived growth factor BB and epidermal growth factor mitogenic signaling. J. Biol. Chem. 271, 16798-16806.

Brown, M.T., Cooper, J.A. (1996). Regulation, substrates and functions of src. Biochimica et Biophysica Acta (BBA) - Reviews on Cancer. 1287, 121-149.

Brugge, J.S. (1986). Interaction of the Rous sarcoma virus protein pp60src with the cellular proteins pp50 and pp90. Curr. Top. Microbiol. Immunol. 123, 1-22.

Brugge, J.S., Erikson, E., Erikson, R.L. (1981). The specific interaction of the Rous sarcoma virus transforming protein, pp60src, with two cellular proteins. Cell 25, 363-372.

Caplan, A.J., Mandal, A.K. & Theodoraki, M.A. (2007) Molecular chaperones and protein kinase quality control. Trends Cell Biol 17, 87-92.

Chen, S., Smith, D.F. (1998). Hop as an adaptor in the heat shock protein 70 (Hsp70) and hsp90 chaperone machinery. J. Biol. Chem. 273, 35194-200.

Chen, S., Sullivan, W.P., Toft, D.O., Smith, D.F. (1998). Differential interactions of p23 and the TPR-containing proteins Hop, Cyp40, FKBP52 and FKBP51 with Hsp90 mutants. Cell Stress Chaperones. 3, 118-29.

Citri, A., Harari, D., Shohat, G., Ramakrishnan, P., Gan, J., Lavi, S., Eisenstein, M., Kimchi, A., Wallach, D., Pietrokovski, S., Yarden, Y. (2006). Hsp90 recognizes a common surface on client kinases. J. Biol. Chem. 281, 14361-9

Cooper, J., Gould, K., Cartwright, C., Hunter, T. (1986). Tyr527 is phosphorylated in pp60c-src: implications for regulation. Science. 231, 1431-1434.

Courtneidge, S., Levinson, A., Bishop, J. (1980). The protein encoded by the transforming gene of avian sarcoma virus (pp60src) and a homologous protein in normal cells (pp60proto-src) are associated with the plasma membrane. Proc. Natl. Acad. Sci. U. S. A. 77, 3783-3787.

Cowan-Jacob, S.W., Fendrich, G., Manley, P.W., Jahnke, W., Fabbro, D., Liebetanz, J., Meyer, T. (2005). The Crystal Structure of a c-Src Complex in an Active Conformation Suggests Possible Steps in c-Src Activation. Structure. 13, 861-87.

Cunningham, C.N., Southworth, D.R., Krukenberg, K.A., Agard, D.A. (2012). The conserved arginine 380 of Hsp90 is not a catalytic residue, but stabilizes the closed conformation required for ATP hydrolysis. Protein Sci. 21: 1162-71.

Dai, K., Kobayashi, R., Beach, D. (1996). Physical interaction of mammalian CDC37 with CDK4. J. Biol. Chem. 271, 22030-22034.

da Rocha Dias, S., Friedlos, F., Light, Y., Springer, C., Workman, P., Marais, R. (2005). Activated B-RAF is an Hsp90 client protein that is targeted by the anticancer drug 17-allylamino-17-demethoxygeldanamycin. Cancer Res. 65, 10686-91.

Dey, B., Caplan, A.J., Boschelli, F. (1996). The Ydj1 molecular chaperone facilitates formation of active p60v-src in yeast. Mol. Biol. Cell. 7, 91-100.

Dill, K.A., Bromberg, S., Yue, K., Fiebig, K.M., Yee, D.P., Thomas, P.D. (1995) Principles of protein folding--a perspective from simple exact models. Protein Sci. 4, 561-602.

Dill, K.A., Chan, H.S. (1997). From Levinthal to pathways to funnels. Nat. Struct. Biol. 4: 10-9.

Dollins, D.E., Warren, J.J., Immormino, R.M., Gewirth, D.T. (2007). Structures of GRP94-nucleotide complexes reveal mechanistic differences between the hsp90 chaperones. Mol. Cell. 28, 41-56.

Eckl, J.M., Rutz, D.A., Haslbeck, V., Zierer, B.K., Reinstein, J., Richter, K. (2013). Cdc37 (cell division cycle 37) restricts Hsp90 (heat shock protein 90) motility by interaction with N-terminal and middle domain binding sites. J. Biol. Chem. 288, 16032-42.

Edelhoch, H. (1967). Spectroscopic determination of tryptophan and tyrosine in proteins. Biochemistry. 6, 1948-1954.

Elble, R. (1992). A simple and efficient procedure for transformation of yeasts. Biotechniques. 13, 18-20.

Ellis, C., Moran, M., McCormick, F., Pawson, T. (1990). Phosphorylation of GAP and GAP-associated proteins by transforming and mitogenic tyrosine kinases. Nature. 343, 377-381.

Fairbanks, G., Steck, T., Wallach, D. (1971). Electrophoretic analysis of the major polypeptides of the human erythrocyte membrane. Biochemistry. 10, 2606-2617.

Falsone, S.F., Leptihn, S., Osterauer, A., Haslbeck, M., Buchner, J. (2004). Oncogenic mutations reduce the stability of SRC kinase. J. Mol. Biol. 344, 281-291.

Fanghänel, J., Fischer, G. (2004). Insights into the catalytic mechanism of peptidyl prolyl cis/trans isomerases. Front Biosci. 9: 3453-78.

Farrell, A. & Morgan, D.O. (2000). Cdc37 promotes the stability of protein kinases Cdc28 and Cak1. Mol. Cell. Biol. 20, 749-754.

Felts, S.J., Karnitz, L.M., Toft, D.O. (2007). Functioning of the Hsp90 machine in chaperoning checkpoint kinase I (Chk1) and the progesterone receptor (PR). Cell Stress Chaperones. 12, 353-63.

Feng, S., Chen, J., Yu, H., Simon, J., Schreiber, S. (1994). Two binding orientations for peptides to the Src SH3 domain: development of a general model for SH3-ligand interactions. Science. 266, 1241-1247.

Fincham, V., Wyke, J., Frame, M. (1995). v-Src-induced degradation of focal adhesion kinase during morphological transformation of chicken embryo fibroblasts. Oncogene. 10, 2247-2252.

Fischer, G., Bang, H., Mech, C. (1984) Determination of enzymatic catalysis for the cis-trans-isomerization of peptide binding in proline-containing peptides. Biomed. Biochim. Acta. 43, 1101-11.

Fling, S., Gregerson, D. (1986). Peptide and protein molecular weight determination by electrophoresis using a high-molarity tris buffer system without urea. Anal. Biochem. 155, 83-88.

Frame, M.C. (2002). Src in cancer: deregulation and consequences for cell behaviour. Biochim. Biophys. Acta. 1602, 114-30.

Freedman, R.B., Hirst, T.R., Tuite, M.F. (1994). Protein disulphide isomerase: building bridges in protein folding. Trends Biochem. Sci. 19, 331-6.

Freeman, B., Myers, M., Schumacher, R., Morimoto, R. (1995). Identification of a regulatory motif in Hsp70 that affects ATPase activity, substrate binding and interaction with HDJ-1. EMBO J. 14, 2281-2292.

Gaiser, A.M., Brandt, F., Richter, K. (2009). The non-canonical Hop protein from Caenorhabditis elegans exerts essential functions and forms binary complexes with either Hsc70 or Hsp90. J. Mol. Biol. 391: 621-34.

Gaiser, A.M., Kretzschmar, A., Richter, K. (2010). Cdc37-Hsp90 complexes are responsive to nucleotide-induced conformational changes and binding of further cofactors. J. Biol. Chem. 285, 40921-32.

Gasteiger, E., Gattiker, A., Hoogland, C., Ivanyi, I., Appel, R., Bairoch, A. (2003). ExPasy: The proteomics served for in-depth protein knowledge and analysis. Nucleic Acids Res. 31, 3784-3788.

Gautschi, M., Mun, A., Ross, S., Rospert, S. (2002). A functional chaperone triad on the yeast ribosome. Proc. Natl. Acad. Sci. U.S.A. 99, 4209-14.

Georgopoulos, C., Welch, W.J. (1993) Role of the major heat shock proteins as molecular chaperones. Annu. Rev. Cell Biol. 9, 601-34.

Ghaemmaghami, S., Huh, W.K., Bower, K., Howson, R.W., Belle, A., Dephoure, N., O'Shea, E.K., Weissman, J.S. (2003). Global analysis of protein expression in yeast. Nature. 425: 737-41.

Gill, S., von Hippel, P. (1989). Calculation of protein extinction coefficients from amino acid sequence data. Anal. Biochem. 182, 319-326.

Go, N., Taketomi, H. (1978). Respective roles of short- and long-range interactions in protein folding. Proc. Natl. Acad. Sci. U S A. 75: 559-63.

Gray, P.J., Prince, T., Cheng, J., Stevenson, M.A., Calderwood, S.K. (2008). Targeting the oncogene and kinome chaperone CDC37. Nat. Rev. Cancer. 8, 491-495.

Grbovic, O.M., Basso, A.D., Sawai, A., Ye, Q., Friedlander, P., Solit, D., Rosen, N. (2006). V600E B-Raf requires the Hsp90 chaperone for stability and is degraded in response to Hsp90 inhibitors. Proc. Natl. Acad. Sci. U. S. A. 103, 57-62.

Gu, J. & Gu, X. (2003). Natural history and functional divergence of protein tyrosine kinases. Gene. 317, 49-57.

Hartl, F.U., Hayer-Hartl, M. (2009). Converging concepts of protein folding in vitro and in vivo. Nat. Struct. Mol. Biol. 16, 574-81.

Hayes, D.B., Stafford, W.F. (2010). SEDVIEW, real-time sedimentation analysis. Macromol. Biosci. 10, 731-5.

Hessling, M., Richter, K., Buchner, J. (2009). Dissection of the ATP-induced conformational cycle of the molecular chaperone Hsp90. Nat. Struct. Mol. Biol. 16, 287-93.

Humphrey, W., Dalke, A., Schulten, K. (1996). VMD - Visual Molecular Dynamics. J. Mol. Graph. 14, 33-38.

Hunter, T. & Poon, R.Y. (1997). Cdc37: a protein kinase chaperone? Trends Cell Biol. 7, 157-161.

Huse, M., Kuriyan, J. (2002). The conformational plasticity of protein kinases. Cell. 109, 275-282.

Hutchison, K.A., Brott, B.K., De Leon, J.H., Perdew, G.H., Jove, R., Pratt, W.B. (1992). Reconstitution of the multiprotein complex of pp60src, hsp90, and p50 in a cell-free system. J. Biol. Chem. 267, 2902-2908.

Iba, H., Takeya, T., Cross, F.R., Hanafusa, T., Hanafusa, H. (1984). Rous sarcoma virus variants that carry the cellular src gene instead of the viral src gene cannot transform chicken embryo fibroblasts. Proc. Natl. Acad. Sci. U S A 81, 4424-4428.

Irby, R., Mao, W., Coppola, D., Kang, J., Loubeau, J., Trudeau, W., Karl, R., Fujita, D., Jove, R., Yeatman, T. (1999). Activating SRC mutation in a subset of advanced human colon cancers. Nat. Genet. 21, 187-190.

Jiang, Y., Bernard, D., Yu, Y., Xie, Y., Zhang, T., Li, Y., Burnett, J.P., Fu, X., Wang, S., Sun, D. (2010). Split Renilla luciferase protein fragment-assisted complementation (SRL-PFAC) to characterize Hsp90-Cdc37 complex and identify critical residues in protein/protein interactions. J. Biol. Chem. 285, 21023-36.

Johnson, D., Agochiya, M., Samejima, K., Earnshaw, W., Frame, M., Wyke, J. (2000). Regulation of both apoptosis and cell survival by the v-Src oncoprotein. Cell Death Differ. 7, 685-696.

Jones, R., Brunton, V., Frame, M. (2000). Adhesion-linked kinases in cancer; emphasis on src, focal adhesion kinase and PI 3-kinase. Eur. J. Cancer. 36, 1595-1606.

Jorgensen, P., Nishikawa, J.L., Breitkreutz, B.J., Tyers, M. (2002). Systematic identification of pathways that couple cell growth and division in yeast. Science. 297: 395-400.

Kamei, T., Machida, K., Nimura, Y., Senga, T., Yamada, I., Yoshii, S., Matsuda, S., Hamaguchi, M. (2000). C-Cbl protein in human cancer tissues is frequently tyrosine phosphorylated in a tumor-specific manner. Int. J. Oncol. 17, 335-339.

Karnitz, L.M. & Felts, S.J. (2007). Cdc37 regulation of the kinome: when to hold 'em and when to fold 'em. Sci. STKE. pe22.

Kamps, M., Buss, J., Sefton, B. (1986). Rous sarcoma virus transforming protein lacking myristic acid phosphorylates known polypeptide substrates without inducing transformation. Cell. 45, 105-112.

Kato, J.Y., Takeya, T., Grandori, C., Iba, H., Levy, J.B., Hanafusa, H. (1986). Amino acid substitutions sufficient to convert the nontransforming p60c-src protein to a transforming protein. Mol. Cell. Biol. 6, 4155-60.

Kellis, M., Birren, B., Lander, E. (2004). Proof and evolutionary analysis of ancient genome duplication in the yeast Saccharomyces cerevisiae. Nature. 428, 617-624.

Kelly, S.M., Jess, T.J., Price, N.C. (2005). How to study proteins by circular dichroism. Biochim. Biophys. Acta. 1751, 119-39.

Kimura, Y., Rutherford, S.L., Miyata, Y., Yahara, I., Freeman, B.C., Yue, L., Morimoto, R.I., Lindquist, S. (1997). Cdc37 is a molecular chaperone with specific functions in signal transduction. Genes Dev. 11, 1775-1785.

Kloss, E., Courtemanche, N., Barrick, D. (2008). Repeat-protein folding: new insights into origins of cooperativity, stability, and topology. Arch. Biochem. Biophys. 469: 83-99.

Kortemme, T., Ramírez-Alvarado, M., Serrano, L. (1998). Design of a 20-amino acid, three-stranded beta-sheet protein. Science. 281: 253-6.

Koulov, A.V., LaPointe, P., Lu, B., Razvi, A., Coppinger, J., Dong, M.Q., Matteson, J., Laister, R., Arrowsmith, C., Yates, JR. 3rd, Balch, W.E. (2010). Biological and structural basis for Aha1 regulation of Hsp90 ATPase activity in maintaining proteostasis in the human disease cystic fibrosis. Mol. Biol. Cell. 21, 871-84.

Krauss, G. (2008). Biochemistry of Signal Transduction and Regulation (Wiley-VCH).

Kroe, R., Laue, T. (2009). NUTS and BOLTS: applications of fluorescence-detected sedimentation. Anal. Biochem. 390, 1-13.

Lakowicz, J. R. (1999). Principles in Fluorescence Spectroscopy (New York: Plenum Press).

Lamphere, L., Fiore, F., Xu, X., Brizuela, L., Keezer, S., Sardet, C., Draetta, G.F., Gyuris, J. (1997). Interaction between Cdc37 and Cdk4 in human cells. Oncogene. 14, 1999-2004.

Langkjaer, R., Cliften, P., Johnston, M., Piskur, J. (2003). Yeast genome duplication was followed by asynchronous differentiation of duplicated genes. Nature. 421, 848-852.

Lee, J.H., Pyon, J.K., Kim, D.W., Lee, S.H., Nam, H.S., Kim, C.H., Kang, S.G., Lee, Y.J., Park, M.Y., Jeong, D.J., Cho, M.K. (2010). Elevated c-Src and c-Yes expression in malignant skin cancers. Journal of Experimental & Clinical Cancer Research. 29: 116.

Lee, P., Rao, J., Fliss, A., Yang, E., Garrett, S., Caplan, A.J. (2002). The Cdc37 protein kinase-binding domain is sufficient for protein kinase activity and cell viability. J. Cell Biol. 159, 1051-1059.

Lee, P., Shabbir, A., Cardozo, C., Caplan, A.J. (2004). Sti1 and Cdc37 can stabilize Hsp90 in chaperone complexes with a protein kinase. Mol. Biol. Cell. 15, 1785-92.

Levy, J.B., Iba, H., Hanafusa, H. (1986). Activation of the transforming potential of p60c-src by a single amino acid change. Proc. Natl. Acad. Sci. U.S.A. 83, 4228-32.

Li, J., Richter, K., Buchner, J. (2011). Mixed Hsp90-cochaperone complexes are important for the progression of the reaction cycle. Nat. Struct. Mol. Biol. 18, 61-6.

Li, J., Richter, K., Reinstein, J., Buchner, J. (2013). Integration of the accelerator Aha1 in the Hsp90 co-chaperone cycle. Nat. Struct. Mol. Biol. 20, 326-31.

Li, J., Soroka, J., Buchner, J. (2012). The Hsp90 chaperone machinery: conformational dynamics and regulation by co-chaperones. Biochim. Biophys. Acta. 1823, 624-35.

Lindquist, S., Craig, E.A. (1988). The heat-shock proteins. Annu. Rev. Genet. 22, 631-77.

Lobley, A., Whitmore, L., Wallace, B. (2002) DICHROWEB: an interactive website for the analysis of protein secondary structure from circular dichroism spectra. Bioinformatics. 18, 211-212.

Lücking, C.B., Brice, A. (2000). Alpha-synuclein and Parkinson's disease. Cell. Mol. Life Sci. 57, 1894-908.

MacGregor, I., Anderson, A., Laue, T. (2004). Fluorescence detection for the XLI analytical ultracentrifuge. Biophys. Chem. 108, 165-185.

MacKerell, A.D. Jr. *et al*. (1998). All-atom empirical potential for molecular modeling and dynamics studies of proteins. J. Phys. Chem. B. 102, 3586-3616.

Macias, M.J., Hyvönen, M., Baraldi, E., Schultz, J., Sudol, M., Saraste, M., Oschkinat, H. (1996). Structure of the WW domain of a kinase-associated protein complexed with a proline-rich peptide. Nature. 382: 646-9.

MacLean, M. & Picard, D. (2003). Cdc37 goes beyond Hsp90 and kinases. Cell Stress Chaperones 8, 114-119.

Mandal, A.K., Lee, P., Chen, J.A., Nillegoda, N., Heller, A., DiStasio, S., Oen, H., Victor, J., Nair, D.M., Brodsky, J.L., Caplan, A.J. (2007). Cdc37 has distinct roles in protein kinase quality control that protect nascent chains from degradation and promote posttranslational maturation. J. Cell Biol. 176, 319-328.

Mandal, A.K., Theodoraki, M.A., Nillegoda, N.B., Caplan, A.J. (2011). Role of molecular chaperones in biogenesis of the protein kinome. Methods Mol. Biol. 787, 75-81.

Manning, G., Whyte, D.B., Martinez, R., Hunter, T., Sudarsanam, S. (2002). The Protein Kinase Complement of the Human Genome. Science. 298, 1912-1934.

Masaki, T., Okada, M., Tokuda, M., Shiratori, Y., Hatase, O., Shirai, M., Nishioka, M., Omata, M. (1999). Reduced C-terminal Src kinase (Csk) activities in hepatocellular carcinoma. Hepatology. 29, 379-384.

Mayer, M.P., Nikolay, R., Bukau, B. (2002). Aha, another regulator for hsp90 chaperones. Mol. Cell. 10, 1255-6.

McLaughlin, S.H., Sobott, F., Yao, Z-ping, Zhang, W, Nielsen, P.R., Grossmann, J.G. (2006). The co-chaperone p23 arrests the Hsp90 ATPase cycle to trap client proteins. J. Mol. Biol. 356, 746-58.

Meyer, P., Prodromou, C., Hu, B., Vaughan, C., Roe, S.M., Panaretou, B. (2003). Structural and functional analysis of the middle segment of hsp90: implications for ATP hydrolysis and client protein and cochaperone interactions. Mol. Cell. 11, 647-58.

Meyer, P., Prodromou, C., Liao, C., Hu, B., Roe, S.M., Vaughan, C.K., Vlasic, I., Panaretou, B., Piper, P.W., Pearl, L.H. (2004). Structural basis for recruitment of the ATPase activator Aha1 to the Hsp90 chaperone machinery. EMBO J. 23, 1402-10.

Meyn, M.A. 3rd, Schreiner, S.J., Dumitrescu, T.P., Nau, G.J., Smithgall, T.E. (2005). SRC family kinase activity is required for murine embryonic stem cell growth and differentiation. Mol. Pharmacol. 68, 1320-30.

Mittag, T. & Forman-Kay, J.D. (2007). Atomic-level characterization of disordered protein ensembles. Curr. Opin. Struct. Biol. 17, 3-14.

Miyata, Y. (2009). Protein kinase CK2 in health and disease: CK2: the kinase controlling the Hsp90 chaperone machinery. Cell. Mol. Life Sci. 66, 1840-1849.

Miyata, Y., Ikawa, Y., Shibuya, M., Nishida, E. (2001). Specific association of a set of molecular chaperones including HSP90 and Cdc37 with MOK, a member of the mitogen-activated protein kinase superfamily. J. Biol. Chem 276, 21841-21848.

Miyata, Y. & Nishida, E. (2004). CK2 controls multiple protein kinases by phosphorylating a kinase-targeting molecular chaperone, Cdc37. Mol. Cell. Biol 24, 4065-4074.

Miyazaki, K., Senga, T., Matsuda, S., Tanaka, M., Machida, K., Takenouchi, Y. (1999). Critical amino acid substitutions in the Src SH3 domain that convert c-Src to be oncogenic. Biochem. Biophys. Res. Commun. 263, 759-64.

Moran, M.F., Koch, C.A., Anderson D, Ellis C, England L, Martin GS. (1990). Src homology region 2 domains direct protein-protein interactions in signal transduction. Proc. Natl. Acad. Sci. U.S.A. 87, 8622-6.

Mort-Bontemps-Soret, M., Facca, C., Faye, G. (2002). Physical interaction of Cdc28 with Cdc37 in Saccharomyces cerevisiae. Mol. Genet. Genomics 267, 447-458.

Myers, E., Miller, W. (1988). Optimal alignments in linear space. Comput.Appl. Biosci. 4, 11-17.

Nada, S., Okada, M., MacAuley, A., Cooper, J., Nakagawa, H. (1991). Cloning of a complementary DNA for a protein-tyrosine kinase that specifically phosphorylates a negative regulatory site of p60c-src. Nature. 351, 69-72.

Nair, S.C., Toran, E.J., Rimerman, R.A., Hjermstad, S., Smithgall, T.E., Smith, D.F. (1996). A pathway of multi-chaperone interactions common to diverse regulatory proteins: estrogen receptor, Fes tyrosine kinase, heat shock transcription factor Hsf1, and the aryl hydrocarbon receptor. Cell Stress Chaperones. 1, 237-250.

Nathan, D.F., Lindquist, S. (1995). Mutational analysis of Hsp90 function: interactions with a steroid receptor and a protein kinase. Mol. Cell Biol. 15, 3917-25.

Nathan, D.F., Vos, M.H., Lindquist, S. (1999). Identification of SSF1, CNS1, and HCH1 as multicopy suppressors of a Saccharomyces cerevisiae Hsp90 loss-of-function mutation. Proc. Natl. Acad. Sci. U.S.A. 96, 1409-14.

Obermann, W.M., Sondermann, H., Russo, A.A., Pavletich, N.P., Hartl, F.U. (1998). In vivo function of Hsp90 is dependent on ATP binding and ATP hydrolysis. J. Cell Biol. 143, 901-10.

Odai, H., Sasaki, K., Iwamatsu, A., Hanazono, Y., Tanaka, T., Mitani, K., Yazaki, Y., Hirai, H. (1995). The protooncogene product c-Cbl becomes tyrosine phosphorylated by stimulation with GM-CSF or Epo and constitutively binds to the SH3 domain of Grb2/Ash in human hematopoietic cells. J. Biol. Chem. 270, 10800-10805.

Okada, M., Nakagawa, H. (1988). Identification of a novel protein tyrosine kinase that phosphorylates pp60c-src and regulates its activity in neonatal rat brain. Biochem. Biophys. Res. Commun. 154, 796-802.

Ozkirimli, E., Yadav, S., Miller, W., Post, C. (2009). An electrostatic network and long-range regulation of src kinases. Protein Sci. 17, 1871-1880.

Ozkirimli, E., Post, C. (2009). Src kinase activation: a switched electrostatic network. Protein Sci. 15, 1051-1062.

Pace, C., Vajdos, F., Fee, L., Grimsley, G., Gray, T. (1995). How to measure and predict the molar absorption coefficient of a protein. Protein Sci. 4, 2411-2423.

Panaretou, B., Prodromou, C., Roe, S.M., O'Brien, R., Ladbury, J.E., Piper, P.W. (1998). ATP binding and hydrolysis are essential to the function of the Hsp90 molecular chaperone in vivo. EMBO J. 17, 4829-36.

Panaretou, B., Siligardi, G., Meyer, P., Maloney, A., Sullivan, J.K., Singh, S. (2002). Activation of the ATPase activity of hsp90 by the stress-regulated cochaperone aha1. Mol. Cell. 10, 1307-18.

Pearl, L.H. (2005). Hsp90 and Cdc37 -- a chaperone cancer conspiracy. Curr. Opin. Genet. Dev. 15, 55-61.

Peng, K., Vucetic, S., Radivojac, P., Brown, C.J., Dunker, A.K., Obradovic, Z. (2005). Optimizing long intrinsic disorder predictors with protein evolutionary information. J. Bioinform. Comput. Biol. 3, 35-60.

Peschek, J., Braun, N., Rohrberg, J., Back, K.C., Kriehuber, T., Kastenmüller, A., Weinkauf, S., Buchner, J. (2013). Regulated structural transitions unleash the chaperone activity of αB-crystallin. Proc. Natl. Acad. Sci. U S A. 110, E3780-9.

Phillips, J.C. *et al*. (2005). Scalable molecular dynamics with NAMD. J. Comput. Chem. 26, 1781-1802.

Picard, D.: http://www.picard.ch/downloads/Cdc37interactors.pdf, date: Dec, 2011.

Picard, D. (2002). Heat-shock protein 90, a chaperone for folding and regulation. Cell. Mol. Life Sci. 59, 1640-8.

Polier, S., Samant, R.S., Clarke, P.A., Workman, P., Prodromou, C., Pearl, L.H.. (2013). ATP-competitive inhibitors block protein kinase recruitment to the Hsp90-Cdc37 system. Nat. Chem. Biol. 9: 307-12.

Pratt, W.B., Morishima, Y., Murphy, M., Harrell, M. (2006). Chaperoning of glucocorticoid receptors. Handb. Exp. Pharmacol. 172, 111-38.

Pridgeon, J., Olzmann, J., Chin, L., Li, L. (2007). PINK1 protects against oxidative stress by phosphorylating mitochondrial chaperone TRAP1. PLoS Biol. 5, e172.

Prince, T., Matts, R.L. (2004). Definition of protein kinase sequence motifs that trigger high affinity binding of Hsp90 and Cdc37. J. Biol. Chem. 279, 39975-81.

Prince, T., Sun, L., Matts, R.L. (2005). Cdk2: a genuine protein kinase client of Hsp90 and Cdc37. Biochemistry. 44, 15287-95.

Prodromou, C., Pearl, L.H. (2003). Structure and functional relationships of Hsp90. Curr. Cancer Drug Targets. 3: 301-23.

Prodromou, C., Siligardi, G., O'Brien, R., Woolfson, D.N., Regan, L., Panaretou, B. Regulation of Hsp90 ATPase activity by tetratricopeptide repeat (TPR)-domain co-chaperones. EMBO J. 18, 754-62.

Prusiner, S.B. (1996). Molecular biology and pathogenesis of prion diseases. Trends Biochem. Sci. 21, 482-7.

Ratzke, C., Berkemeier, F., Hugel, T. (2012). Heat shock protein 90's mechanochemical cycle is dominated by thermal fluctuations. Proc. Natl. Acad. Sci. U.S.A. 109, 161-6.

Ren, M., Santhanam, A., Lee, P., Caplan, A. & Garrett, S. (2007). Alteration of the Protein Kinase Binding Domain Enhances Function of the Saccharomyces cerevisiae Molecular Chaperone Cdc37. Eukaryot. Cell. 6, 1363-1372.

Richter, K., Haslbeck, M., Buchner, J. (2010). The heat shock response: life on the verge of death. Mol Cell 40, 253-66.

Richter, K., Muschler, P., Hainzl, O., Reinstein, J., Buchner, J. (2003). Sti1 is a non-competitive inhibitor of the Hsp90 ATPase. Binding prevents the N-terminal dimerization reaction during the atpase cycle. J. Biol. Chem. 278, 10328-33.

Richter, K., Soroka, J., Skalniak, L., Leskovar, A., Hessling, M., Reinstein, J. (2008). Conserved conformational changes in the ATPase cycle of human Hsp90. J. Biol. Chem. 283, 17757-65.

Riddihough, G. (1994). More meanders and sandwiches. Nat. Struct. Biol. 1: 755-7.

Roe, S.M., Ali, M.M.U., Meyer, P., Vaughan, C.K., Panaretou, B., Piper, P.W. (2004). The Mechanism of Hsp90 regulation by the protein kinase-specific cochaperone p50(cdc37). Cell. 116, 87-98.

Roskoski, R. Jr. (2004). Src protein-tyrosine kinase structure and regulation. Biochem. Biophys. Res. Commun. 324, 1155-64.

Roussel, M., Saule, S., Lagrou, C., Rommens, C., Beug, H., Graf, T., Stehelin, D. (1979). Three new types of viral oncogene of cellular origin specific for haematopoietic cell transformation. Nature. 281, 452-5.

Ruddock, L.W., Klappa, P. (1999). Oxidative stress: Protein folding with a novel redox switch. Curr. Biol. 9, R400-2.

Russell, R.B., Breed, J., Barton, G.J. (1992). Conservation analysis and structure prediction of the SH2 family of phosphotyrosine binding domains. FEBS Lett. 304: 15-20.

Rutkowska, A., Mayer, M.P., Hoffmann, A., Merz, F., Zachmann-Brand, B., Schaffitzel, C. (2008). Dynamics of trigger factor interaction with translating ribosomes. J. Biol. Chem. 283, 4124-32.

Schaller, M., Hildebrand, J., Shannon, J., Fox, J., Vines, R., Parsons, J. (1994). Autophosphorylation of the focal adhesion kinase, pp125FAK, directs SH2-dependent binding of pp60src. Mol. Cell. Biol. 14, 1680-1688.

Schiene, C., Fischer, G. (2000). Enzymes that catalyse the restructuring of proteins. Curr. Opin. Struct. Biol. 10: 40-5.

Schlaepfer, D., Hunter, T. (1996). Evidence for in vivo phosphorylation of the Grb2 SH2-domain binding site on focal adhesion kinase by Src-family protein-tyrosine kinases. Mol. Cell. Biol. 16, 5623-5633.

Schmid, A.B., Lagleder, S., Gräwert, M.A., Röhl, A., Hagn, F., Wandinger, S.K., Cox, M.B., Demmer, O., Richter, K., Groll, M., Kessler, H., Buchner, J. (2012). The architecture of functional modules in the Hsp90 co-chaperone Sti1/Hop. EMBO J. 31, 1506-17.

Schneider, C., Sepp-Lorenzino, L., Nimmesgern, E., Ouerfelli, O., Danishefsky, S., Rosen, N., Hartl, F.U. (1996). Pharmacologic shifting of a balance between protein refolding and degradation mediated by Hsp90. Proc. Natl. Acad. Sci. U.S.A. 93, 14536-14541.

Sen, B., Johnson, F.M. (2011). Regulation of Src Family Kinases in Human Cancers. Journal of Signal Transduction. Vol. 2011: Article ID 865819.

Shao, J., Grammatikakis, N., Scroggins, B.T., Uma, S., Huang, W., Chen, J.J., Hartson, S.D., Matts, R.L. (2001). Hsp90 regulates p50(cdc37) function during the biogenesis of the active conformation of the heme-regulated eIF2 alpha kinase. J. Biol. Chem. 276, 206-214.

Shao, J., Irwin, A., Hartson, S.D. & Matts, R.L. (2003). Functional dissection of cdc37: characterization of domain structure and amino acid residues critical for protein kinase binding. Biochemistry. 42, 12577-12588.

Shao, J., Prince, T., Hartson, S.D. & Matts, R.L. (2003). Phosphorylation of serine 13 is required for the proper function of the Hsp90 co-chaperone, Cdc37. J. Biol. Chem. 278, 38117-38120.

Shen, Z., Batzer, A., Koehler, J.A., Polakis, P., Schlessinger, J., Lydon, N.B., Moran, M.F. (1999). Evidence for SH3 domain directed binding and phosphorylation of Sam68 by Src. Oncogene.18: 4647-53.

Shiau, A.K., Harris, S.F., Southworth, D.R., Agard, D.A. (2006). Structural Analysis of E. coli hsp90 reveals dramatic nucleotide-dependent conformational rearrangements. Cell. 127, 329–40.

Shibata, N., Hirano, A., Yamamoto, T., Kato, Y., Kobayashi, M. (2000). Superoxide dismutase-1 mutation-related neurotoxicity in familial amyotrophic lateral sclerosis. Amyotroph. Lateral Scler. Other Motor Neuron Disord. 1, 143–61.

Shimamura, T., Lowell, A.M., Engelman, J.A., Shapiro, G.I. (2005). Epidermal growth factor receptors harboring kinase domain mutations associate with the heat shock protein 90 chaperone and are destabilized following exposure to geldanamycins. Cancer Res. 65, 6401-8.

Shukla, D., Meng, Y., Roux, B., Pande, V.S. (2014). Activation pathway of Src kinase reveals intermediate states as targets for drug design. Nat. Commun. 5, 3397.

Siligardi, G., Panaretou, B., Meyer, P., Singh, S., Woolfson, D.N., Piper, P.W., Pearl, L.H., Prodromou, C. (2002). Regulation of Hsp90 ATPase activity by the co-chaperone Cdc37p/p50cdc37. J. Biol. Chem. 277, 20151-20159.

Silverstein, A.M., Grammatikakis, N., Cochran, B.H., Chinkers, M., Pratt, W.B. (1998). p50(cdc37) binds directly to the catalytic domain of Raf as well as to a site on hsp90 that is topologically adjacent to the tetratricopeptide repeat binding site. J. Biol. Chem. 273, 20090-5.

Smart, J.E., Oppermann, H., Czernilofsky, A.P., Purchio, A.F., Erikson, R.L., Bishop, J.M. (1981). Characterization of Sites for Tyrosine Phosphorylation in the Transforming Protein of Rous Sarcoma Virus (pp60v-src) and Its Normal Cellular Homologue (pp60c-src). Proc. Natl. Acad. Sci. 78, 6013-6017.

Smith, J.R., de Billy, E., Hobbs, S., Powers, M., Prodromou, C., Pearl, L., Clarke, P.A., Workman, P. (2013). Restricting direct interaction of CDC37 with HSP90 does not compromise chaperoning of client proteins. Oncogene.

Smith, J.R., Workman, P. (2009). Targeting CDC37: an alternative, kinase-directed strategy for disruption of oncogenic chaperoning. Cell Cycle. 8: 362-72.

Snyder, M.A., Bishop, J.M., McGrath, J.P., Levinson, A.D. (1985). A mutation at the ATP-binding site of pp60v-src abolishes kinase activity, transformation, and tumorigenicity. Mol. Cell. Biol. 5, 1772-9.

Sontag, E.M., Vonk, W.I., Frydman, J. (2014). Sorting out the trash: the spatial nature of eukaryotic protein quality control. Curr. Opin. Cell Biol. 26: 139-46.

Sreeramulu, S., Jonker, H.R., Langer, T., Richter, C., Lancaster, C.R., Schwalbe, H. (2009). The human Cdc37.Hsp90 complex studied by heteronuclear NMR spectroscopy. J. Biol. Chem. 284, 3885-3896.

Stéhelin, D. (1976). The transforming gene of avian tumor viruses. Pathol. Biol. (Paris). 24: 513-5.

Stehelin, D., Varmus, H.E., Bishop, J.M., Vogt, P.K. (1976). DNA related to the transforming gene(s) of avian sarcoma viruses is present in normal avian DNA. Nature. 260, 170-3.

Stepanova, L., Leng, X., Parker, S.B., Harper, J.W. (1996). Mammalian p50Cdc37 is a protein kinase-targeting subunit of Hsp90 that binds and stabilizes Cdk4. Genes Dev. 10, 1491-502.

Taipale, M., Jarosz, D.F., Lindquist, S. (2010). HSP90 at the hub of protein homeostasis: emerging mechanistic insights. Nat. Rev. Mol. Cell Biol. 11, 515-28.

Taipale, M., Krykbaeva, I., Koeva, M., Kayatekin, C., Westover, K.D., Karras, G.I., Lindquist, S. (2012). Quantitative analysis of HSP90-client interactions reveals principles of substrate recognition. Cell. 150, 987-1001.

Takeya, T., Hanafusa, H. (1983). Structure and sequence of the cellular gene homologous to the RSV src gene and the mechanism for generating the transforming virus. Cell. 32, 881-890.

Tanaka, S., Amling, M., Neff, L., Peyman, A., Uhlmann, E., Levy, J., Baron, R. (1996). c-Cbl is downstream of c-Src in a signalling pathway necessary for bone resorption. Nature. 383, 528-531.

Taylor, S. & Kornev, A. (2011). Protein kinases: evolution of dynamic regulatory proteins. Trends Biochem. Sci. 36, 65-77.

Terasawa, K., Yoshimatsu, K., Iemura, S., Natsume, T., Tanaka, K., Minami, Y. (2006). Cdc37 interacts with the glycine-rich loop of Hsp90 client kinases. Mol. Cell. Biol. 26, 3378-3389.

Trepel, J., Mollapour, M., Giaccone, G., Neckers, L. (2010). Targeting the dynamic HSP90 complex in cancer. Nat. Rev. Cancer. 10, 537-549.

Turnbull, E.L., Martin, I.V. Fantes, P.A. (2005). Cdc37 maintains cellular viability in Schizosaccharomyces pombe independently of interactions with heat-shock protein 90. FEBS J. 272, 4129-4140.

Twamley-Stein, G., Pepperkok, R., Ansorge, W., Courtneidge, S. (1993). The Src family tyrosine kinases are required for platelet-derived growth factor-mediated signal transduction in NIH 3T3 cells. Proc. Natl. Acad. Sci. U. S. A. 90, 7696-7700.

Vaughan, C.K., Gohlke, U., Sobott, F., Good, V.M., Ali, M.M., Prodromou, C., Robinson, C.V., Saibil, H.R., Pearl, L.H. (2006). Structure of an Hsp90-Cdc37-Cdk4 complex. Mol. Cell. 23, 697-707.

Vaughan, C.K., Mollapour, M., Smith, J.R., Truman, A., Hu, B., Good, V.M., Panaretou, B., Neckers, L., Clarke, P.A., Workman, P., Piper, P.W., Prodromou, C., Pearl, L.H. (2008). Hsp90-Dependent Activation of Protein Kinases Is Regulated by Chaperone-Targeted Dephosphorylation of Cdc37. Mol. Cell. 31, 886-895.

Vaughan, C.K., Piper, P.W., Pearl, L.H., Prodromou, C. (2009). A common conformationally coupled ATPase mechanism for yeast and human cytoplasmic HSP90s. FEBS J. 276, 199-209.

Walter, P., Ron, D. (2011). The unfolded protein response: from stress pathway to homeostatic regulation. Science. 334: 1081-6.

Wang, D.S., Shaw, G. (1995). The association of the C-terminal region of beta I sigma II spectrin to brain membranes is mediated by a PH domain, does not require membrane proteins, and coincides with a inositol-1,4,5 triphosphate binding site. Biochem. Biophys. Res. Commun. 217: 608-15.

Wang, D.S., Shaw, R., Winkelmann, J.C., Shaw, G. (1994). Binding of PH domains of beta-adrenergic receptor kinase and beta-spectrin to WD40/beta-transducin repeat containing regions of the beta-subunit of trimeric G-proteins. Biochem. Biophys. Res. Commun. 203: 29-35.

Wegele, H., Haslbeck, M., Reinstein, J., Buchner, J. (2003). Sti1 is a novel activator of the Ssa proteins. J. Biol. Chem. 278, 25970-6.

Welch, W., Feramisco, J. (1982). Purification of the major mammalian heat shock proteins. J. Biol. Chem. 257, 14949-14959.

Wilbur, W., Lipman, D. (1983). Rapid similarity searches of nucleid acid and protein data banks. Proc. Natl. Acad. Sci. U S A. 80, 726-730.

Whitmore, L. & Wallace, B. (2004). DICHROWEB, an online serve for protein secondary structure analyses from circular dichroism spectroscopic data. Nucleid Acids Res. 32, W668-673.

Whitmore, L. & Wallace, B. (2008). Protein secondary structure analyses from circular dichroism spectroscopy: methods and reference databases. Biopolymers. 89, 392-400.

Williams, J.C., Weijland, A., Gonfloni, S., Thompson, A., Courtneidge, S.A., Superti-Furga, G., Wierenga, R.K. (1997). The 2.35 A crystal structure of the inactivated form of chicken Src: a dynamic molecule with multiple regulatory interactions. J. Mol. Biol. 274: 757-75.

Wolozin, B. (2014). Physiological protein aggregation run amuck: stress granules and the genesis of neurodegenerative disease. Discov. Med. 17: 47-52.

Xu, W., Doshi, A., Lei, M., Eck, M.J., Harrison, S.C. (1999a) Crystal structures of c-Src reveal features of its autoinhibitory mechanism. Mol. Cell. 3, 629-38.

Xu, Y., Lindquist, S. (1993). Heat-shock protein hsp90 governs the activity of pp60v-src kinase. Proc. Natl. Acad. Sci. U S A. 90, 7074-8.

Xu, W., Mollapour, M., Prodromou, C., Wang, S., Scroggins, B.T., Palchick, Z., Beebe, K., Siderius, M., Lee, M.J., Couvillon, A., Trepel, J.B., Miyata, Y., Matts, R., Neckers, L. (2012). Dynamic tyrosine phosphorylation modulates cycling of the HSP90-P50(CDC37)-AHA1 chaperone machine. Mol. Cell. 47, 434-43.

Xu, Y., Singer, M.A., Lindquist, S. (1999b). Maturation of the tyrosine kinase c-src as a kinase and as a substrate depends on the molecular chaperone Hsp90. Proc. Natl. Acad. Sci. U S A. 96, 109-14.

Xu, W., Yuan, X., Xiang, Z., Mimnaugh, E., Marcu, M., Neckers, L. (2005). Surface charge and hydrophobicity determine ErbB2 binding to the Hsp90 chaperone complex. Nat. Struct. Mol. Biol. 12, 120-6

Yang, Y., Li, Z. (2005). Roles of heat shock protein gp96 in the ER quality control: redundant or unique function? Mol. Cell. 20, 173-182.

Yao, L., Kawakami, Y., Kawakami, T. (1994). The pleckstrin homology domain of Bruton tyrosine kinase interacts with protein kinase C. Proc. Natl. Acad. Sci. U S A. 91: 9175-9.

Young, J.C., Hartl, F.U. (2000). Polypeptide release by Hsp90 involves ATP hydrolysis and is enhanced by the co-chaperone p23. EMBO J. 19, 5930-40.

Yu, H., Chen, J., Feng, S., Dalgarno, D., Brauer, A., Schreiber, S. (1994). Structural basis for the binding of proline-rich peptides to SH3 domains. Cell. 76, 933-945.

Zhang, A., Hu, P., MacGregor, P., Xue, Y., Fan, H., Suchecki, P., Olszewski, L., Liu, A. (2014). Understanding the conformational impact of chemical modifications on monoclonal antibodies with diverse sequence variation using hydrogen/deuterium exchange mass spectrometry and structural modeling. Anal. Chem. 86, 3468–75.

Zhang, T., Li, Y., Yu, Y., Zou, P., Jiang, Y., Sun, D. (2009). Characterization of celastrol to inhibit hsp90 and cdc37 interaction. J. Biol. Chem. 284, 35381-35389.

Zhang, W., Hirshberg, M., McLaughlin, S.H., Lazar, G.A., Grossmann, J.G., Nielsen, P.R., Sobott, F., Robinson, C.V., Jackson, S.E., Laue, E.D. (2004). Biochemical and structural studies of the interaction of Cdc37 with Hsp90. J. Mol. Biol. 340, 891-907.

Zhao, Q., Boschelli, F., Caplan, A.J., Arndt, K.T. (2004). Identification of a conserved sequence motif that promotes Cdc37 and cyclin D1 binding to Cdk4. J. Biol. Chem. 279, 12560-4.

Zimmerman, S.B., Trach, S.O. (1991). Estimation of macromolecule concentrations and excluded volume effects for the cytoplasm of Escherichia coli. J. Mol. Biol. 222, 599-620.

8. Acknowledgements

This thesis was prepared at the Technische Universität München, Department Chemie, Lehrstuhl Biotechnologie under supervision of Prof. Dr. Johannes Buchner from December 2010 to December 2014.

I would like to thank Prof. Dr. Johannes Buchner for offering me the scientific tasks, for giving me the opportunity to prepare my PhD thesis in his group on this highly exciting topic and for giving me exceptional advice and support during my work.

I want to thank my collarboration partners Ville Kaila, Andreas Seidl and most of all Marco Dehling, with whom I always had a lot of fun during our joint project. Also I would like to thank my friend and colleague Oliver Lorenz for having been a true help concerning any technical and personal challenges. Most importantly, I would like to thank all PhD students, post-docs and CTAs/BTAs of our group for the nice and stimulating cooperation during the whole time. Finally, I would like to thank my parents, my girlfriend and my friends for always being there.

9. Declaration

I, Edgar Erik Boczek, hereby declare that this thesis was prepared independently using only the references and resources stated here. This work has not been presented to any examination board yet. Parts of this work have been submitted and / or published in scientific journals.

Hiermit erkläre ich, Edgar Erik Boczek, dass ich die vorliegende Arbeit selbständig verfasst und nur die angegebenen Quellen und Hilfsmittel verwendet habe. Die Arbeit wurde bisher keiner Prüfungskommission vorgelegt. Teile dieser Arbeit wurden in wissenschaftlichen Journalen eingereicht und / oder veröffentlicht.

_____

Edgar E. Boczek

München, 01. Dezember 2014